LOW LOSS MICROWAVE POWER COMBINERS/DIVIDERS

Thijs Waardenburg

A dissertation submitted to the Faculty of Engineering, University of Cape Town, in fulfilment of the requirement for the Degree of Master of Science in Engineering.

Cape Town 1986.

DECLARATION

I declare that this dissertation is my own, unaided work. It is submitted for the degree of Master of Science in Engineering at the University of Cape Town. It has not been submitted before for any degree or examination in any other University.

Signed by candidate

(Signature of candidate)

14th day of APRIL 1986

ABSTRACT

As many current applications require microwave solid state sources with output powers greater than that available from a single device a need for combining the power from these devices is required. N-way combiners/dividers may be used to achieve this. For high output powers these combiners/dividers must have a high combining efficiency.

This dissertation describes various power combining techniques and essentially a power combiner/divider that is both planar and low loss is required. The planar structure is a requirement if efficient heat dissipation is to be achieved.

Cylindrical resonant cavity structures give very high combining efficiencies, however, they are non planar and have narrow bandwidths. N-way planar combiners/dividers fabricated on microstrip provide the desired planar structure but due to the characteristics of microstrip are lossy.

As a culmination of this work a low loss 8-way planar stripline combiner/divider was constructed that gave a peak combining efficiency of 94 percent which approaches the combining efficiency of 98 percent that was obtained with the cylindrical resonant cavity combiner. The former offers its broader bandwidth and planar structure as advantages.

ACKNOWLEDGEMENTS

The author is indebted to the following:

Professor B.J. Downing for his supervision and constant encouragement.

Diana, my wife, for her typing and constant support.

The CSIR for financial assistance.

CONTENTS

	PAGE
ABSTRACT	(iii)
ACKNOWLEDGEMENTS	(iv)
Chapter	
1. REVIEW OF MICROWAVE SOLID STATE AMPLIFYING DEVICES	1
1.1 Introduction	1
1.2 The Bipolar Transistor a Brief Review	1
1.3 The Field Effect Transistor	3
1.4 The GaAs Field Effect Transistor Versus the Silicon Bipolar Transistor	9
1.5 Techniques Used to Increase the Output Power of FETs	10
1.6 Conclusion	17
2. COMBINING ON THE CIRCUIT LEVEL	18
2.1 Introduction	18
2.2 Chain and Tree Combining Structures	20
2.3 N-Way Combining Structures	23
2.3.1 Resonant Cavity Combining Structures	23
2.3.2 Non-Resonant Combining Structures	26
2.4 Conclusion	28
3. RESONANT CAVITY COMBINERS	29
3.1 Introduction	29
3.1.1 Measurement Equipment	30
3.2 The Cylindrical Resonant Cavity Combiner/Divider	30
3.2.1 Results and Discussion	36

3.2.2 Conclusions and Possible Improvements to the Resonant Cavity Combiner 42
3.3 Rectangular Waveguide Combiner/Divider 43
3.3.1 Introduction 43
3.3.2 The Design Procedure 44
3.3.3 Results and Discussion 50
3.3.4 Conclusions 53
3.4 Summary 54

4. WILKINSON AND CORPORATE WILKINSON COMBINERS/DIVIDERS 55
4.1 Introduction 55
4.2 The 2-Way Wilkinson Combiner/Divider 55
4.2.1 Construction of the Combiner/Divider and Results Obtained 59
4.2.2 Conclusions 62
4.3 The Corporate Wilkinson Combiner/Divider 63
4.3.1 Results and Discussion 64
4.3.2 Analysis of the Corporate Combiner/Divider on TOUCHSTONE 66
4.3.3 Results of the Second Version of the Corporate Wilkinson Combiner/Divider 72
4.3.4 Conclusions 75

5. PLANAR N-WAY COMBINERS/DIVIDERS 77
5.1 Introduction 77
5.2 Microstrip 77
5.2.1 Introduction 77
5.2.2 Design Formulae for Microstrip 80
5.2.3 Losses in Microstrip 82
5.3 Stripline 87

5.3.1 Design Equations for Stripline 88

5.3.2 Stripline Losses 88

5.4 Planar N-Way Combiner/Divider 91

5.4.1 Design of a Planar 4-Way Combiner/Divider 92

5.4.2 Conclusions 108

5.5 An 8-Way Planar Combiner/Divider 109

5.5.1 Design of the Combiner/Divider 109

5.5.2 Results Obtained for the 8-Way Combiner/Divider 112

5.5.3 Combining Efficiency of the 8-Way Combiner/Divider 118

5.6 Loss from Rampart Antennae Structure on RTDUROID 5880 119

5.6.1 Results Obtained 120

5.7 The Reduction of Loss in Microstrip and Stripline Structures 123

5.7.1 Results Obtained with the Air Substrates 125

5.8 A Low Loss 8-Way Combiner/Divider 131

5.9 Conclusion 135

6. CONCLUSION 137

APPENDIX A: BESSEL FUNCTION TABLES 139

APPENDIX B: TOUCHSTONE/RF - VERSION 1.3 1985 140

APPENDIX C: METHOD EMPLOYED TO SHOW OUTPUT MATCHES WHEN A DIVIDER IS USED AS A COMBINER 144

REFERENCES 147

CHAPTER 1 REVIEW OF MICROWAVE SOLID STATE AMPLIFYING DEVICES

1.1 Introduction

Increasing the output power from field effect transistors (FETs) by enlarging their size or by wire bonding several of them in parallel within a package eventually reach practical and economic limitations. Technically, limitations such as extremely low input impedance occur when a large number of cells are combined in parallel which further leads to matching problems. As the size increases phasing problems at high frequencies occur as well as a higher heat dissipation.

As many current applications require microwave solid state power sources with output powers greater than that available from a single device a need for combining these devices is required. N-way combiners/dividers may be used to achieve this.

This chapter goes onto give a brief overview of the development of the gallium arsenide field effect transistor (GaAs FET) and the silicon bipolar transistor. Emphasis will be placed on FETs and their power handling capabilities in an endeavour to justify the requirement of power combiners/dividers to increase the output power available from solid state amplifiers.

1.2 The Bipolar Transistor - a Brief Review

It took seventeen years from the initial introduction of the bipolar transistor in 1948 until microwave transistors with practical gain and noise figure became available. The first transistors to enter the microwave industry were germanium

transistors. These first appeared in 1965 and were available in the L-band with noise figures of 6dB. Since 1968 rapid progress has been made in obtaining high power capability and low noise performance from silicon bipolar transistors up to X-band.

An indication of the progress made can be seen from the fact that in 1968 the state of the art bipolars had an fmax of 6GHz with a maximum gain of 8dB at 2GHz and an associated noise figure of 6dB[1]. In 1976 bipolars had noise figures in the region of 3.9dB at 8GHz and an associated gain of 3.8dB. Power transistors at this stage could deliver 1W CW with a 6dB power gain at 8GHz. At 2GHz a single transistor chip delivered up to 30W CW output power with 7dB power gain and 32 percent power added efficiency[2]. By 1979 the state of the art bipolars could deliver 60-W CW output with an associated gain of 11dB and a power added efficiency of 46,3 percent at 2GHz[3].

The upper frequency limit of bipolar transistors is determined by the ratio of carrier mobility to emitter length. The electron mobility is determined by the characteristics of doped silicon, so the emitter is the controlling factor. This width is dependent on the state of the art of electron beam photolithography, which today allows geometries in the 0,25

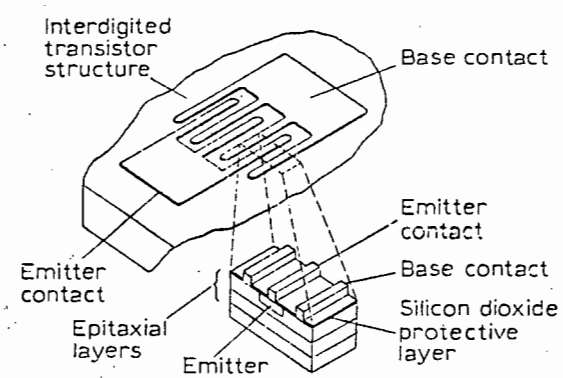

Fig. 1.1 Interdigitated planar transistor structure (from ref 4).

micron range. Figure 1.1 shows a typical interdigitated planar structure of a bipolar transistor. To increase the output power of a single packaged device several cells are connected in parallel into a single microwave package. The direct parallel connection of a large number of cells (greater than 4) requires stringent controls on the uniformity of the cells as there is no isolation between the cells. Any matching circuits used must be identical for each cell if phasing errors are not to occur and if each cell is to be driven equally. Another disadvantage is that the device becomes electrically wide as cells are combined and limitations are reached in trying to maintain equal phasing. Note that these problems also hold when trying to combine individual cells in FETs.

1.3 The Field Effect Transistor

One of the oldest three terminal devices is the field effect transistor (FET) that was proposed in 1952 by William Schokley. Due to technological and fabrication problems it was not until the 1960's that the first viable device appeared.

There are three main types of FET in use. The simplest FET is the JFET which came into use at about the same time as the bipolar transistor. Further technological advances in FET fabrication led to the MOSFET which is also called the insulated-gate FET (IGFET). These devices are manufactured with silicon. Neither of these devices could compete with the silicon bipolar transistor and it was not until the advent of gallium arsenide technology which allowed the development of the MESFET, often called the GaAs FET, that the FET was considered seriously for microwave use.

A GaAs FET is similar to a JFET, except that instead of a diffusion process at the p-n junction, a Schottky barrier contact having a very short storage time is used. In a p-n junction the current is carried by minority carriers, this is not the case for Schottky barriers where the current is carried by the the majority carriers. Whereas minority carriers limit the frequency response of the p-n junction, the Schottky barrier has no such limit, thus making it ideal for use at microwave frequencies.

In the late 1960's the first solid state amplifiers began to replace travelling wave tube amplifiers in the L and S bands. These amplifiers utilised bipolar transistors. However, further TWT replacement stopped after 1972 above 5GHz due to the high cost of bipolar transistors for these frequencies, and because the TWT was superior. Higher frequency solid state amplifiers

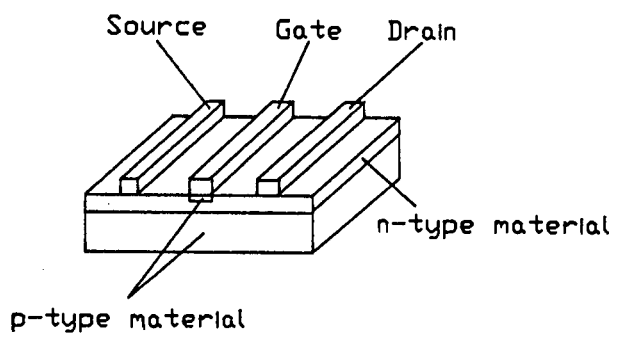

Fig. 1.2 (a) Junction FET (JFET).

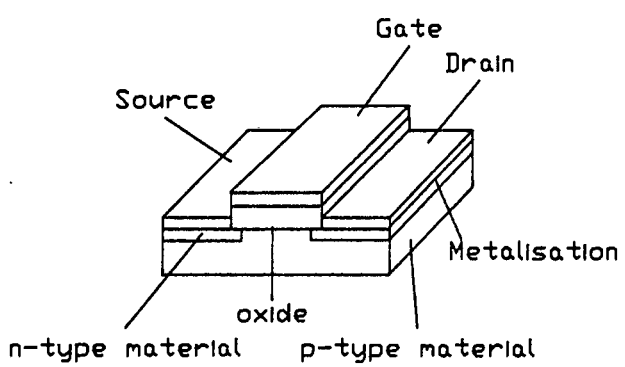

Fig. 1.2 (b) Metal oxide semiconductor FET (MOSFET).

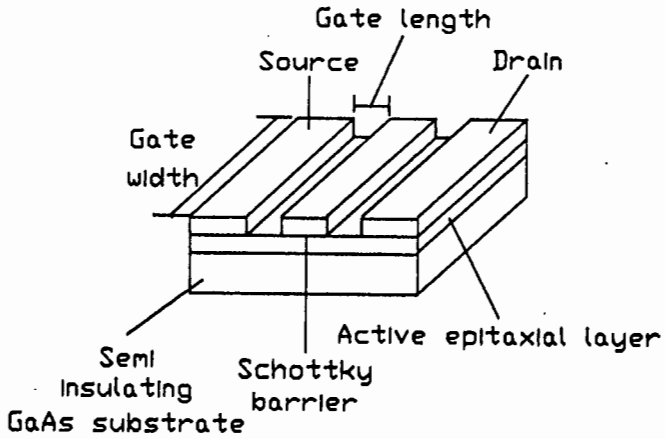

Fig. 1.2 (c) Metal semiconductor FET (GaAs FET or MESFET).

started to make their debut with the commercial availability of the GaAs FET, and now low noise TWTs are being replaced by solid state devices which have improved reliability and better performance.

In mid 1975 the first commercially available X-band (8-12GHz) was introduced. Since the introduction of the GaAS FET, the output power capabilities have increased rapidly as shown in figure 1.3. These figures were the state of the art results as reported by Bell Laboratories[5].

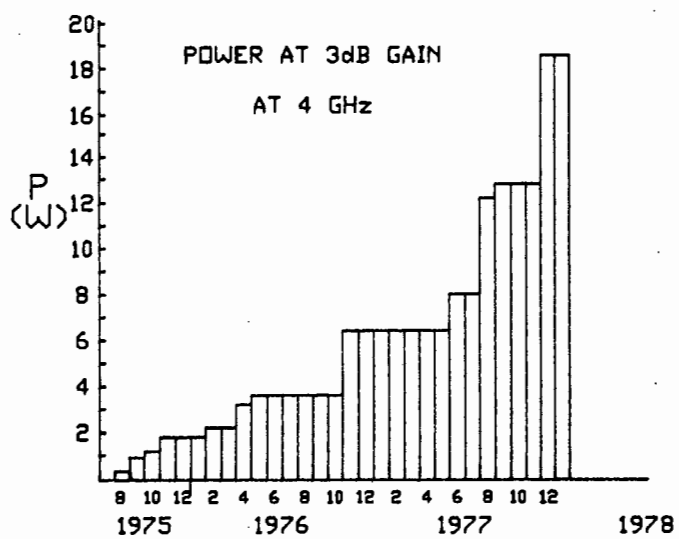

Fig. 1.3 Progress of power GaAs FETs at Bell Laboratories as a function of time.

With the advent of GaAs, a 1μm MESFET was fabricated on GaAs which gave an fmax of 50GHz[2]. These devices had a useful gain up to 18GHz. In 1972 it became apparent that GaAs FETs were capable of very low noise figures and a noise figure of 3,5dB with 6,6dB of gain at 10GHz was reported[2].

The first power GaAs FET was reported in 1973[2]. These devices were of a planar structure as shown in figure 1.4. A MESFET with 20 gates, each 1μm long and 400μm wide operated in parallel and interconnected with a second metallisation layer was designed by Fukuta and other co-workers. This FET exhibited an output power of 1,6W with a power gain of 5dB at 2GHz and a power added efficiency of 21 percent[2].

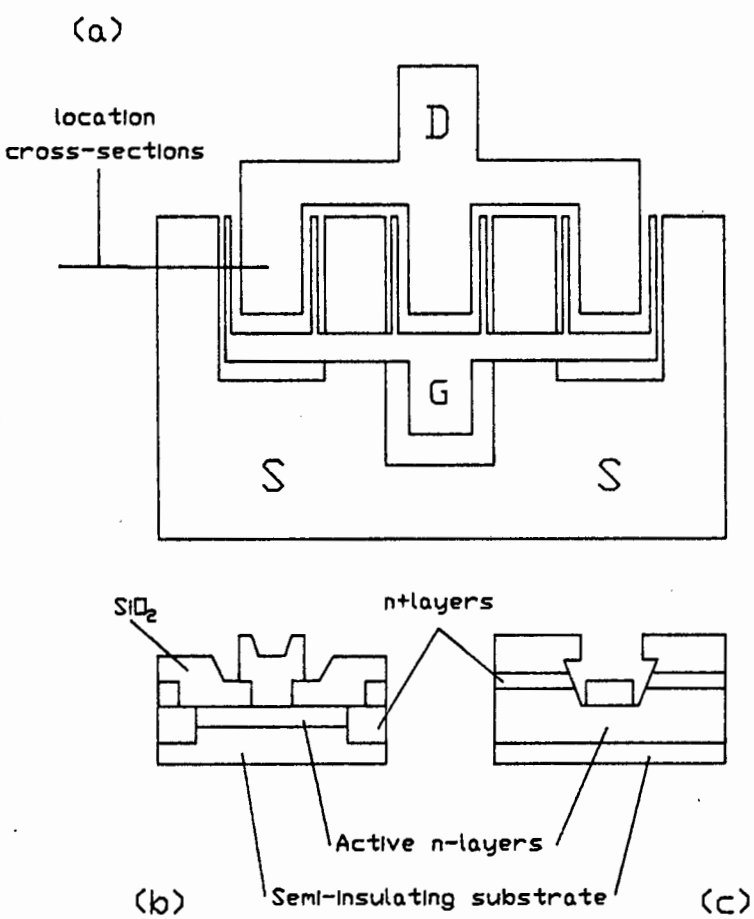

Fig. 1.4 Schematic of the metallisation of a planar power MESFET produced at Fujitsu laboratories.

In 1978 the highest CW power outputs from single GaAs FETs ranged from close to 20W at 4GHz to several watts at 10GHz[6]. The best reported efficiencies at the time ranged from 70 percent at 4GHz to 30 - 40 percent at X-band. The best commercially available devices at that time delivered an output of 5W at 6GHz and 1W at 12GHz[6]. The power outputs and power efficiencies continue to improve, Fujitsu have commercially available devices capable of 39dBm at 7GHz with a power added efficiency of 29 percent, this data comes from their Semiconductor Selector Guide, June 1985. A new method for increasing the total gate width was proposed by B. Turner et al in 1981[7]. Their proposed technique involved the application of a polymide dielectric overlay technology to a GaAs structure. Results with this structure gave an output of 950mW at 8GHz with 4,0dB associated gain. With increased V_{DS} an output of 1017mW was obtained with 4,3dB gain and a power added efficiency of 27 percent.

As FETs continue to develop more and more devices are internally matched and in 1981 Yasuo Mitsui et al[8] reported the development of a 10GHz 10W internally matched flip chip GaAs FET. In their configuration the gate and drain electrodes were connected directly to the lumped matching capacitors using no bond wires. The flip chip technology reduced both parasitics and thermal resistance. Results obtained for their device are shown in figure 1.5.

The latest FETs are the matched field effect transistors (MFETs) as reported by F.M. Magalhaes et al[9] It is a new design approach for microwave integrated amplifier modules. It uses one

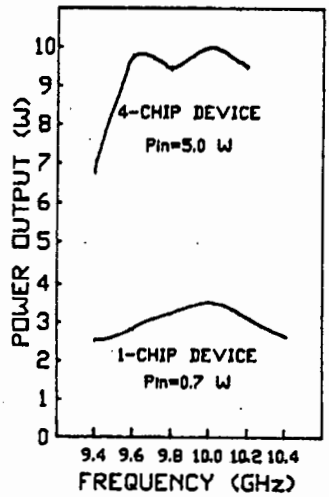

Fig. 1.5 Frequency response of 4-chip and 1-chip devices with internal matching.

or more GaAs FET chips for active elements and has input and output matching and bias circuits fabricated on two additional GaAs chips. It is contained in a hermetically sealed package that may be inserted in to a standard 50ohm transmission line system without external matching or biasing circuitry. Figure 1.6 shows the M-FET layout.

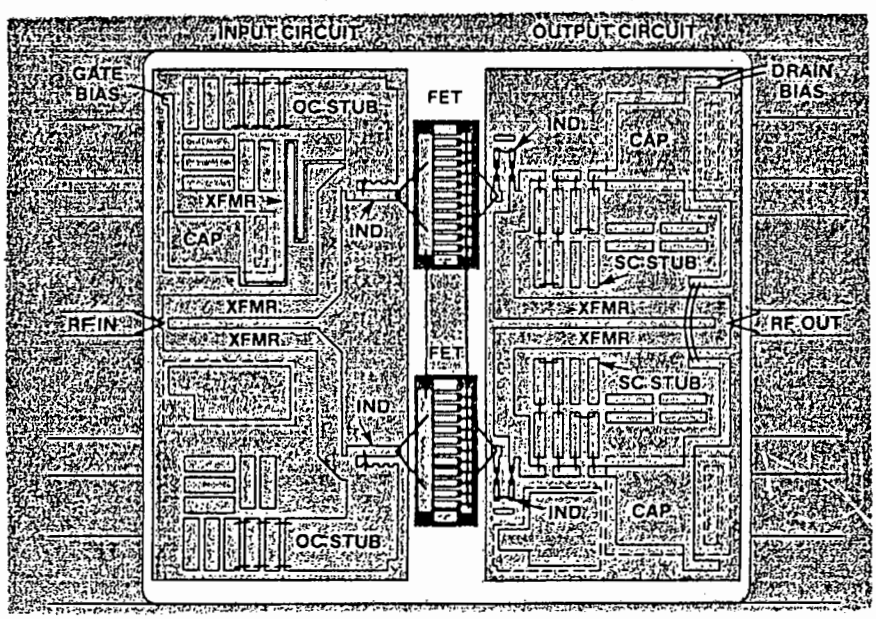

Fig. 1.6 M-FET circuit layout (From ref. 9).

1.4 The GaAs Field Effect Transistor Versus the Silicon Bipolar Transistor

Comparing the GaAs FET with the silicon bipolar transistor it is found that the maximum operating frequency of a GaAs FET is the ratio of gate length to carrier mobility. Although the same photolithography limitations apply to FETs as to bipolars the carrier mobility of GaAs is roughly six times that of silicon and electrons travel with peak velocities up to twice that in silicon[10]. This immediately implies GaAs FETs will predominate at the higher frequencies.

It is possible to use GaAs FETs at the lower limits of the microwave spectrum with expected improvements in noise figures over the best available bipolars. However, at frequencies below 1 or 2 GHz the input impedance becomes very high making impedance matching very difficult. At about 4 to 5 GHz a trade off point is reached and FETs provide unquestionably better performance and are worth the extra cost and design difficulties associated with them. Bipolars are however, competitive at 4GHz and can provide output powers comparable to FETs. In 1981 R. Basset and D. McCombs[11] reported a seven cell bipolar transistor that produced an output of 6W at 4GHz which at that time was unattainable with FETs. Tables 1.1 and 1.2 give a comparison between some commercially available FETs and bipolar transistors. The data are from the Fujitsu Microwave Semiconductors Selector Guide, June 1985.

From the tables it can be seen that high powers are available below 1GHz and below this frequency solid state amplifiers are replacing travelling wave tube amplifiers (TWTAs).

Table 1.1 Comparison between low noise FETs and bipolar transistors.

GaAs FET				Bipolar			
Type No.	Freq (GHz)	Gain (dB)	NF (dB)	Type No.	Freq (GHz)	MAG (dB)	NF (dB)
				FJ201	2,0	10,0	4,0
FSC10	4,0	13,0	0,6	FJ451	4,0	10,5	4,0
FSC11	4,0	13,0	1,0	FJ401	4,0	10,5	3,5
FSX51	8,0	9,5	2,5				

Table 1.2 Comparison between power FETs and bipolar transistors.

GaAs FET				Bipolar			
Type No.	Freq (GHz)	G_{1dB} (dB)	P_{1dB} (W)	Type No.	Freq (GHz)	Gain (dB)	Power (W)
				FJ0880-28	0,86	5,0	80,0
FLL10ME	2,3	12,0	0,7	FJ2301B-24	2,3	10,5	1,1
FLL100	2,3	8,0	7,9	FJ2306B-24	2,3	8,0	6,0
FLC253MH8	8,5	8,0	2,5				
FLK202MH-14	10,0	6,0	1,8				

1.5 Techniques Used to Increase the Output Power of FETs

The maximum output available from power FETs is limited by several factors. Firstly, there is a limit to the size of the device. If the distribution of voltages and currents is to be kept uniform, the transistor cell dimensions must be kept to a fraction of the operating wavelength. The gate width cannot be made too long either, as this must be less than about a tenth of a wavelength. Further, the longer the gate width the lower the impedance, and the more difficult it becomes to match the device for wideband applications. Design of power FETs now incorporate

matching networks that are placed as close to the transistor cell as possible.

Another limiting factor as regards the output power of FETs is the maximum allowable temperature rise of the cell. The mean time before failure (MTBF) of a GaAs FET generally decreases exponentially with an increase in temperature[6]. It is therefore necessary to minimise the thermal resistance of the devices since most power devices have to dissipate tens of watts of DC power. One method that is used to reduce thermal resistance is a flip chip technology. This involves plating metal posts on the sources, gates and drains of the FETs and then flip chip the device on to berrylia carriers for example.

In the majority of FETs the three terminals lie on the same plane on the surface of the die. This creates a problem for manufacturers because they must be able to make contact with multiple source contacts, and the sources must be interconnected while minimising inductance, shunt capacitance and dielectric loss. The source contacts can dissipate heat and hence the source connections should also have minimum thermal resistance to the heat sink.

In order to achieve maximum power, various structures have been employed in the design and fabrication of GaAs FETs and various goals have been striven for. These are:-

a) to obtain the maximum gate width for the frequency of interest
b) to minimise electrical parasitics
c) to reduce thermal impedance

d) to achieve a device capable of sustaining high drain source potential

e) to achieve a materials technology which gives consistent and reproducible effects.

One method to increase the gate width simply involves paralleling a large number of unit cells by wire bonding. This method bonds the individual source pads together with gold wire, thus preventing dielectric crossover loss and providing fairly low conductor loss. Devices as large as 9,6mm total gate width for operation at 9GHz and 24mm gate width for operation at 4GHz have been successfully assembled this way. The multiple bond approach allows a simple processing technology but makes device assembly more difficult, highly labour intensive and can have increased parasitics, namely inductance due to the wire bonds.

Another approach uses a dielectric insulator deposited on the chip surface and interconnects the sources with a deposited metal overlay. A device produced by Fujitsu employs gate over source cross-overs with SiO_2 as the dielectric. The main advantage of this approach is that it makes the most efficient use of real estate and minimises the number of bonds required to assemble a large device. The processing is more complex, although less labour intensive than wire bonding, and additional parasitics are involved in the crossover as well as increased dielectric loss.

Another method providing very low thermal resistance involves a flip chip technique which provides large, plated up source contacts on the FET die and the die inversion so the plated up areas make contact with a copper heat sink. Not many devices

have been made this way, mainly because a great deal of care in mounting is required and quality control is a difficulty.

Interconnecting via air bridges is a newer method. In 1978 the method was still in the development stage. Another approach uses holes etched through the substrate, plated up and used to interconnect the sources from the backside. This can also result in very low thermal resistances. Refer to figures 1.7, 1.8, 1.9, 1.10 and 1.11.

For given device parameters, the maximum available gain (MAG) falls off at 6dB per octave increase in frequency. For this reason minimisation of electrical parasitic effects is particularly important in the design of higher frequency FETs to prevent the gain from becoming unacceptably low.

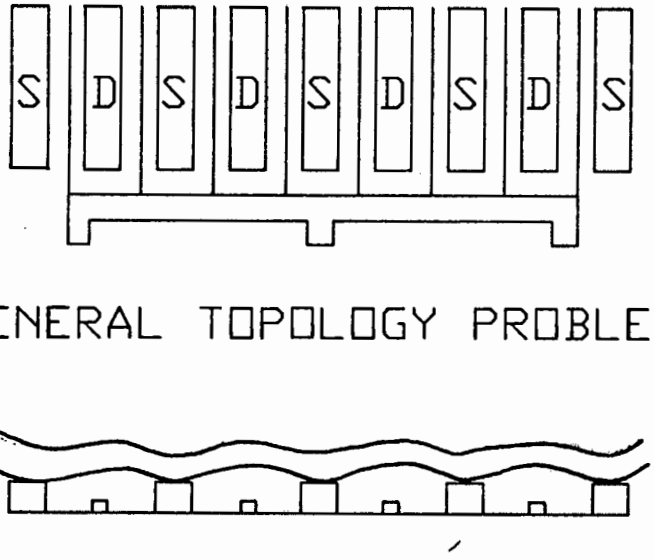

Fig. 1.7 Wire bonding of the sources, process is labour intensive.

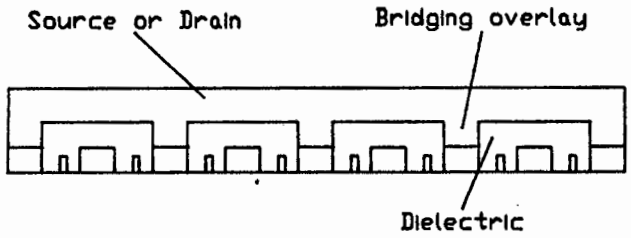

Fig. 1.8 Fujitsu bonding method includes dielectric insulator with metal overlay.

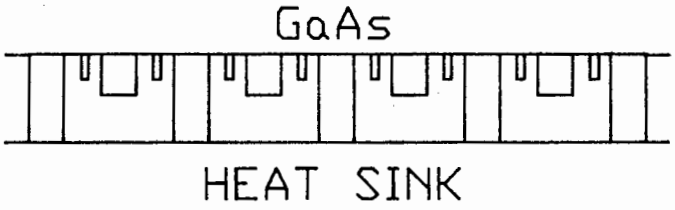

Fig. 1.9 Flip chip technique - requires precise mounting, low source inductance.

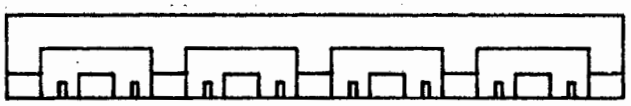

Fig. 1.10 Air bridge to minimise loss and shunt capacitance.

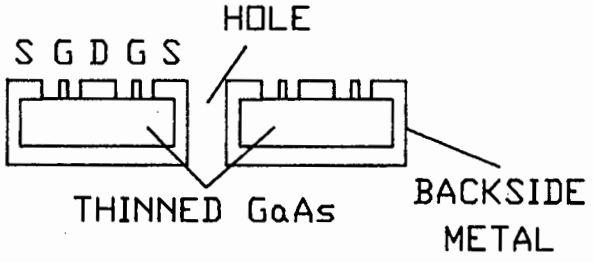

Fig. 1.11 Through hole plating limits thermal resistance and assembly labour.

There are a large number of parasitic effects that must be considered in power FET design. The most significant parasitic effect is the source lead inductance. Minimisation of this inductance is much more difficult for power FETs than for small signal devices. Most power FET designs involve the combination of several cells and each cell has several parallel gate fingers. The cells must be combined either during processing in which case they are integrated on the chip or during the bonding operation. In principle, cells can be added until the impedance becomes too low for it to be matched in the microwave circuit. If the source lead inductance and resistance are neglected it can be shown that the maximum available gain (MAG) is unchanged as cells are combined. Unless special care is taken the MAG will, however, be reduced because of the source lead inductance which is not reduced proportionally as cells are added. The combining efficiency is defined as

$$\eta = \left. \frac{P_{out}\ (n\ cells)}{nP_{out}\ (1\ cell)} \right|_{\text{constant gain}} \qquad 1.1$$

A method of reducing source inductance is shown in figure 1.12 Here the four single-cell chips are mounted side by side with the sources independently grounded. This effectively reduces the source lead inductance which in turn then has a lesser effect on the cell combination.

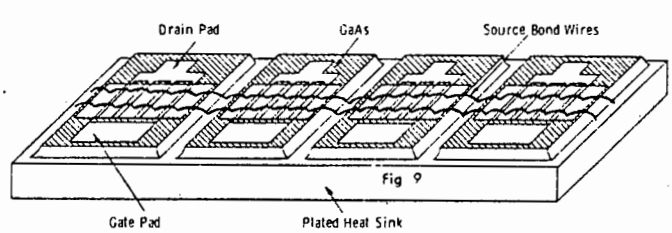

Fig. 1.12 A Texas instruments plated heat sink FET (from ref. 5).

Another method that is used to reduce source inductance is shown in figure 1.13. This shows the cross section and cell layout of a FET with low inductance via connections through the substrate. This device has a plated heatsink.

There have been several other approaches to minimise the source lead inductance in the development of GaAs power FETs. One of the most promising is flip chip mounting. This is not widely used as already mentioned because of the difficulty of implementation. Y. Mitsui et al[12] developed a flip chip device in 1979. The fabrication procedure used is similar to that used for conventional MESFETs.

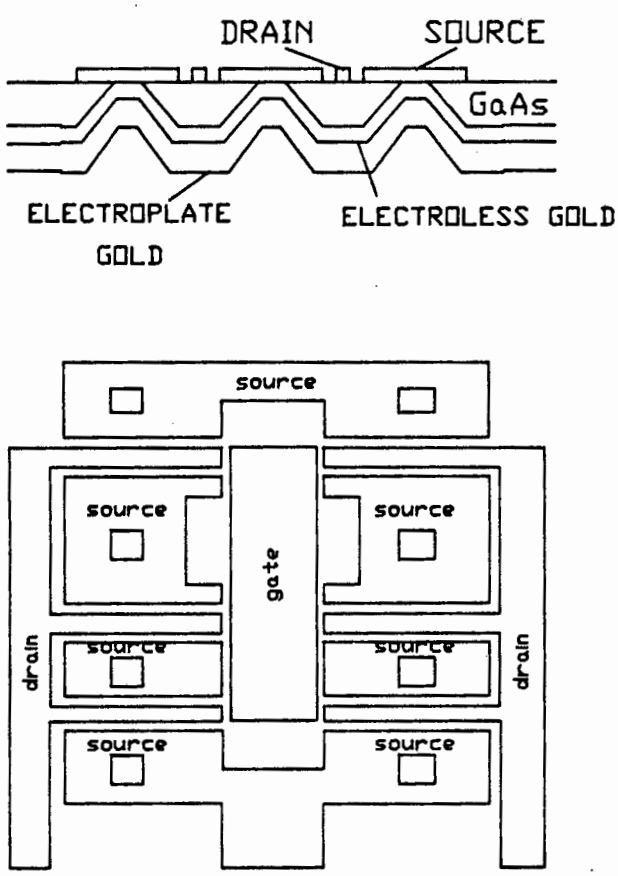

Fig. 1.13 Bell Laboratories FET (a) cross-section (b) top view.

The source and drain metallisations consisted of multiple layers

of Au, Ni and alloyed Au-Ge films. Gold was electroplated on to the source. The metal layers were formed between the gold post and the aluminium gate pad which prevented Al-Au interaction. The chip was then turned over and all the metal posts connected directly to the corresponding bonding area in the package by thermo compression bonding. Since the source electrodes were bonded directly to a gold plated copper heatsink, the source lead inductances were greatly reduced as was the thermal resistance. The results obtained are shown in table 1.3.

Table 1.3 Performance of a flip chip mounted FET (from ref. 12).

FREQUENCY (GHz)	POWER (P1dB) Watts	POWER (Psat) Watts	LINEAR POWER GAIN (dB)	η (%)	TOTAL GATE WIDTH (m)
10	4,5	6,0	5,0	17	9600
12	3,4	4,1	4,0	16	7200
12	2,5	2,8	5,8	19	4800
12	1,0	1,3	6,9	27	2400
13	1,2	1,5	6,0	17	2400
15	1,9	2,5	4,8	12	4800

1.6 Conclusion

In order to increase the output power capabilities of solid state amplifiers any further, another approach will have to be employed. This approach takes the form of power combiners/dividers which combine the outputs of several devices at the circuit level. These passive devices will be introduced in the next chapter.

CHAPTER 2 COMBINING ON THE CIRCUIT LEVEL

2.1 Introduction

As mentioned in the previous chapter increasing the power handling capabilities of solid state devices by continuing to increase their size eventually runs into various problems such as concentrated heat dissipation, parasitics and impedance matching. This then creates the need for power combining at the circuit level if solid state amplification with performance comparable to travelling wave tube amplifiers is to be achieved.

In order to combine n amplifiers the input power is divided n ways and is then fed to n amplifiers. The n amplifier outputs are combined using an n-way combiner, which is a n-way divider used in "reverse", that is the combiner inputs are the divider outputs.

One advantage that the power combining of several solid state devices has over a single TWTA is graceful degradation of the combined amplifier. In a power combiner/divider the match and isolation provided by them are essential for graceful degradation of the combined amplifier in the event that one or more of its component amplifiers suffer arbitary modes of failure because, in that case, such failures would not affect the impedances presented to the remaining amplifiers. In other words there is no complete loss of output power, which is usually the case with a TWTA, where hard failure is the norm. If m out of n amplifiers fail it can be shown that the output of the combined amplifier reduces by

$$-20\log(1-\frac{m}{n})\ \text{dB} \qquad 2.1$$

This assumes of course that the isolation between each device is infinite.

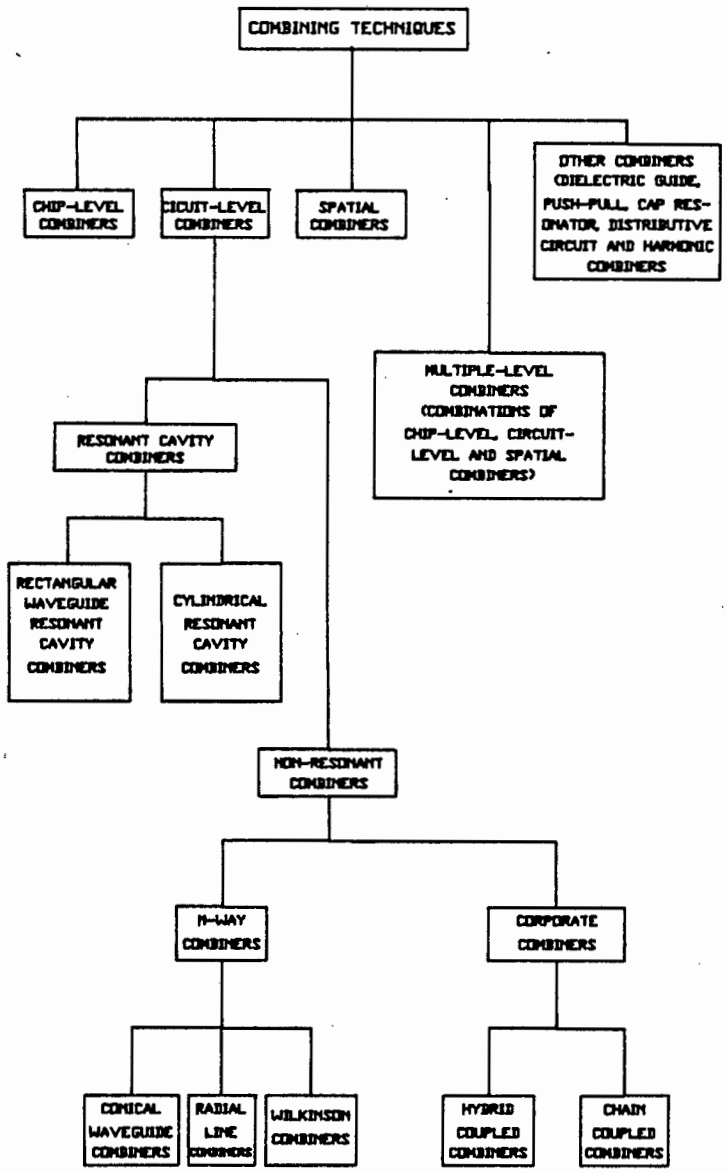

Fig. 2.1 Different types of combining techniques that are available.

Combining approaches can be separated into two general categories, those which combine the output of n devices in a single step and those which do not. The former are called n-way combiners. The latter type of combiner is simpler and more widely used, although it must be stressed that it does not

provide the most efficient technique, which is important for the combination of high power devices. Fig 2.1 shows the different types of combining techniques. As mentioned earlier, circuit level combining will be dealt with here.

2.2 Chain and Tree Combining Structures

Figure 2.2 Shows a method of combining power using two way dividers. This is usually called a corporate (or tree) structure.

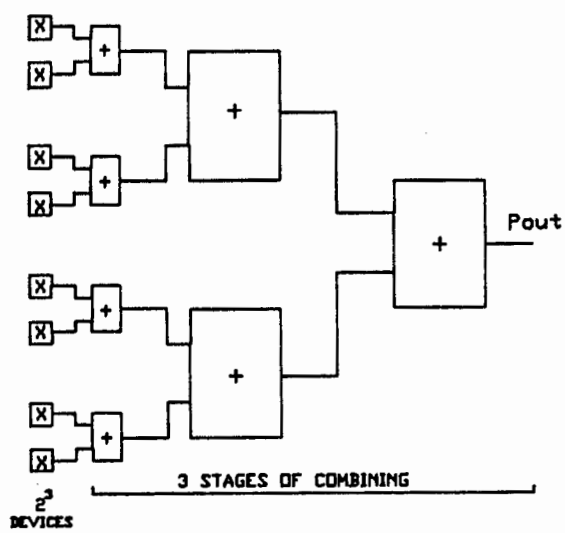

Fig 2.2 A corporate structure for combining power.

In theory, any amount of power could be obtained this way if each of the two way dividers were lossless. However, in practice each of the combiners/dividers used has an associated loss, which means that efficient combining of power is limited, especially as the number of two way dividers used increases. Another limiting factor, when using this approach is the fact that only 2^N amplifiers may be combined where N is the number of combining stage's used.

The combining efficiency of the corporate structure is given as

$$\text{Efficiency} = [\text{antilog}(\frac{-(N \times \text{loss per divider})}{10})] \times 100\% \qquad 2.2$$

Examples of different two way combiners/dividers that may be used in a corporate structure are shown in figure 2.3.

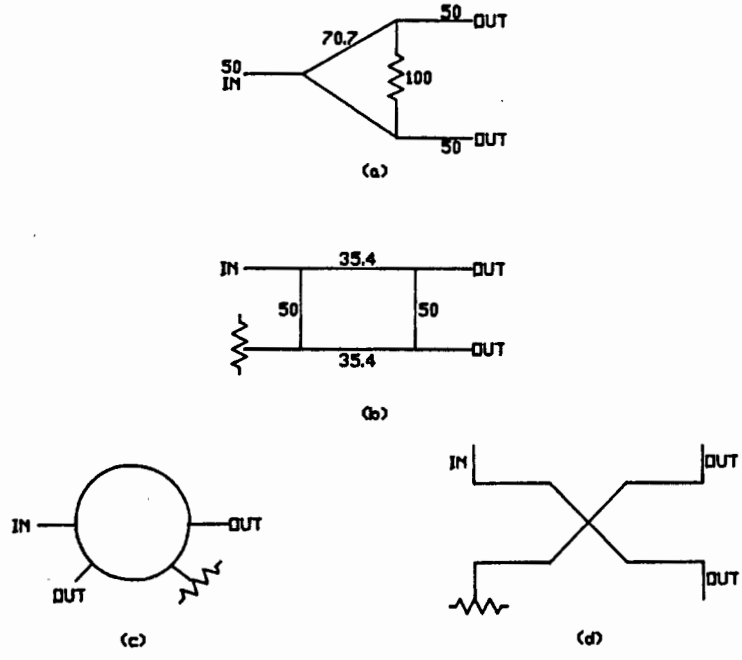

Fig. 2.3 Common forms of 2-way power combiners and couplers that can be used in corporate structures. (a) 2-way Wilkinson (b) branch arm coupler (c) rat race (d) coupled line directional coupler (eg. Lange coupler).

The Wilkinson combiner/divider will be discussed in more detail in chapter 4, as this type of combiner is a classic and many of the n-way combiners/dividers are based upon it.

The branch arm coupler of figure 2.3 (b) divides the power to give two outputs that are in quadrature. This implies that some thought has to be used in the design of a corporate structure so that all outputs are in phase. The rat race coupler, shown in fig 2.3 (c), also has ouputs that are not in phase. It is the basis of the reversed-phase hybrid ring which has a wide bandwidth

approaching an octive or more. Once again they are not well suited for low loss n-way combiners. The coupled line directional coupler, for example, the Lange coupler, also has outputs that are in quadrature. This coupler has an octive bandwidth capability. However, construction of these couplers is difficult and requires a very precise etching process as well as bonding facilities. As none of these types of power combiner/divider lend themselves to the design of high efficiency combiners, which is the topic of this dissertation, they will not be covered in any further detail; they are covered widely in the literature[13-19].

The chain type of combiner is shown in figure 2.4. In this type of combiner each successive stage or coupler adds 1/N of the output power to the output. The coupling for a particular stage therefore depends on the number of that stage. The necessary coupling of the N^{th} stage is thus 10logN in dB's, assuming that there is no loss. The chain combining approach is non binary, and in principle, any number could be combined. Losses in the couplers reduce the combining efficiency. It is also difficult to build couplers in microstrip with the high coupling coefficient required as the number of stages increases. The combining efficiency of this structure is lower than for the corporate structure for the same number of devices combined[20].

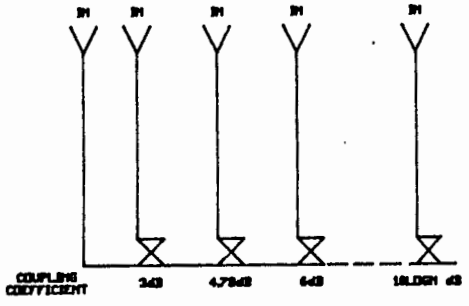

Fig. 2.4 A chain combining structure.

2.3 N-way Combining Structures

N-way combiners are those combiners that combine n devices directly in one step without having to proceed through several combining stages. This immediately indicates that a higher combining efficiency should be possible with these type of combiners than with either the corporate or chain structures. The n-way combiners/dividers can be divided into two categories, resonant cavity and non-resonant structures.

2.3.1 Resonant Cavity Combining Structures

In general these type of combiners sum the output powers from a number of devices by coupling their outputs to a single resonator. They are generally low loss because they are a waveguide structure, but have very narrow bandwiths due to the resonant cavity. Methods of broadening the bandwidth of these structures have been investigated[21-23].

There are basically two types of resonant cavity structures that can be used as combiners. These are a rectangular waveguide structure and a cylindrical resonant cavity combiner. The waveguide version was described by Kurokawa and Magalhaes in 1971, fig 2.5 shows the layout[20]. Using this approach the power from twelve IMPATT diodes were combined. To properly couple to the waveguide cavity, the devices must be located at the magnetic field maxima of the cavity, and therefore the diode pairs in this case, must be spaced one half wavelength, $\frac{\lambda g}{2}$, apart along the waveguide. This form of combiner may be adapted to combine the power of FETs. The structure would essentially be

planar allowing effective heat dissipation, a problem associated with cylindrical resonant cavities. An idea involving rectangular waveguide as a combiner/divider is given in chapter 3.

The more successful resonant combining technique, and hence more widely used, is the cavity combiner shown in figure 2.6. The combiner shown in the figure combines the output power of 12 diodes. These are placed around the circular periphery of a cylindrical cavity resonant in a $TM_{0\,m\,0}$ mode. The more common

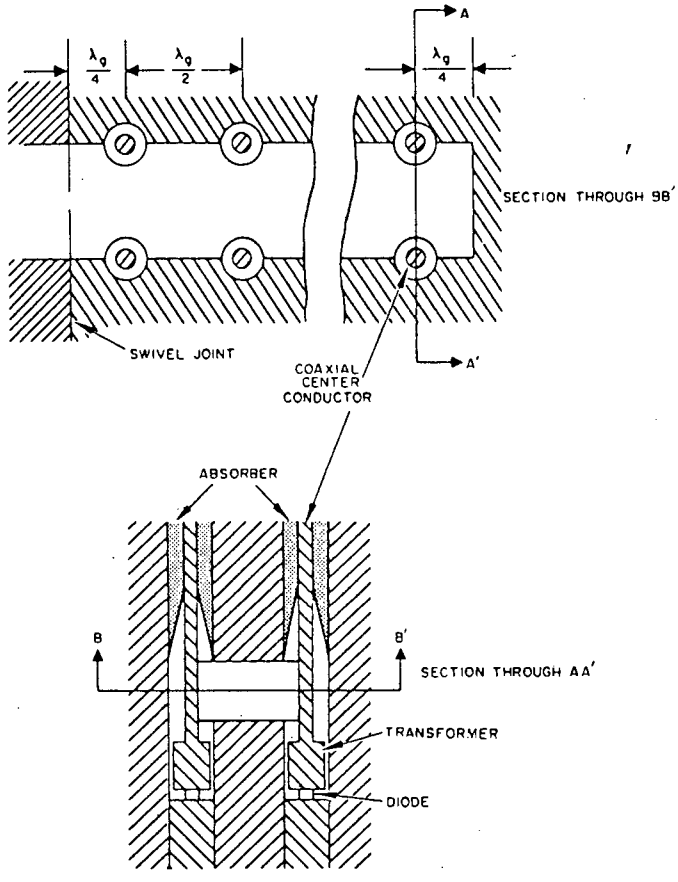

Fig. 2.5 Two cross-sections of the Kurokawa waveguide combiner.

mode used is the $TM_{0\,1\,0}$ mode. These modes have a maximum of the electric field at the central axis of the combiner, and the output is obtained from the combiner by placing a probe at this

point. This resonant cavity may be used to combine several FETs as shown by Y. Tokumitsu et al[21]. A further discussion of this combiner will will be given in chapter 3.

An important feature of the cylindrical cavity is that the cavity fields are azimuthally symmetric, and thus there is no minimum spacing between probes. However, there are practical limits, such as the size of the devices to be combined.

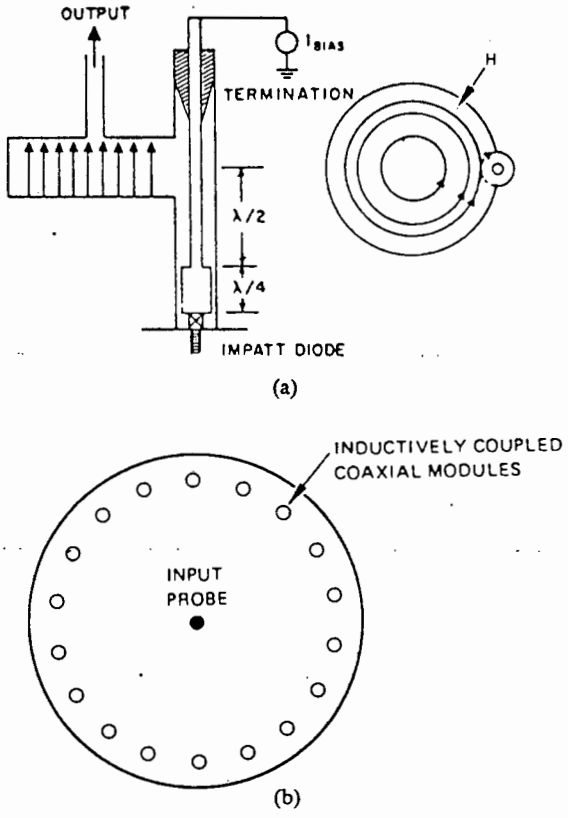

Fig. 2.6 Cylindrical resonant cavity combiner. (a) A single coaxial module illustrating magnetic coupling to TM_{010} cavity. (b) Top view of resonant cavity showing module portions around pheriphery[20].

The combining efficiency of these structures is very high. The combining efficiency has been demonstrated to increase with the number of devices combined, especially diodes[20].

2.3.2 Non-resonant Combining Structures

A large number of non-resonant combiner/divider structures have been proposed and because of their non-resonant structure allow a fairly wide bandwidth.

The simplest of these is the two way Wilkinson, which is also one of the oldest combiners. This classic combiner will be discussed in chapter 4. The Wilkinson may be extended to an n-way structure however, it no longer remains planar due to the placing of the isolation resistors.

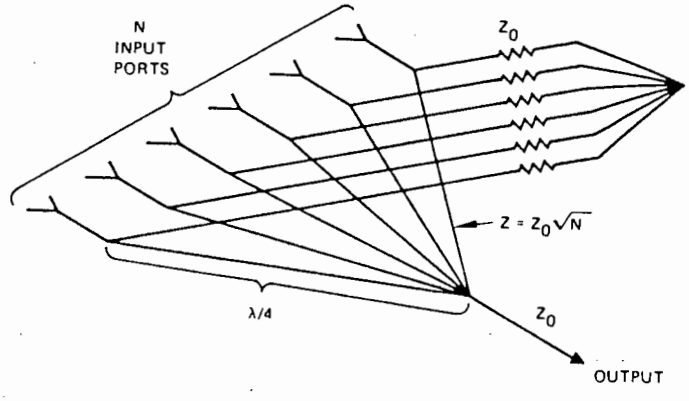

Fig. 2.7 Wilkinson N-way combiner.

A majority of the planar combiners are generalisations of the Wilkinson combiner. One such combiner is the n-way combiner proposed by Z. Galani and S.J. Temple[24]. Figure 2.8 shows the principle involved. This type of combiner/divider will be discussed in detail in chapter 5.

An example of a radial line combiner which has been developed for

use as a 12-way transistor combiner for X-band is shown in figure 2.9. Although the essential part of the radial hybrid is planar, a combined amplifier using two such hybrids would be non-planar.

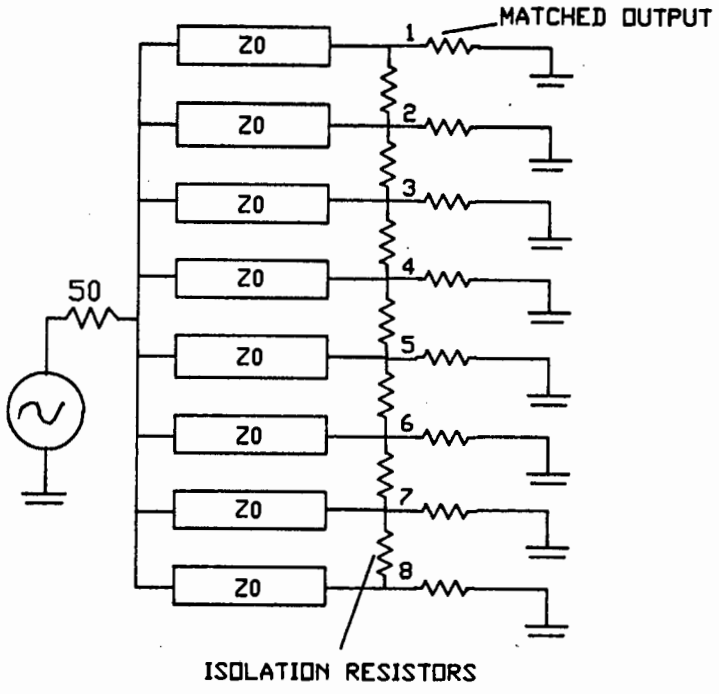

Fig. 2.8 Planar n-way combiner/divider.

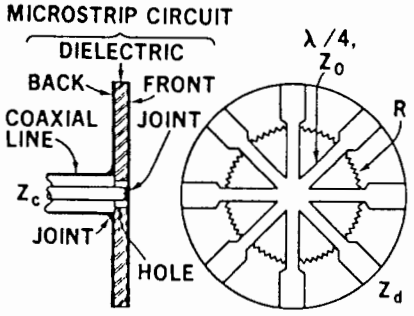

Fig 2.9 The radial n-way power combiner/divider.

The radial transmission line is accomplished on microstrip. Coaxial transmission lines with abrupt stepped transitions to the microstrip radial lines are used for input and output. The combiner has demonstrated a combining efficiency of 87,4 percent

and 1dB bandwidth of 20 percent at 8,5GHz operating as an amplifier[20].

It must be noted at this stage that there are both planar and non planar versions of n-way combiners/dividers. A planar version is preferred due to the better heat dissipation that can be obtained than from a radial type of combiner. Other types of planar combiners available are the travelling wave combiner/divider which was proposed by A. Bert and D. Kaminsky in 1980[25]. This is not essentially an n-way combiner/divider but is closer to a corporate structure. N. Nagai et al[26] proposed a new n-way hybrid power divider in 1977 and is in some ways similar to that proposed by Gallani. These types of combiner are just mentioned for completeness.

2.4 Conclusion

In this chapter various types of power combining techniques have been briefly discussed. As a generality the non-planar versions are usually of a radial structure and as such are more efficient than their planar counterparts. However they do have the problem of heat dissipation which is significant when high power outputs are required.

The aim of this dissertation is therefore to investigate various types of combiner/divider in an effort to design an efficient planar combiner that can compete with the cylindrical resonant combiner/divider that until now has proved to be the most efficient and practical.

CHAPTER 3 RESONANT CAVITY COMBINERS

3.1 Introduction

In general, a cavity resonator is a metallic enclosure that confines electromagnetic energy. A given resonator has an infinite number of resonant modes, and each mode corresponds to a definite resonant frequency. When the frequency of an impressed signal is equal to a resonant frequency, a maximum amplitude of the standing wave occurs, and the peak energies stored in the electric and magnetic fields are equal. The mode with the lowest resonant frequency is known as the dominant mode.

As previously stated, the key to high output powers from solid state amplifiers is efficient power combiners. One such combiner is the resonant cavity combiner. The TM_{0m0} mode is suitable for use as the resonant combiner/divider as it is easy to separate the associated mode from other undesired modes. It is also easy to obtain multiports because it has a constant electromagnetic field in the azimuthal direction.

Disadvantages with this type of combiner are:

(a) the narrow bandwidth, although there are ways of overcoming this problem.

(b) the non-planar structure as far as the cylindrical cavity combiner is concerned; this causes heat dissipation problems for the combined amplifier because of the cylindrical structure.

This chapter deals with the design of two types of resonant combiners. Practical results are given and broadbanding techniques are discussed for the cylindrical cavity combiner.

3.1.1 Measurement Equipment

All experimental measurements were taken with the HP 8410C network analyser. This apparatus is controlled by an HP 85 computer that uses an accuracy enhancement package.

3.2 The Cylindrical Resonant Cavity Combiner/Divider

A circular cavity resonator is a circular waveguide with two ends closed by a metal wall; refer to figure 3.1

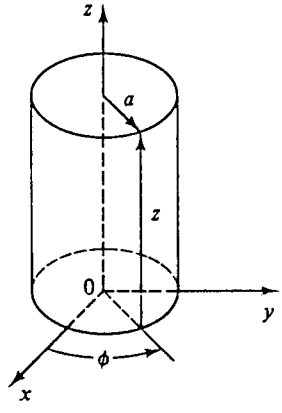

Fig. 3.1 Co-ordinates of a circular resonator

The electromagnetic field inside the cavity should satisfy Maxwell's equations, subject to the boundary conditions that the electric field tangential to and the magnetic field normal to the metal walls must vanish. These conditions are met if:

$$H_z = H_{0z} J_n\left[\frac{X'_{np} r}{a}\right] \cos(n\phi) \sin\left[\frac{q\pi z}{d}\right] \qquad TE_{npq} \qquad 3.1$$

where n = 0, 1, 2, 3... is the number of the periodicity in the ϕ direction

p = 1, 2, 3... is the number of zeros of the field in the radial direction

q = 1, 2, 3, 4... is the number of half wavelengths in the

axial direction

J_n = Bessell's function of the first kind

H_{oz} = The amplitude of the magnetic field

and

$$E_z = E_{oz} J_n\left[\frac{X_{np} r}{a}\right] \cos(n\phi) \cos\left[\frac{q\pi z}{d}\right] \qquad TM_{npq} \qquad 3.2$$

where n = 0, 1, 2, 3...

p = 1, 2, 3, 4...

q = 0, 1, 2, 3...

E_{oz} = the amplitude of the electric field.

The wave number k is given as $k = w\sqrt{\mu\varepsilon}$. The resonant frequencies for TE and TM modes are

$$f_r = \frac{1}{2\pi\sqrt{\mu\varepsilon}} \sqrt{\left[\frac{X'_{np}}{a}\right]^2 + \left[\frac{q}{d}\right]^2} \qquad (TE) \qquad 3.3a$$

$$f_r = \frac{1}{2\pi\sqrt{\mu\varepsilon}} \sqrt{\left[\frac{X_{np}}{a}\right]^2 + \left[\frac{q}{d}\right]^2} \qquad (TM) \qquad 3.3b$$

Also $k = X'_{np}$ for the TE mode

$k = X_{np}$ for the TM mode 3.4

For cavities where 2a>d the dominant mode is the TM_{010} mode and for d>2a the TE_{111} mode is dominant.

For the design of the combiner the mode of interest is the TM_{npq} mode, and if other undesirable modes are to be supressed it is safer to consider the TM_{010} mode. This means that n = 0, p = 1 and q = 0. This then leaves the following

$$E_z = E_{oz} J_0\left[\frac{X_{01} r}{a}\right] \qquad 3.5a$$

$$f_r = \frac{1}{2\pi\sqrt{\mu\varepsilon}}\left[\frac{X_{01}}{a}\right] \qquad 3.5b$$

To find the resonant frequency let r = a, as at this point the electric field must be zero, which in turn means that $J_0(X_{01})=0$. For this to be the case $X_{01}=2,405$ from Bessel function tables, given in appendix A. The radius of the resonant cavity using equation 3.5b can now be determined. For a centre frequency of 4GHz the radius, a, turns out to be 28,71mm; in other words a diameter of 57,42mm.

The required diameter for the cavity has therefore been determined. The depth of the cavity must be less than 57,42mm if the TM_{010} mode is to be dominant. Before deciding on the other dimensions and the positioning of the probes, various points must be considered. Firstly figure 3.2 gives the basic cross-section of the design, the dimensions of which have to now be determined.

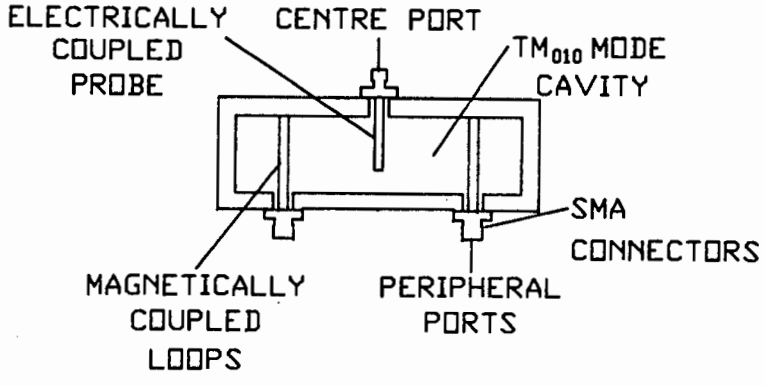

Fig. 3.2 Cross-section of the circular resonant cavity combiner.

The unloaded Q, Q_0 for a cylindrical cavity operating in the dominant mode is given by equation 3.6.

$$Q_0 = \frac{\eta}{R_s} * \frac{X_{01}}{2\left[\frac{a}{h}+1\right]} \qquad 3.6$$

Where η = the intrisic impedance, 377 ohms

R_s = surface resistivity

a = radius of the cavity

h = depth of the cavity.

Equation 3.6 is quoted as being 40 to 200 percent accurate[27]. The reason for this is the surface roughness of the cylindrical walls. The surface roughness effects the surface resistivity and careful measurements of this parameter must be made if accurate determination of R_s is required.

As Q_0 cannot be determined practically, a more informative Q is the external Q, Q_E, which is given by

$$Q_E = \frac{Q_0}{\beta} \qquad 3.7$$

where β is the coupling coefficient. From equation 3.7 it can be seen that the external Q, Q_E, decreases with an increase in the coupling coefficient. As Q_0 depends on the cavity only, the coupling coefficient is an important factor in the resulting Q_E. The coupling coefficient may be determined from

$$\beta = \frac{2Q_0 h \eta \lambda_0}{Z_0} \left[\frac{J_0\left[\frac{X_{01} r}{a}\right]}{2\pi a J_1[X_{01}]}\right]^2 \qquad 3.8$$

where λ_0 is the wavelength at the resonant frequency.

The self inductance of the coupling (outer probes) may be obtained by considering the cavity as an outer conductor of an eccentric transmission line, as depicted in figure 3.3.

$$L_s = \frac{Z_{oe}}{C} * h = \frac{Z_{oe}}{\omega} \tan\left[\frac{X_{01}}{a}\right] \qquad 3.9a$$

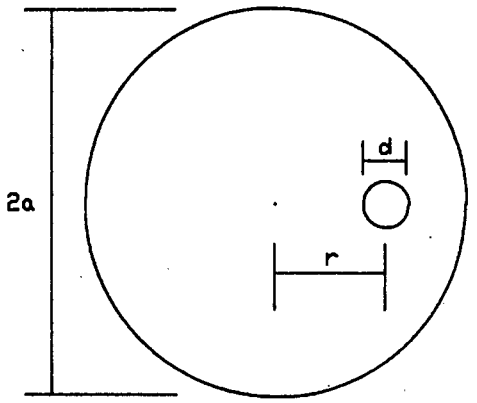

Fig. 3.3 Eccentric transmission line.

where L_e is the self inductance of the outer probe

and $$Z_{oe} = \frac{60}{\sqrt{\varepsilon_r}} \cosh^{-1}\left[\frac{1}{2}\left[\frac{4a^2+d^2-4r^2}{2ad}\right]\right] \qquad 3.9b$$

This self inductance modifies the coupling to

$$\beta_1 = \frac{\beta}{1+\left[\frac{\omega L_e}{Z_0}\right]^2} \qquad 3.10$$

Equations 3.6 to 3.10 are standard equations that have been used by various authors[20,27,28]. From 3.8 it is seen that for a high β, Q_0 has to be high. However, if Q_0 is high, it also means that Q_{ext} becomes high, and ideally a low Q_{ext} is required for a higher bandwidth. Y. Tokumitsu et al[20], discovered that the lower the depth of the cavity, the lower Q_E. As a result, it was decided to make the depth of the cavity, h, 10mm.

Another point which effects the coupling coefficient is the positioning of the probes. For a higher coupling coefficient, that is a broader bandwidth, the probes must be placed as close

to the centre as possible where the maximum coupling will occur. This is at r = 0, as can be seen from equation 3.8. In the case of a TM_{010} structure the coupling will steadily increase towards the centre of the cavity, however, this is not true if other modes are considered, because there are points where the electrical field is zero. This may be seen from equations 3.2 to 3.4.

The positioning of the probes is controlled by the physical size of the SMA connectors used. The size of the connectors, 12,5mm square, imply that the probes have to be placed on a radius of 22,5mm or greater for an 8-way combiner. The diameter of the probes should ideally be as large as possible[20], however, again this is determined by the connectors used, in this case SMA, resulting in 3mm diameter probes. The final dimensions of the cavity were

$$2a = 57,4\text{mm}$$

$$h = 10\text{mm}$$

$$d = 3\text{mm}$$

Figure 3.4 shows a photograph of the 8-way TM_{010} mode combiner/divider.

The depth of the central probe, the output when used as a combiner, was determined experimentally. That is, its depth was adjusted by small amounts until the match was optimum. Note that the periphery probes are placed so as to form magnetic loops, refer to figure 3.2.

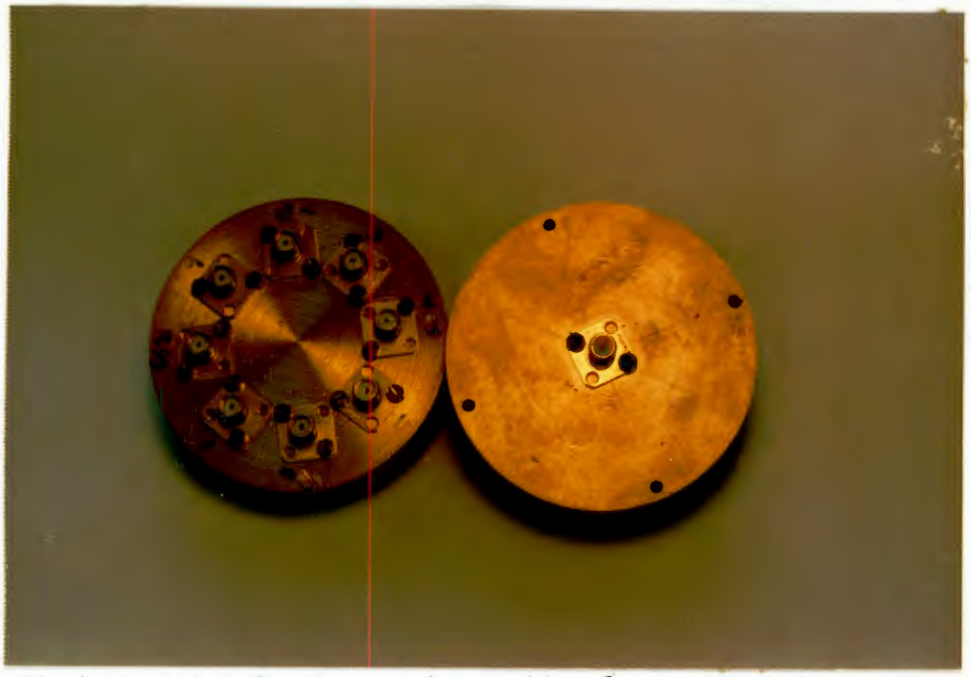

Fig. 3.4 Photograph of resonant cavity 8-way combiner/divider.

3.2.1 Results and Discussion

In the following discussion the resonant cavity will be considered as a divider unless otherwise stipulated. This means that the centre port is the input and is numbered port 1. The output ports are numbered 2 to 9.

The input match was adjusted by altering the centre probe depth with all other ports terminated in 50 ohms. The resulting match gave a return loss of better than 40dB. This occurred at a centre frequency of 4,27GHz as shown in figure 3.5.

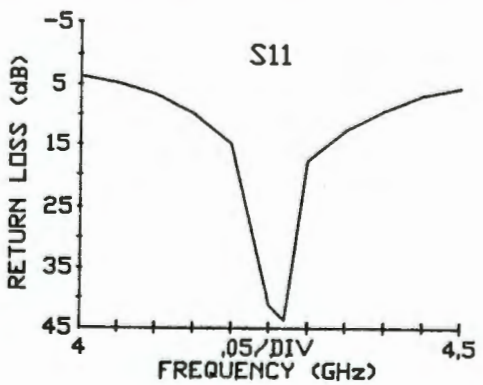

Fig. 3.5 Input match versus frequency.

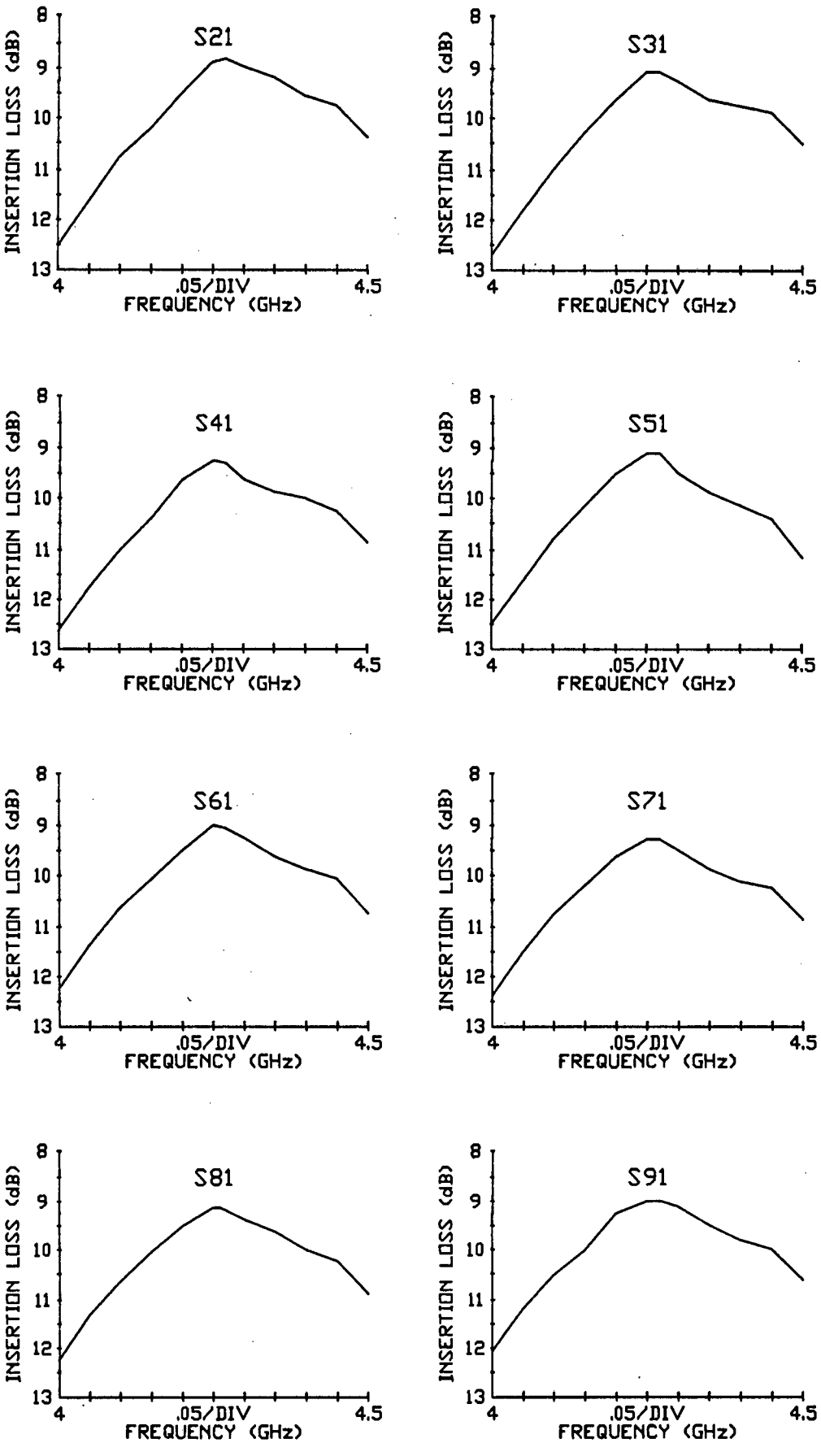

Fig. 3.6 Outputs obtained from the cylindrical resonant cavity power combiner/divider.

The power at each of the outputs should be an eighth of the total input power, assuming that there is no insertion loss. Therefore, the expected insertion loss from ports 1 to any of the output ports should be 9,03dB. The actual results obtained are shown in figure 3.6. These results show that the outputs track well, with no more than 0,5dB between any port. From the results obtained, an insertion loss of 0,1dB with respect to 9dB was determined for the combiner/divider. This indicates an efficiency of 98 percent at the centre frequency. It was however, decided that the best way to determine both the bandwidth and efficiency of the combiner was to build another and place the two "back to back". Another combiner was fabricated, its response being very similar to the first. The centre frequency of the second was at 4,25GHz. The construction of this type of combiner/divider is therefore very repeatable. The two combiners were placed "back to back" and the results obtained are shown in figure 3.7.(a) and (b).

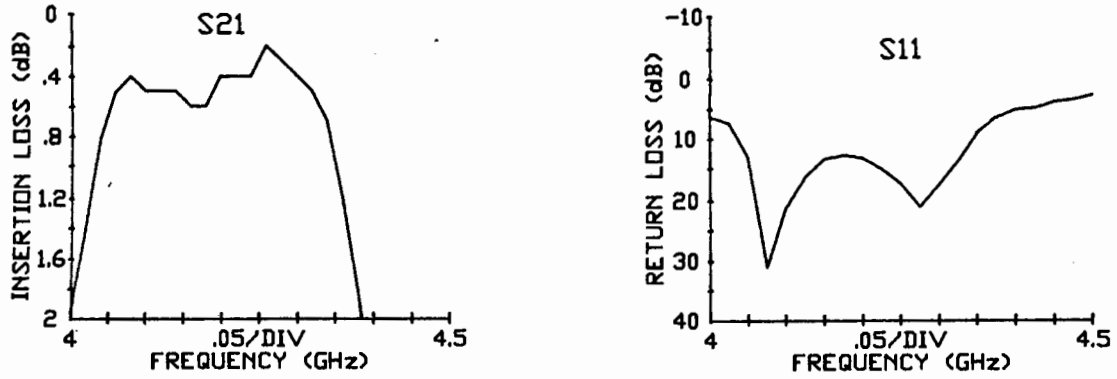

(a) (b)

Fig. 3.7.(a) Insertion loss of two resonant cavities placed "back to back". (b) The input return loss of the combined cavities.

The minimum insertion loss measured was 0,2dB at a frequency of

4,26GHz. This insertion loss corresponds to an overall combining efficiency of 95,5 percent, or the efficiency of each combiner is 97,7 percent. From the results obtained it can be seen that the bandwidth is very narrow. The 0,2dB bandwidth is 110MHz and the 1dB bandwidth is 300MHz.

Figure 3.7 (b) shows the input match. From this figure it can be seen that there are two points corresponding to a good match. The reason for these two "notches" was put down to the slightly different centre frequencies of the two combiners used.

The isolation obtained between various ports is shown in figure 3.8. Note that the isolation between any other two ports will be the same as one of the graphs shown in figure 3.8 due to the symmetry of the device.

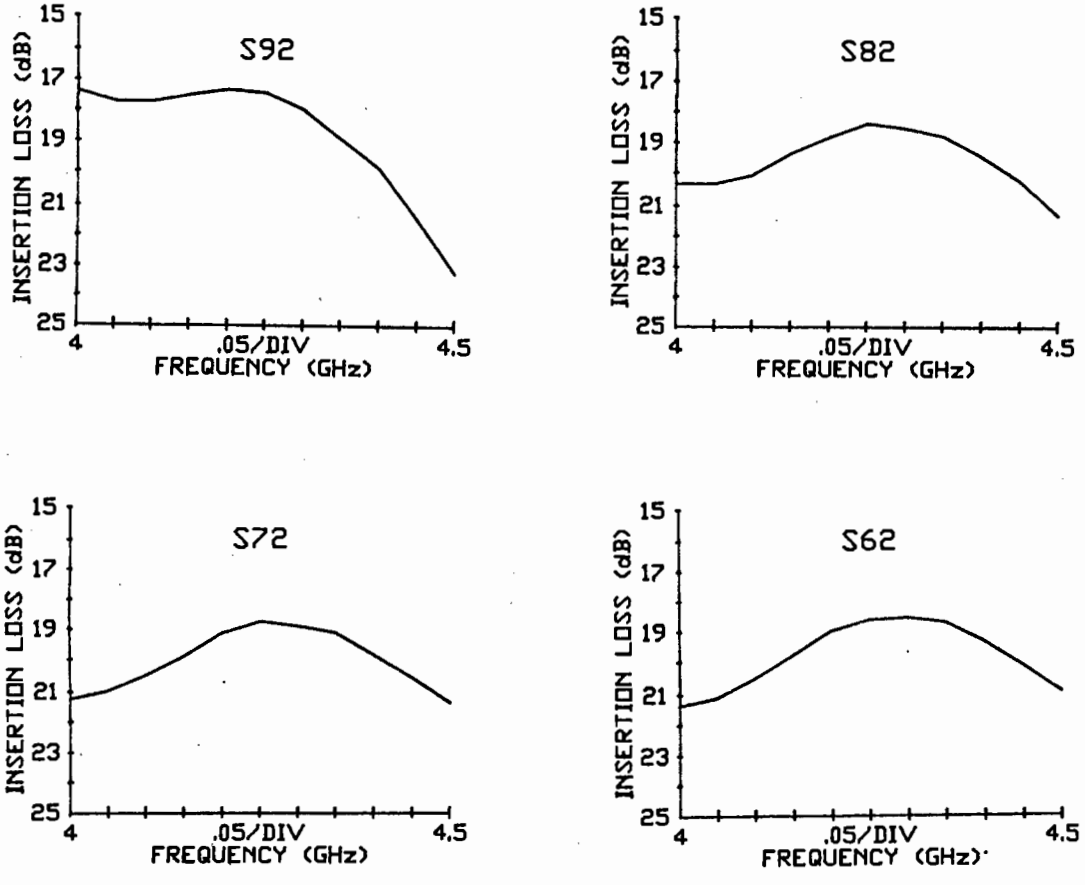

Fig. 3.8 The isolation between various ports.

The theoretical isolation at the centre frequency is 18dB. This may be calculated by considering the combiner as an 8-way combiner consisting of quarter wavelength transformers as shown in figure 3.9.

At point A the impedance seen by port 1 must be 50 ohms at the centre frequency. This means that each of the transformers must transform 50 ohms to 400 ohms, which gives them a characteristic impedance of 141,42 ohms. Now consider port 2 as the input

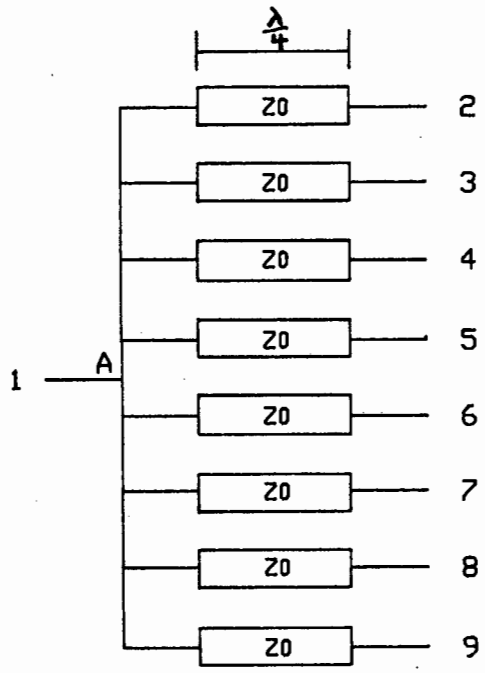

Fig. 3.9 A possible analogous circuit used to determine the theoretical isolation.

with all other ports terminated in 50 ohms. The impedance at point A would be 50 ohms in parallel with 400/7 ohms which is 26,67 ohms. This gives an impedance of 750 ohms at port 2. A reflection coefficient of 0,875 would result. Therefore for an input of 1 watt at port 2, 0,234 watts is transmitted. At point A this power is divided in the ratio 0,4667: 0,533. The output

power at port 1 is therefore 0,1247 watts, and the power output at the other seven ports is 0,0156 watts. This gives an isolation of -10log(0,0156)=18,06dB and an S_{12} of -9,03dB. The match at port 2 gives a return loss of -1,16dB. Note that the analogy used to calculate the above values is only true at the centre frequency.

Figure 3.8 shows that the isolations obtained for the combiner/divider are slightly higher than the 18dB expected. The results obtained for some of the output matches are shown in figure 3.10. The results shown in figure 3.10 correlate well with those predicted, giving strength to the analogy used.

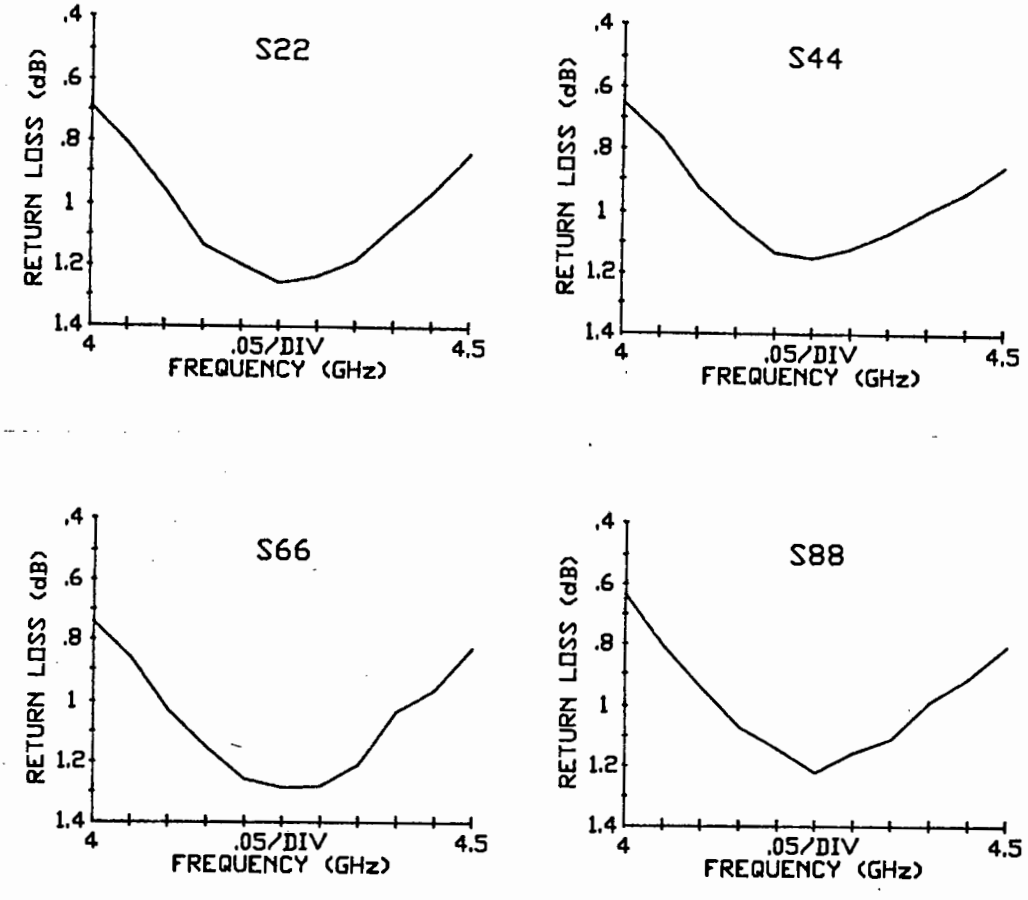

Fig. 3.10 Output return loss for the resonant cavity combiner/divider.

Note that the output matches appear to be very poor. This is due to the conditions under which they were measured. That is, in order to determine the S-parameters of the device it is necessary to feed power into one port only and terminate the others with 50 ohm loads. However, in practice all the outputs will be driven simultaneously when the combiner/divider is used as a combiner. In this situation the output (now input) ports will appear matched to the driving sources. This is because the device is a passive one, and as such must be reciprocal. Appendix C shows this for the 2-way Wilkinson, which is discussed in chapter 4.

The measured values obtained for the output matches are important when considering the effect an amplifier which has blown up would have on the other non failed amplifiers. This in turn is also tied up with isolation because as more amplifiers blow up the input and output match gets worse and if, for example, all but one of the amplifiers fail, the remaining amplifier will be left with a very poor match at its input and output. Depending on the device used, this could in turn cause the last amplifier to also fail. However, most devices are now short circuit protected. In order to prevent such failures it is worthwhile to use isolators in the amplifier circuits when the price of individual FETs are very high.

3.2.2 Conclusions and Possible Improvements to the Resonant Cavity Combiner

In summary, the resonant cavity combiner/divider described is both efficient and repeatable. Its major drawbacks are its narrow bandwidth and non-planar structure. The non-planar

structure, as mentioned before makes heat dissipation difficult. However, the structure is physically small and offers that as an advantage.

The bandwidth may be improved by altering certain dimensions. The main adjustment that can be carried out is the depth of the cavity, but this has practical limitations as does increasing the diameter of the probes, which is another way in which the bandwidth may be increased. Other methods have been proposed. One such method uses double cavities[20]. This provides a double tuned circuit composed of TM_{010} and TM_{020} mode cavities. Another method is that proposed by G.W. Swift[22]. The design is based upon traditional matching filter synthesis techniques employed to realise octave bandwidth performance in the form of a radial wave matching filter. Another point to note is that the loaded Q, $Q_l = Q_e / \sqrt{2}N$ where N is the number of devices. This means that the larger N, the broader the bandwidth.

3.3 Rectangular Waveguide Combiner/Divider

3.3.1 Introduction

The combiner/divider to be described consists of a rectangular waveguide, one end of which is short circuited. The outputs are coupled to the electric field maxima, and are therefore placed half a wavelength apart. This differs from the more common rectangular waveguide combiner/divider (ref 22 p174) that couples at the magnetic field maxima found in the cavity walls also a half wavelengh apart.

3.3.2 The design procedure

Figure 3.11 shows a cross-section of the waveguide combiner/divider. The design procedure will be outlined in this section; expected performance from the combiner/divider will also be given.

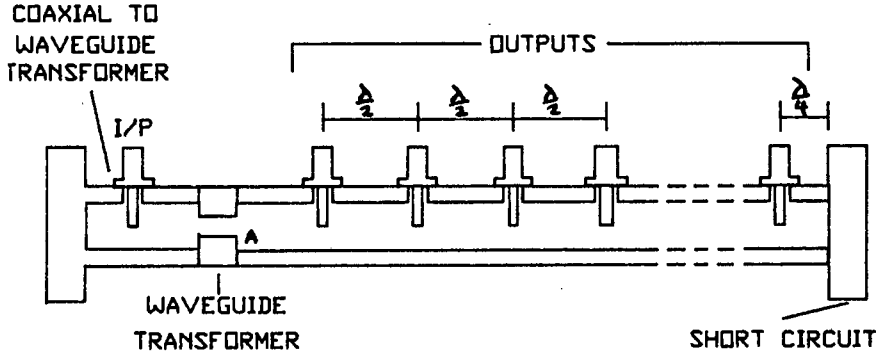

Fig. 3.11 Cross-section of the rectangular waveguide combiner/divider.

The principle of operation of this combiner is as follows:
Each of the outputs is matched to 50 ohms. This means that the impedance seen at point A is the parallel combination of all the impedances at the outputs. This impedance is then transformed via a quarter wavelength transformer in waveguide to allow a match at the input. The idea is analogous to a transmission line that is short circuited at one end, and has 50 ohm loads placed at half wavelength intervals upon it. A quarter wave section then transforms the parallel combination back to 50 ohms. The equivalent circuit is shown in figure 3.13. The above analogy was implemented on TOUCHSTONE, a microwave CAD program designed by EEsof, refer to appendix B for further information. Z_0 was taken to be 50 ohms, which means that Z1 must be 17,67 ohms. The circuit file and results obtained are shown in figure 3.14. The

graph shows that the transmission measurements give the expected

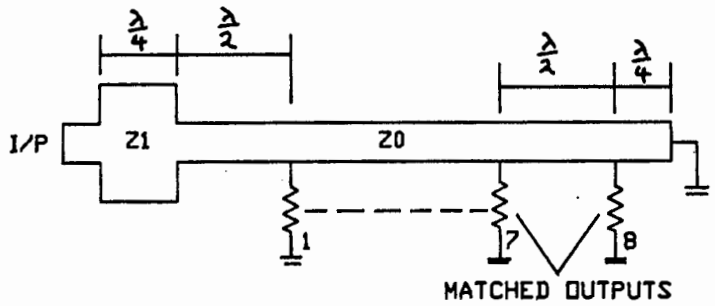

Fig. 3.13 Equivalent circuit of the rectangular waveguide combiner/divider.

```
VAR
  RL=50

CKT
  TLIN 1 2 Z=17.667 E=90 F=10
  TLIN 2 3 Z=50 E=180 F=10
! RES 3 0 R^RL
  TLIN 3 4 Z=50 E=180 F=10
  RES 4 0 R=50
  TLIN 4 5 Z=50 E=180 F=10
  RES 5 0 R=50
  TLIN 5 6 Z=50 E=180 F=10
! RES 6 0 R^RL
  TLIN 6 7 Z=50 E=180 F=10
  RES 7 0 R^RL
  TLIN 7 8 Z=50 E=180 F=10
  RES 8 0 R^RL
  TLIN 8 9 Z=50 E=180 F=10
  RES 9 0 R=50
  TLIN 9 10 Z=50 E=180 F=10
! RES 10 0 R^RL
  TLIN 10 11 Z=50 E=270 F=10
  SHOR 11
  DEF4P 1 3 6 10 TEST

OUT
  TEST DB[S21] GR1
  TEST DB[S31] GR1
  TEST DB[S41] GR1

FREQ
  SWEEP 8 12 .2

GRID
  GR1 0 -20 2
```

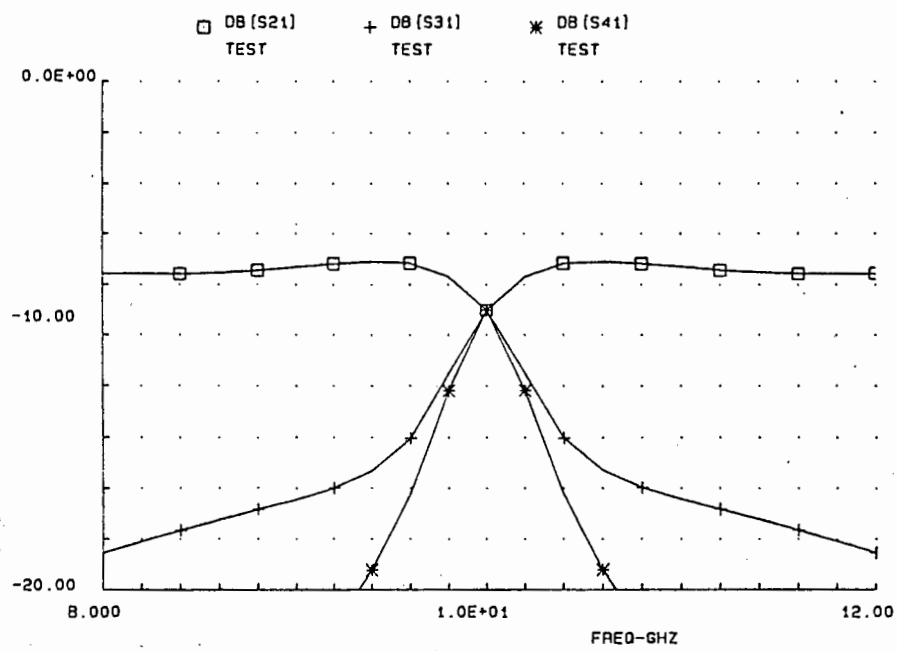

Fig. 3.14 Output expected from the rectangular waveguide combiner/divider using the analogy depicted by the TOUCHSTONE circuit file.

9,03dB insertion loss. The bandwidth was however, narrower than expected. Another feature that was not expected was the narrowing of the bandwidth as the last output port was approached.

Even though these results indicated very narrow bandwidths it was decided to go ahead and build the combiner/divider to see what correlation there would be with the measured and expected results.

Firstly various values have to be determined such as the waveguide wavelength. The dimensions of the rectangular waveguide are as shown in figure 3.15.

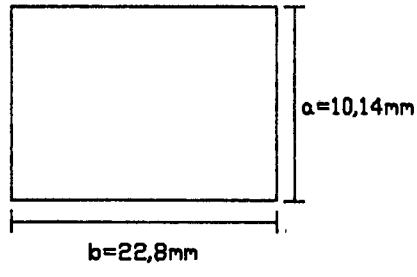

Fig. 3.15 Dimensions of the rectangular waveguide.

The dominant mode of operation in rectangular waveguides is the TE_{01} mode. The cut off frequency is given by

$$f_c = \frac{1}{2\pi\sqrt{\mu_0\varepsilon_0}}\sqrt{\frac{m^2}{a^2}+\frac{n^2}{b^2}} \qquad 3.11$$

where m = 0

n = 1

μ_0 = permeability of free space

ε_0 = permittivity of free space.

The waveguide wavelength λ_g, is given by

$$\lambda_g = \frac{\lambda_0}{\sqrt{1-\left[\frac{f_c}{f}\right]^2}} \qquad 3.12$$

where λ_0 is the wavelength in free space at frequency f.
For the dimensions of figure 3.15 the cut off frequency is 6,56GHz and λ_g is 3,98cm at 10GHz. This gives $\lambda_g/2$ = 1,99cm and $\lambda_g/4$ = 0,995cm.

The first requirement in the design of this combiner/divider was to determine the depth of the coupling probe to obtain a perfect match into the waveguide. This is in priciple a coaxial to waveguide transformer. A connector was placed a quarter of a wavelength, at 10GHz, from the short circuited end of a piece of rectangular waveguide. The depth of the probe was adjusted to give a good match when looking in from the coaxial side. Once a return loss of better than 25dB was obtained a template was made that enabled all probes to be cut to exactly the same length.

The next stage in the design was the quarter wave transformer. This involves impedance considerations in waveguide, so that the new waveguide dimensions can be determined. The characteristic impedance of a waveguide is given by

$$Z_g = \frac{\eta \lambda_g}{\lambda_0} \qquad 3.13$$

where η is the intrinsic impedance of air, which is approximately 377 ohms.

This impedance is effectively the resistance per unit area of the waveguide cross-section and equation 3.13 can be rewritten as

$$Z_0 = \frac{\eta \lambda_g a}{\lambda_0 b}$$ 3.14 (ref28)

where a and b are the waveguide dimensions.

It requires $Z_0/8$ to be transformed to Z_0. This therefore requires a characteristic impedance of Z_0' for the waveguide transformer.

This is given by $$[Z_0']^2 = \frac{Z_0^2}{8}$$ 3.15

which is the standard equation transforming impedances with quarter qavelength transmission lines, $Z_0^2 = Z_{in} Z_{out}$.

Therefore $$Z_0' = \frac{\eta \lambda_g a}{\lambda_0 b} * \frac{1}{\sqrt{8}}$$ 3.16

As both b and λ_0 remain the same the following results.

$$\frac{\lambda_g a'}{\lambda_0 b} = \frac{\lambda_g a}{\lambda_0 b} * \frac{1}{\sqrt{8}}$$

Which gives an a' of 3,58mm.

The dimensions of the waveguide transformer are therefore:

a = 3,58mm

b = 22,14mm

l = 9,95mm

where l is the waveguide length.

This leaves the placing of the probes. Each probe is spaced half a wavelength apart so that all probes have identical coupling and the last probe is a quarter wavelength from the short circuit resulting in all the probes being coupled to an electric field

maxima. The first probe is placed a half wavelength from the waveguide transformer, therefore all eight probes are in parallel and connected to one side of the quarter wavelength transformer. Figure 3.16 is a photograph of the combiner/divider. The coaxial to waveguide transformer is not present and is placed on the right hand side.

Note that this type of combiner/divider can only be effectively used as a pair. This is because each output is different in phase. Hence they will have to be used "back to back" with ports 2 and 9 connected together as shown in figure 3.17 which ensures that all path lengths are the same.

Fig. 3.16 Photograph of the rectangular waveguide combiner/divider.

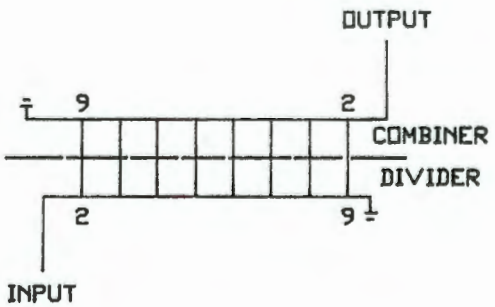

Fig. 3.17 The correct connection of two such combiners/dividers.

3.3.3 Results and Discussion

The input match obtained is shown in figure 3.18. As can be seen the bandwidth is very narrow. The measured value approached a return loss of 35dB. This cannot be seen in the figure because the frequency steps were too large to pick up the centre point. The centre frequency is at 10,17GHz.

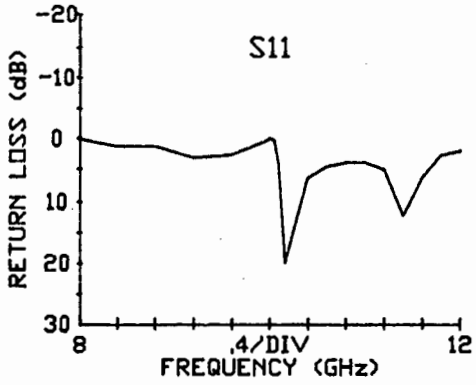

Fig. 3.18 Return loss of the input, port 1.

The results obtained at the outputs were different to those expected. This can be seen from figures 3.19 (a), (b), (c) and (d).

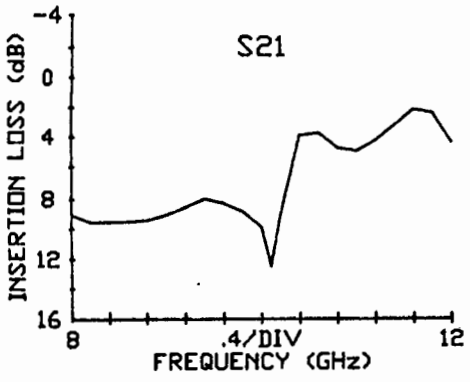

(a)

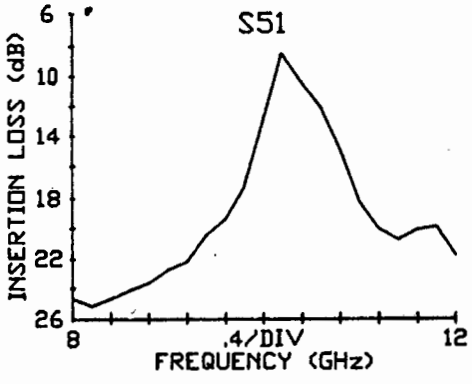

(b)

Fig 3.19 (a) S_{21} and (b) S_{51} of the rectangular combiner/divider.

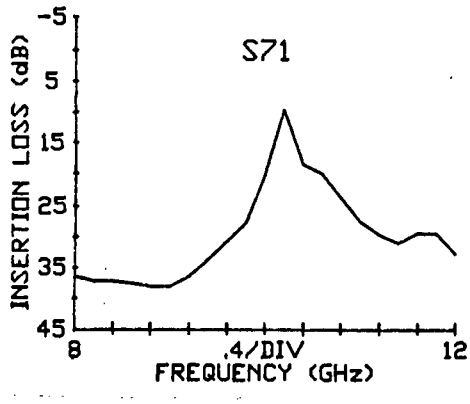

(c)

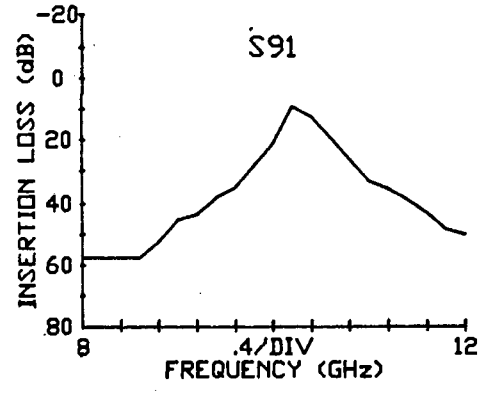

(d)

Fig. 3.19 (c) S_{71} and (d) S_{91} of the rectangular combiner/divider.

From these figures it can be seen that the bandwidth of this type of combiner would obviously be very narrow. The expected result for S_{21} differed the most in shape from that measured, refer to figure 3.14. Due to this it was anticipated that various factors, such as the spacing of the probes, their depth etc must be critical in the construction of the combiner. An investigation of the various effects was carried out on TOUCHSTONE.

Firstly, the effect of varying the probe depth was investigated. This variation would be similar to changing the loads of the analogous circuit, provided the changes are not too large. Secondly, the effect of spacing between probes was examined, this was simply done by changing the transmission length between the loads on the model. Thirdly, the effect of changing the short circuit position from the last probe and fourthly the effect of changing the distance between the first probe and the quarter wavelength transformer were examined. The results obtained are shown in figures 3.20 (a), (b), (c) and (d).

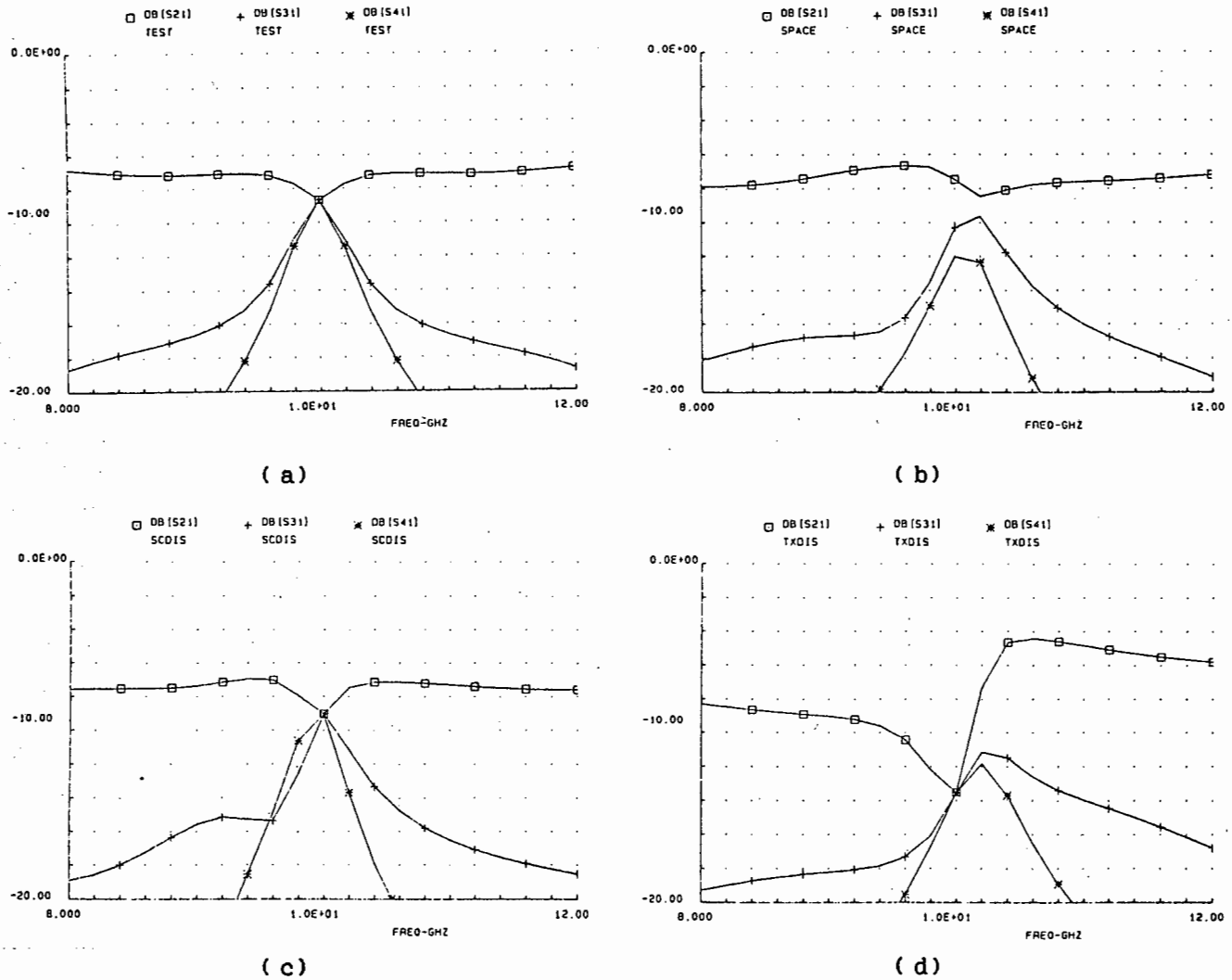

Fig. 3.20 (a) Effect of changing load. (b) Effect of changing probe spacing. (c) Effect of changing short circuit positition. (d) Effect of changing quarter wavelength section.

From these results, it was found that the factor which produced the most dramatic change was the distance between the first probe and the quarter wavelength transformer. As a result of this investigation it was decided that spacers of various thicknesses should be placed between the waveguide and the transformer section. As a result it was found that the predicted performance could be approximated more closely. The best result that could be achieved was with a 0,9mm spacer. Results obtained for S_{21} are shown in figure 3.21 for 0,9 and 1.6mm spacers.

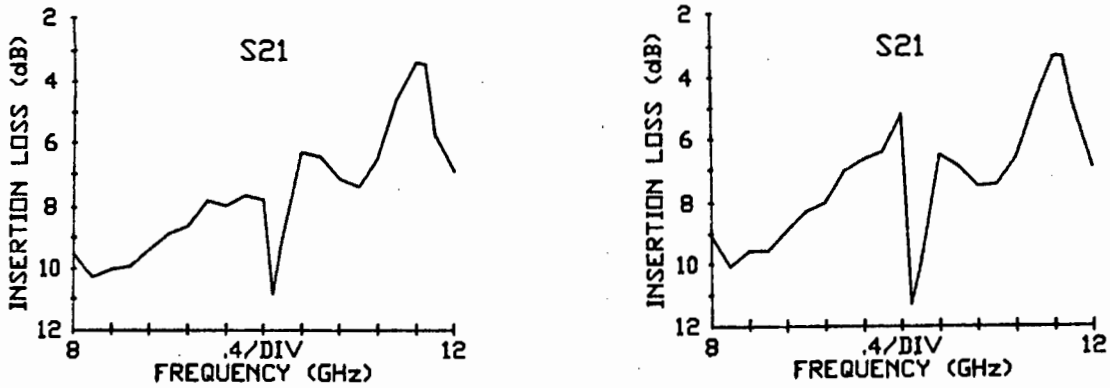

(a) (b)

Fig. 3.21 (a) S_{21} with a 0,9mm spacer (b) S_{21} with a 1,6mm spacer.

The results obtained for the other transmission measurements were similar to those obtained previously. This was predicted as can be seen from figure 3.20(d). The results for S_{21} are shown because the effect is more pronounced.

From the experience gained, it was concluded that there were too many variables that could cause variations from the ideal, and as such the idea is not a practical solution fo a combiner/divider.

3.3.4 Conclusions

From the results obtained it can be seen that this type of combiner is not very practical. The major disadvantage being the critical construction required if one is to get reasonable results, and then the bandwidth is extremely narrow to make this effort worthwhile.

3.4 Summary

It was found that the cylindrical resonant cavity provides an efficient way of power combining several devices together. Other factors in its favour are the physical size and repeatability of the results. Its disadvantages are its narrow bandwidth and its non-planar structure which makes effective heat dissipation difficult. The bandwidth can however, be improved by various techniques, as previously mentioned.

The rectangular waveguide combiner/divider discussed was not very successful; the construction being far too critical.

CHAPTER 4 WILKINSON AND CORPORATE WILKINSON COMBINERS/DIVIDERS

4.1 Introduction

The Wilkinson divider was first proposed by E.J. Wilkinson in 1960[30]. Since then many generalisations of the Wilkinson divider have been developed. For example L.I. Parad and L. Moynihan[31] published a more complex version of the Wilkinson combiner/divider. Their combiner/divider provided two in phase isolated outputs with a constant arbitary power division. These types of combiners/dividers are three port devices, the characteristics of which will be discussed in a later section. These three port devices were then arranged into corporate structures to provide isolated in phase outputs for binary power splits. This chapter deals with both a Wilkinson 2-way combiner/divider and extends this to a corporate 4-way combiner/divider.

4.2 The 2-Way Wilkinson Combiner/Divider

Figure 4.1 shows the standard Wilkinson combiner/divider.

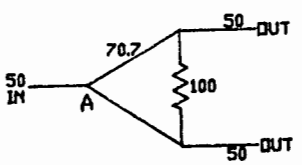

Fig. 4.1 2-way Wilkinson combiner/divider.

The device is a three port network that divides the input power equally to give equiphase outputs. This division is achieved as

follows:

(a) Ports 2 and 3 terminated with 50 ohm loads (no isolation resistor). In order to achieve a match at port 1 each of the quarter wavelength transformers must transform 50 ohms to 100 ohms. The parallel combination of the 100 ohms giving the required 50 ohms. The characteristic impedance of the quarter wave transformer must therefore be 70,7 ohms. The division at port 1 is thus equal because two equal loads are seen at this point. The outputs are in phase because of the equal path lengths travelled.

(b) Ports 1 and 3 are terminated with 50 ohm loads (no isolation resistor) and port 2 is now the input. The impedance at port 1 will be 50 ohms in parallel with 100 ohms giving a resultant impedance of 33,33 ohms. This impedance is transformed by the 70,7 ohm quarter wave transformer to 150 ohms. Thus the impedance seen at port 2 is 150 ohms and the reflection coefficient, ρ, is 0,5. This allows three quarters of the incident power to be transmitted. At point A this power is split such that the output at port 1 is two thirds of the incident power arriving at point A and the other one third goes to port 3. This gives a transmission of -3dB between ports 2 and 1 which is expected because the device is passive and therefore reciprocal. The transmission from port 2 to 3 is -6dB which is the isolation between the two output ports without an isolation resistor. Obviously this is not good enough if the one output is not to effect the other when used as a power combiner/divider.

Before elaborating on the subject of isolation it is worth mentioning that if the device were operating as a combiner, both

ports 2 and 3 would be driven simultaneously and under these conditions ports 2 and 3 are in fact matched. The reason again is the reciprocal action of the passive device. To prove this point, it was decided to analyse the device on TOUCHSTONE with ports 2 and 3 driven simultaneously and port 1 terminated in 50 ohms. The transmission lines are assumed to be loss free and the results obtained are shown in figure 4.2. The technique used to obtain these results on TOUCHSTONE is discussed in appendix C. From figure 4.2 it is seen that S_{22} is in fact matched. Note that S_{21} is -3dB which is expected as the system is now a divider. S_{12}, however, is 3dB which proves that the power driven into port 3 is the same magnitude as that driven into port 2 and that the device is operating as a combiner. The output power at port 1 would therefore be twice the input power at port 2.

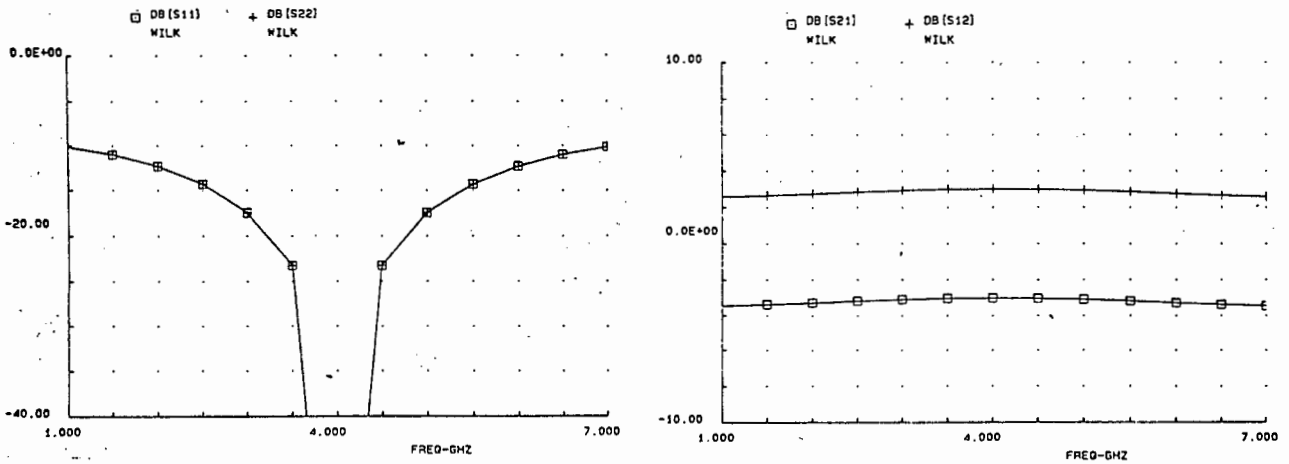

(a) (b)

Fig. 4.2 Input/output matches when port 2 and 3 are driven simultaneously, no isolation resistor (b) S_{21} and S_{12} under the same conditions.

The isolation obviously needs improving if such a combiner/divider is to used for combining the power of two amplifiers and the effect of input and output matching is to have little or no effect on the other two devices. The method used to

achieve this is to place a resistor between the two output ports. Its value may be determined as follows. Let port 3 be short circuited. For perfect isolation port 2 should remain perfectly matched. Also the transmission from port 2 to 1 must be -3dB, which means that half the power must be dissipated in the resistor. Figure 4.3 shows the circuit layout.

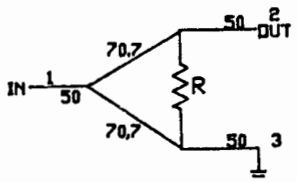

Fig. 4.3 Circuit layout with port 3 short circuited.

Under these conditions the impedance at port 2 will be 100 ohms. The short circuit at port 3 is transformed to an open circuit at port 1. This then means that 50 ohms is transformed to 100 ohms at port 2. If port 2 is to be matched, the parallel combination of 100 ohms and R must be 50 ohms, which gives a value of 100 ohms for R. This also satisfies the requirement that half the input power will be dissipated in R, and half will be transmitted.

Isolation is also provided between the output ports under normal operating conditions. If either port 2 or 3 are mismatched in any way the reflected power from port 2, say, will travel one half wavelength before arriving at port 3. The resistor has no physical length in the ideal case, therefore cancelation will occur due to the 180 degree phase shift. It must also be noted then, that when the combiner/divider is operating as a combiner, the two inputs, ports 2 and 3 now, must be driven with both the

same amplitude and phase if the combiner is to operate efficiently. Any variations in phase and amplitude will cause some power loss across the isolation resistor. Figures 4.4 (a) and (b) give the theoretical results for a Wilkinson combiner/divider.

The bandwidth of the Wilkinson combiner/divider depends very much on definition. If the input match is an important factor the bandwidth would be from 3,25 to 4.75GHz for a match of better than 20dB. In other words a bandwidth of 37,5 percent. The same bandwidth is obtained if isolation is the important factor in a particular design. The limit is also 20dB. If S_{21} is the only important factor, a bandwidth of 2,25 to 5,75GHz (87,5%) results for a 0,22dB ripple.

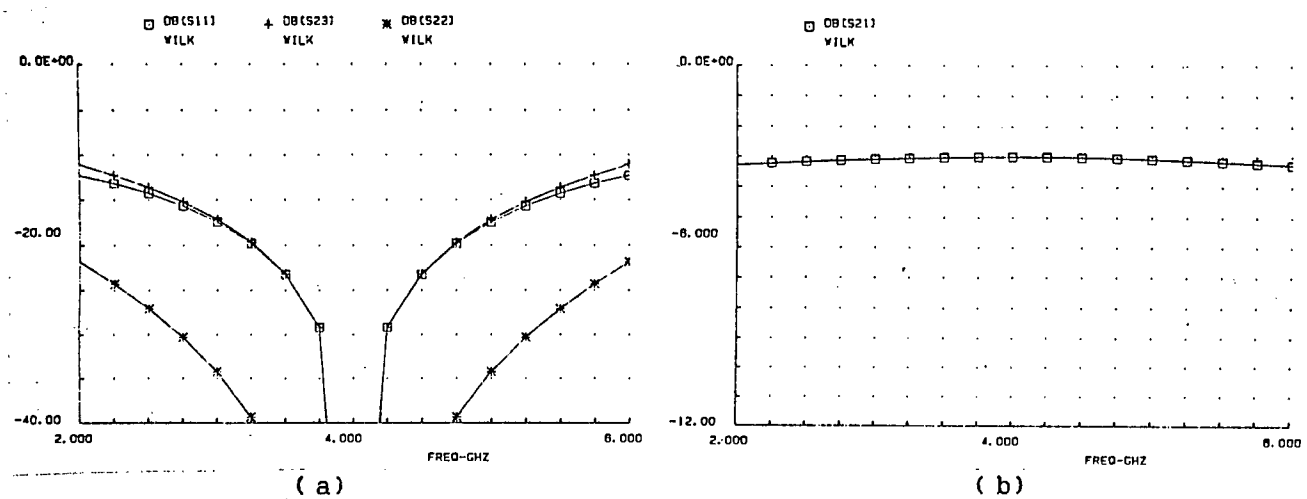

Fig. 4.4 (a) S_{11}, S_{22} and S_{23} for the Wilkinson combiner/divider. (b) S_{21} for the same device.

4.2.1 Construction of the Combiner/Divider and Results Obtained

The circuit of figure 4.1 was implemented on softboard microstrip (RTDUROID 5880). A discussion on microstrip will be given in the

next chapter. The layout is shown in figure 4.5. Note that the outputs were not placed on the same edge of the microstrip board for ease of construction and testing. The isolation resistor used was a 100 ohm chip resistor.

Dimensions

70,7 ohms: width = 1,39mm

λ_m(at 4GHz) = 55,3mm

50 ohms : width = 2,46mm

λ_m(at 4GHz) = 53.8mm

Fig. 4.5 Microstrip layout of the 2-way Wilkinson combiner/divider.

Results obtained for this device are given in figures 4.6 (a), (b), (c), (d) and (e). S_{21} and S_{31} are shown in figures 4.6 (a) and (b). From these figures it is seen that the split is fairly even, with a measured maximum variation of 0,6dB which occurred at only one frequency. The mean variation was 0,3dB and the insertion loss at the centre frequency of 3,8GHz was 0,3dB for the one path and 0,25dB for the other.

Figure 4.6(d) shows the input return loss for the Wilkinson combiner/divider (port 1). The best match was at a frequency of 3,8GHz which is close to the design frequency of 4GHz. The match was not very good, with a return loss of only 14,3dB at 3,8GHz. This corresponds to a VSWR of 1,48. One possible explanation for this poor match is the effect of the discontinuity found at ports 2 and 3 where there is a 90 degree bend. Bends introduce various parasitic effects such as increased capacitance, and therefore change the impedance at that point. As this point occurs at one

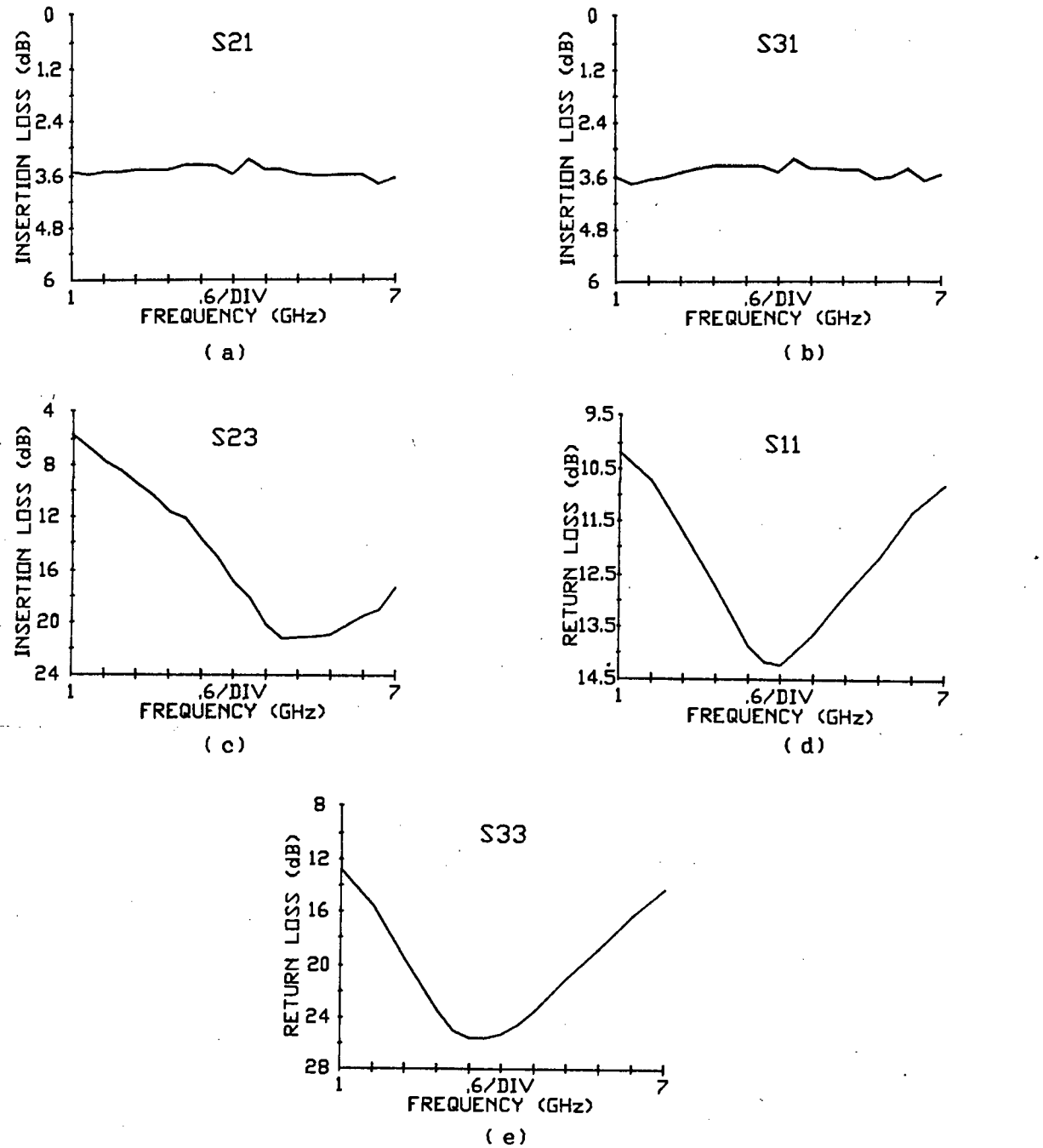

Fig. 4.6 (a) S_{21}, (b) S_{31}, (c) S_{23}, (d) s_{11}, (e) S_{22} and (f) S_{33} for the 2-way Wilkinson combiner/divider.

end of the quarter wave transformer, it will be transformed, and as such magnified. For example if the impedances at the bends were changed to say 60 ohms, the impedance seen at port 1 would be 41,7 ohms, which already produces a VSWR of 1,2. The effect of the bend could be further enhanced if the characteristic

impedance of the 70,7 ohm transmission lines was out. If for example the impedance was 65 ohms instead, the input match would now be 35,2 ohms (still assumes a match of 60 ohms at ports 2 and 3). This corresponds to a VSWR of 1,41 and it shows that variations of this type can easily cause the poor match at the input. To show the tolerances required, it is interesting to note that the line width required for the 65 ohms is 1,6mm compared to 1,4mm required for the 70,7 ohm line. This is a difference of only 0,2mm, which indicates that the etching process must be carried out with great care. The matches for S_{22} and S_{33} were, however, very good with a return loss of 24dB and 26dB respectively. Figure 4.6 (d) shows S_{22} is very similar to S_{33}. The isolation was measured as 22dB at 5,8GHz and is shown in figure 4.6 (e). The reason for this shift in centre frequency compared to the centre frequency for best match of 3.8GHz is definitely the resistor size, which in practice does have a physical length and subsequently causes a phase shift.

4.2.2 Conclusions

The Wilkinson 2-way combiner/divider was fabricated in microstrip. The results obtained were not ideal, however, the principles were demonstrated and valuable experience was gained in the design of circuits on microstrip. The tolerances were slightly more critical than at first thought, and a good deal of care is required in the layout of the circuit. Effects such as discontinuities must be considered more carefully, the most probable reason for the poor match at the input, as already mentioned. The divider on the whole, however, provides a method of power division that is simple to implement and that can

provide very good results with more care taken in the construction stage. The bandwidth depends very much on definition and depends on the application of the combiner/divider as previously discussed. The insertion loss was in the region of 0,3dB. which corresponds to a combining efficiency of 93,3 percent.

4.3 The Corporate Wilkinson Combiner/Divider

A 4-way combiner was constructed using three Wilkinson combiners/dividers in a corporate structure. The corporate type of combiner was discussed in chapter 2.

Initially, the first version fabricated, used the layout of the 2-way Wilkinson combiner/divider discussed in the previous section for each of the 2-way dividers. The layout is shown in figure 4.7.

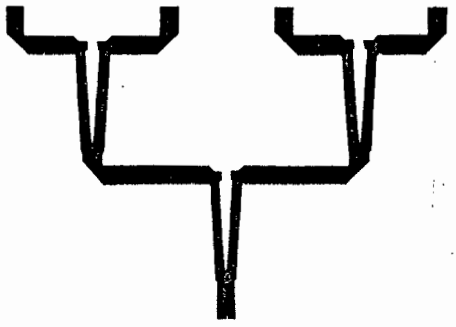

Dimensions for line widths are as for the 2-way Wilkinson as there are no other impedance lines other than 50 and 70,7 ohm lines.

Fig. 4.7 Layout of the 4-way corporate Wilkinson combiner/divider.

From the layout, it is seen that a length of 50 ohm line connects the first Wilkinson to the next one. The size of the connectors

at the output control this length, as well as the 50 ohm lines found at the output. The path lengths from the input to each of the outputs must be the same. It will be noticed that a ninety degree bend is accompanied by a mitred corner. This is necessary to reduce any parasitic reactances that are introduced by a bend. The ideal dimensions for such a bend are given in figure 4.8[32]

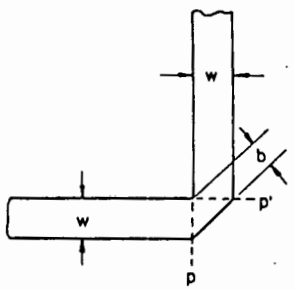

b = 0,57w

Fig. 4.8 The ideal amount of mitre required for a 90 degree bend.

The layout was once again etched on to microstrip (RTDUROID 5880).

4.3.1 Results and Discussion

The input match obtained for this power combiner divider is shown in figure 4.9. From this figure it can be seen that there are two frequencies at which the device was well matched. These frequencies are at 2,0GHz and 5,0GHz. The match at 2,0GHz is 28dB and at 5,0GHz 21dB. Both are good matches, however, they are not at the design frequency of 4GHz. At first it was thought that some error must have been made in the layout, such as the quarter wavelength sections being too long. This proved not to be the case. What was more striking, was that the layout of each Wilkinson divider was the same as that used previously, which did work at the centre frequency. One possible explanation lay in

the connection between the dividers. This was investigated on TOUCHSTONE. From the results obtained it was found that the interconnection between the dividers was important as well as the the transmission lines at the output. These results will be discussed in more detail once other results for this combiner/divider have been presented.

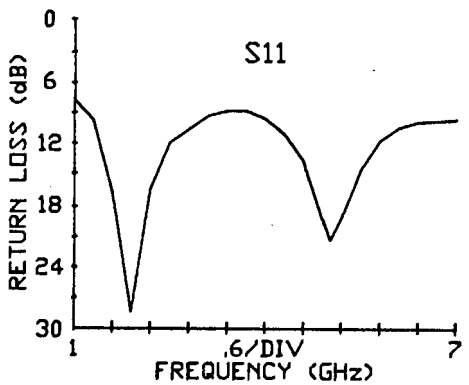

Fig. 4.9 Input match for the corporate combiner/divider.

The through transmissions tracked well, and are shown in figures 4.10 (a), (b), (c) and (d).

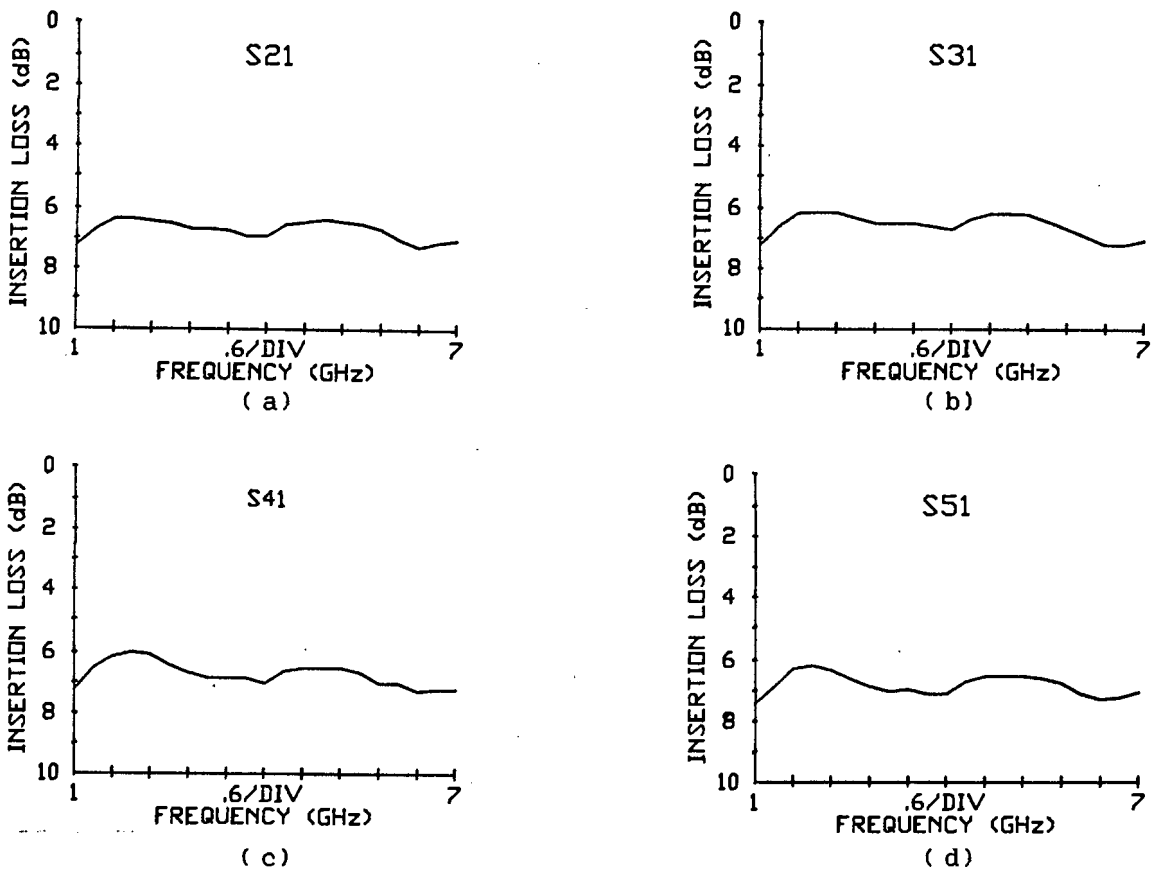

Fig. 4.10 (a) S_{21}, (b) S_{31}, (c) S_{41}, and (d) S_{51}.

From these figures it is seen that the outputs approach the required 6dB insertion loss at the two "centre" frequencies indicated by the input match, namely at 2,0GHz and 5,0GHz. The insertion loss between S_{21}, S_{31}, S_{41} and S_{51} varied by less than 0,4dB. The loss, with respect to 6,0dB, was 0,3dB at 2GHz and 0,35dB at 5GHz. The loss is lower than expected, especially when the loss measured for the Wilkison 2-way is 0,25dB. A loss of at least 0,5dB would be expected. The reason for this is two fold. Firstly the network analyser used to determine these results cannot measure insertion losses more accurately than to 0,1dB, and hence the lower the loss the more unreliable the result. Secondly, in the case of the Wilkinson 2-way combiner/divider the input match was not very good, which means some power will be lost due to reflection at the input, and for the corporate structure the input match is good and consequently the power lost due to reflection at the input was lower.

4.3.2 Analysis of the Corporate Combiner/Divider on TOUCHSTONE

The objective of this analysis is to determine the reason for the response obtained for the combiner/divider shown in figure 4.9. Ideally the response is easily predicted and is shown in figure 4.11. If the 2-way combiners are connected with 50 ohm lines the response should not be effected in any way, except for a possible increase in bandwidth if quarter wavelengths are used. This section describes the process used to determine what factors influence the response of the combiner/divider in an attempt to give an explanation for the response depicted by figure 4.9.

From figures 4.11 (a) and (b) it is seen that there is a centre frequency where the response is optimum, and the response is very similar to the 2-way Wilkinson, except that the split gives an S_{21} of -6dB as opposed to -3dB. It was then decided to investigate the effect a length of 50 ohm transmission line has on the response when placed between the first divider and the other two dividers.

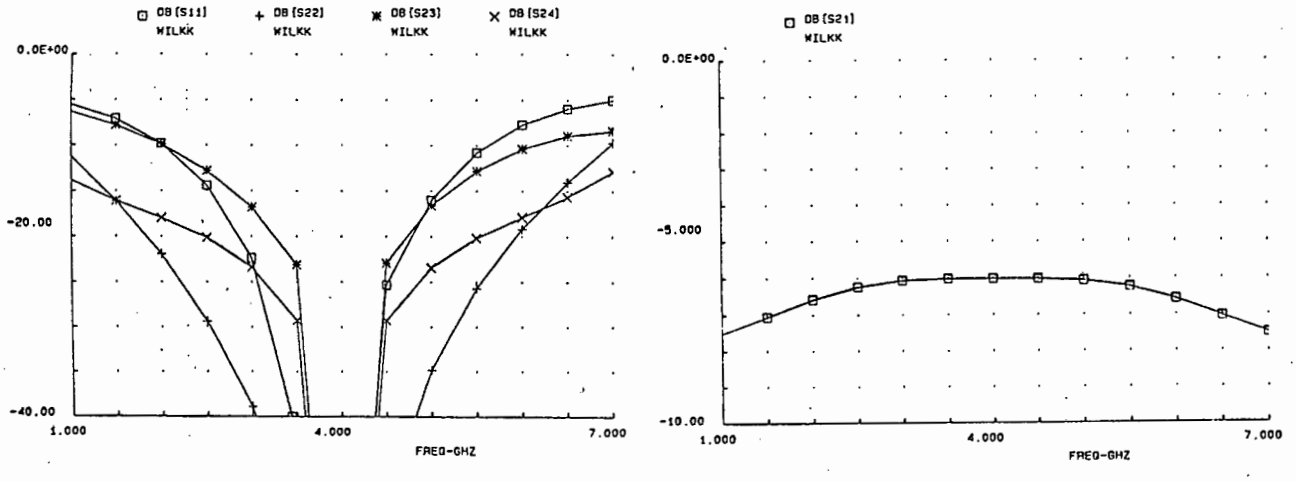

(a) (b)

Fig. 4.11 (a) Ideal S_{11}, S_{22}, S_{23} and S_{24} for the 4-way corporate combiner/divider (b) S_{21} for the same device.

Firstly the length between the dividers was measured on the layout used. This turned out to be slightly more than a quarter of a wavelength. This length was totally accidental, as it was chosen so that the connectors could be placed next to each other on the board. This length of transmission line was then placed

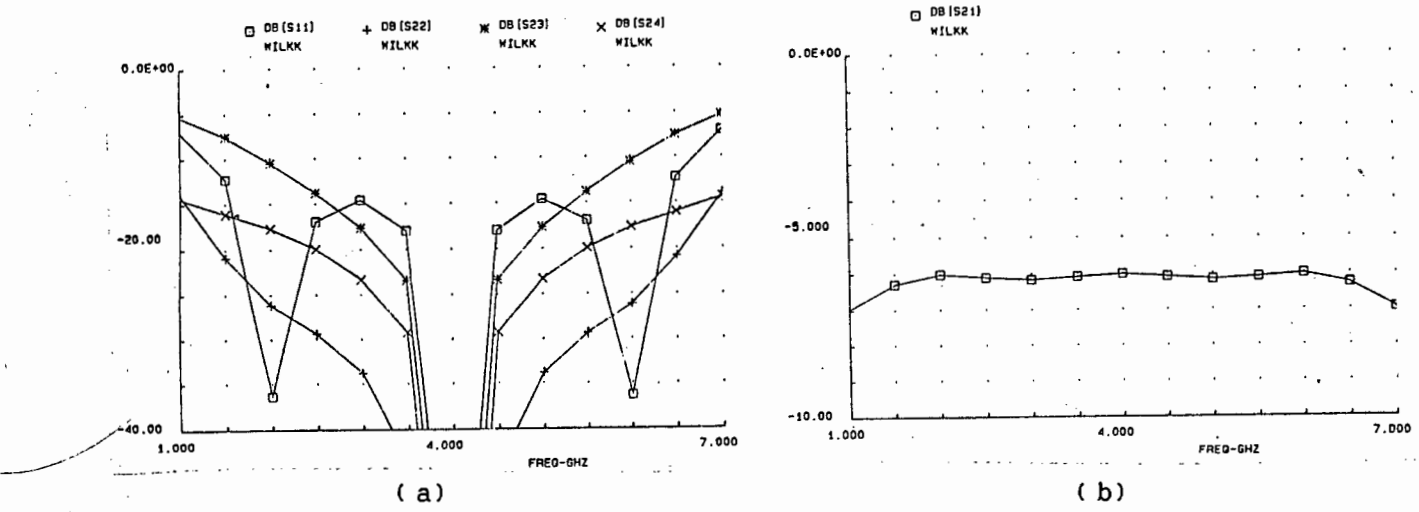

Fig. 4.12 Response of the corporate structure with a 50 ohm quarter wavelength of transmission line interconnecting the dividers (a) S_{11}, S_{22}, S_{23} and S_{24} (b) S_{21}.

between the dividers on the TOUCHSTONE model. The results obtained are shown in figures 4.12 (a) and (b). From figure 4.12 it is seen that good matches occur at three frequencies, namely 2GHz, 6GHz and at the centre frequency of 4GHz. Already this starts to approach the results obtained with the actual device. From the layout given in figure 4.7 the length of 50 ohm lines at the four outputs is almost a quarter of a wavelength. It was decided to add these lengths of transmission lines to the model on TOUCHSTONE as well. The response remained the same as that predicted in figure 4.12, which was expected. As the measured results indicated a mismatch for S_{11} at 4GHz it was decided to change the impedance of the lines connecting the dividers to 40 ohms. The results obtained are shown in figure 4.13 (a). From these results it is seen that there is now a worse match at the input at 4GHz. For interest it was then decided to change the impedance of the output transmission lines to 40 ohms as well. The results obtained are shown in figure 4.13 (b).

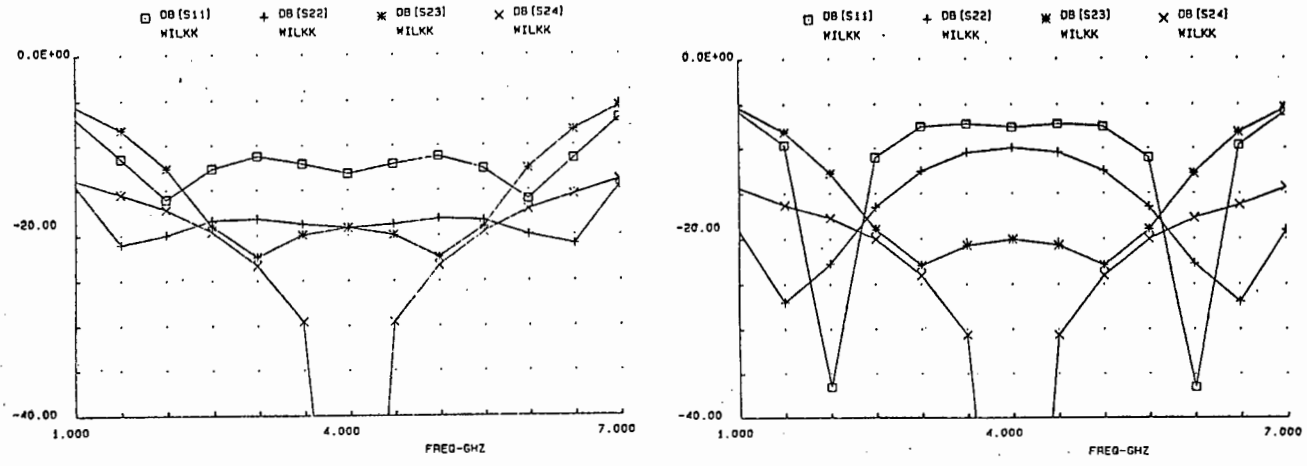

(a) (b)

Fig. 4.13 (a) S_{11}, S_{22}, S_{23}, S_{24}, obtained with 0,25λ 40 ohm transmission lines connecting the 2-way dividers and with 0,25λ 50 ohm lines at the output (b) results with both output and connecting transmission lines set to 40 ohms and 0,25λ long.

Here the response of S_{11} approached the measured results, with good input matches at 2 and 6GHz and a poor match at 4GHz. Figure 4.13 (c) gives S_{21} for this situation.

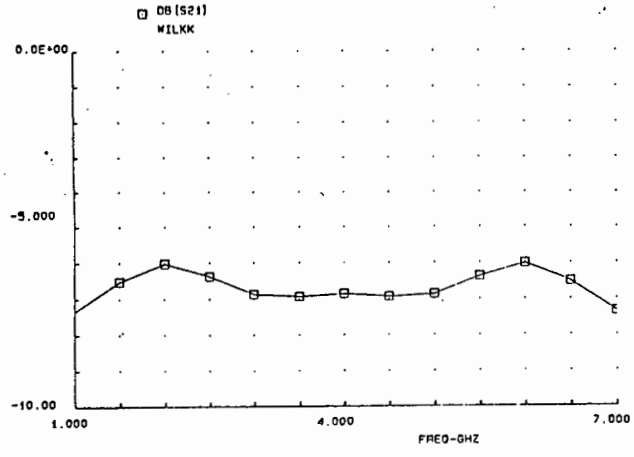

Fig. 4.13 (c) S_{21} for the set up as in (b).

It was now decided to keep the interconnecting transmission lines at 50 ohms and see what the effect is with 40 ohm lines at the outputs. The results obtained are shown in figure 4.14. Here it is evident that the input match is poor over most of the bandwidth

and is slightly improved at 4GHz.

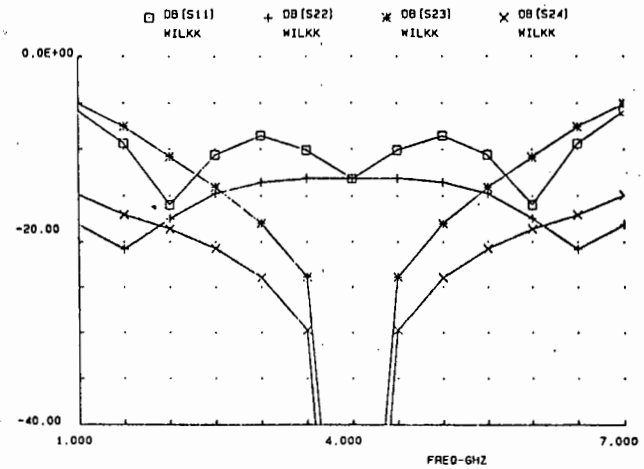

Fig. 4.14 S_{11}, S_{22}, S_{23} and S_{24} where the interconnecting lines are 50 ohms 0,25λ long and the output lines are 40 ohms 0,25 λ long.

Continuing with this investigation, results obtained with 40 ohm connecting lines 0,5 λ long and 50 ohm 0,25λ lines at the output are shown in 4.15 (a). Here the response is almost ideal. The response is more affected if the output lines are changed to 40 ohms and the interconnecting lines to 50 ohms. The lengths being the same as for the previous case. These results are shown in figure 4.15 (b).

From the results obtained, the most important factor appears to be the impedance of the output lines. If this impedance is poor, the effect is more enhanced by the presence of quarter wave transmission lines. The choice of lengths for the output and connecting lines was thus poor, although it was accidental. These results also show that the impedance of the lines is important, and great care must be taken in the fabrication of the circuit board layout.

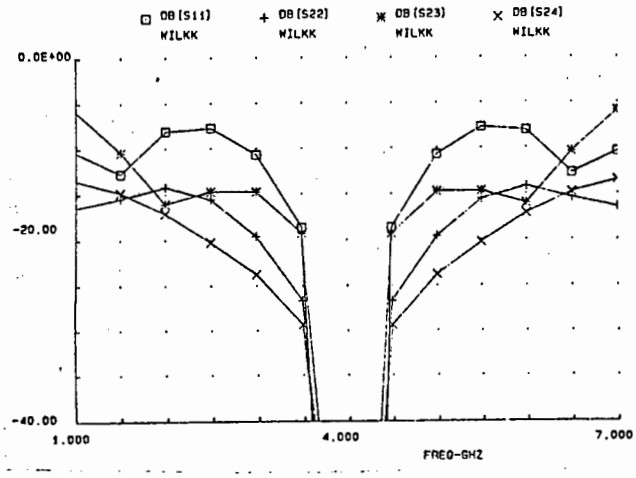

(a)

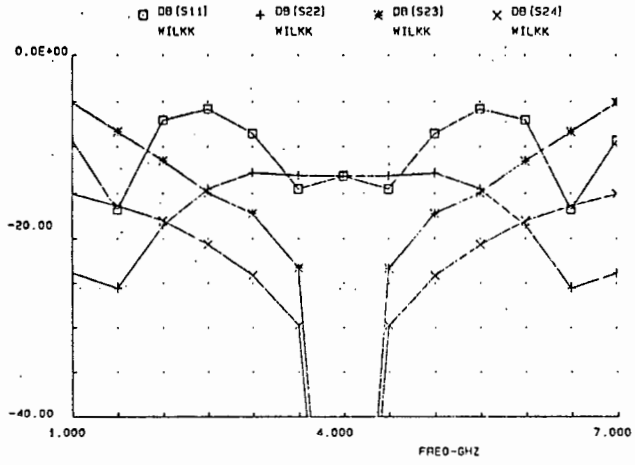

(b)

Fig. 4.15 (a) 0,5λ 40 ohm connecting lines; 0,25λ 50 ohm output lines (b) 0,5λ 50 ohm connecting lines; 0,25λ 40 ohm output lines.

Note that the results obtained show a match at 5GHz as opposed to 6GHz. The reason for this is the fact that the model on TOUCHSTONE used connecting transmission lines that were exactly a quarter of a wavelength long. However, on the actual device this length was 16mm, this is slightly longer than a quarter of a wavelength, which is 13,5mm. This would mean that the frequency at which the next multiple of a quarter wavelength occurs will be lower than the true frequency. To show this, the length of the connecting lines was changed to 106 degrees. The output lines were kept at 0,25λ and both output and connecting lines at 40 ohms. The results obtained are shown if figures 4.16 (a) and (b). From this figure it is noted that the upper frequency has shifted to 5,5GHz. Any further shift in frequency could be due to the fact that the effective dielectric constant changes with frequency. This means that the microstrip wavelength, λ_m, does not change linearly with frequency, and can therefore cause shifts in frequency. This effect is discussed in chapter 5.

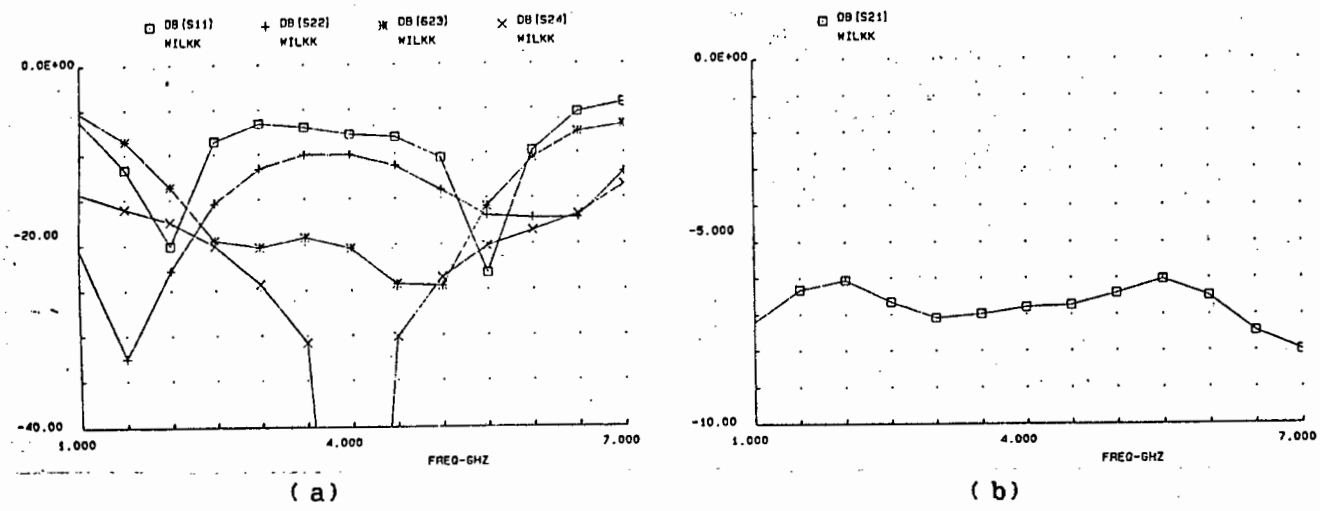

(a) (b)

Fig. 4.16 (a) Results for the 106 degrees 40 ohm interconnecting lines; 0,25 λ 40 ohm output lines (b) S_{21} for the same model.

As a result of the predictions obtained from TOUCHSTONE, it was decided that a second corporate divider be constructed which had no interconnecting transmission lines. The results obtained are discussed in the next section.

4.3.3 Results of the Second Version of the Corporate Wilkinson Combiner/Divider

The layout of the second version of the 4-way corporate combiner/divider is shown in figure 4.17. Here it will be noted that the 2-way Wilkinsons are connected directly to one another. Also note that meandering lines are required at the outputs to obtain equiphased outputs. Each of these lines is equal in physical length. Their positioning is controlled by the physical size of the SMA connectors and the fact that these connectors have to be placed in the same plane if the device is to operate as a combiner as well as a divider.

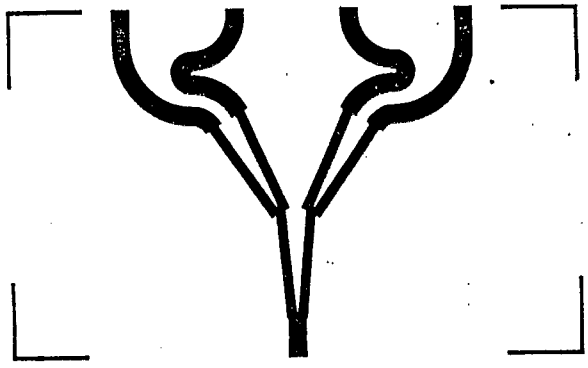

Dimensions as before.

Fig. 4.17 Layout of the second version of the 4-way combiner/divider.

The results obtained are best summarised by examining figures 4.18 through 4.21. Figure 4.18 shows the input match which occurs at 3,65GHz and has a return loss of 40dB. The centre frequency is slightly out because of the effect of the discontinuities found at the changes in line widths. Such a discontinuity changes the effective length of the transmission lines[32]. Figures 4.19 (a) and (b) show S_{21} and S_{21} with S_{31} respectively. The outputs tracked to within 0,2dB of one another. The insertion loss was found to be 0,3dB. The phase response, however, was not good with a difference of 10 degrees at 3,65GHz between S_{21} and S_{31}, which was the same as the difference between S_{41} and S_{51}. Note that the responses of S_{21} and S_{51} are the same, as are the responses for S_{31} and S_{41}. The phase discrepancy is most likely due to the sharp bend found in the paths for S_{31} and S_{41}.

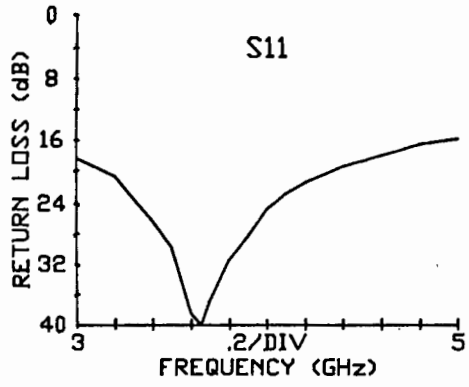

Fig. 4.18 Input match for the 4-way corporate combiner/divider.

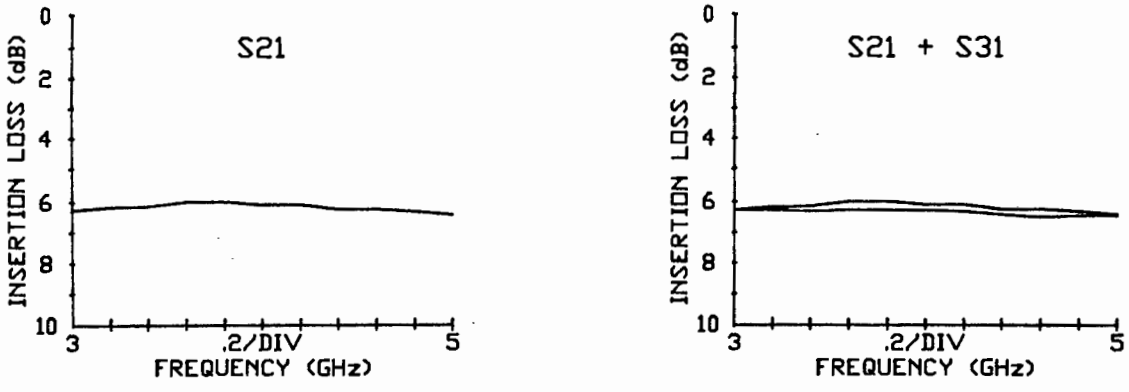

(a) (b)

Fig. 4.19 (a) S_{21} (b) $S_{21} + S_{31}$ for the corporate combiner/divider.

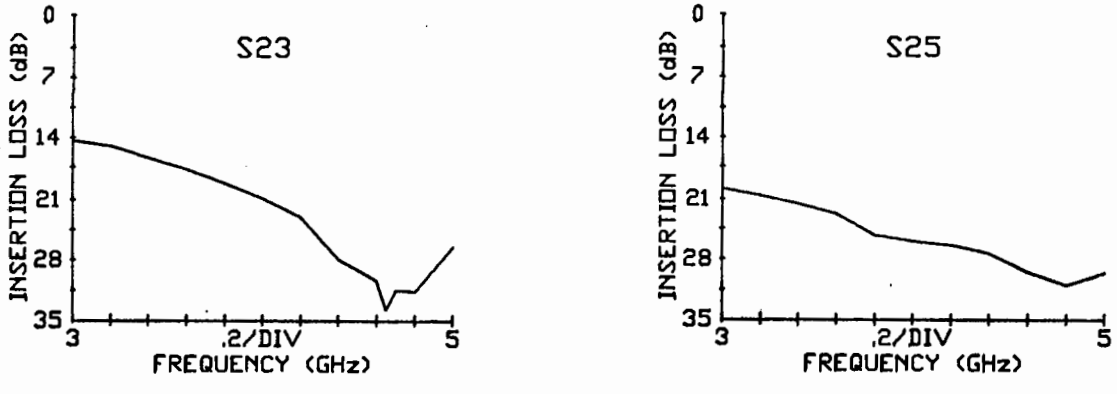

(a) (b)

Fig. 4.20 (a) S_{23} (b) S_{25} for the corporate combiner/divider.

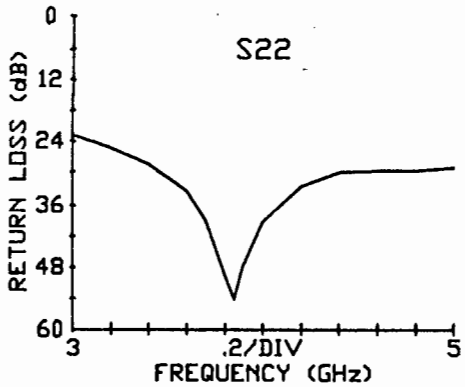

Fig. 4.21 S_{22} for the 4-way corporate combiner/divider.

This sharp bend probably causes some phase shifting, and also coupling probably takes place between the lines running parallel to one another. The phase error could be improved by making another device and reducing the bend curvature and increasing the distance between the lines. However, as the prime aim of this dissertation is the design of an 8-way combiner it was felt that the experience gained for this device will be put to better use in the design of the other combiners/dividers which will also have phasing problems to sort out. Figures 4.20 (a) and (b) show the isolation between ports 2 and 3 and ports 2 and 5. The centre frequency is shifted to around 4,5GHz. Once again this is ascribed to the physical lengths of the isolation resistor. The isolation, however, is good being around 30dB. Figure 4.21 shows the output match, S_{22}. The return loss was 54dB at 3,8GHz.

4.3.4 Conclusions

The corporate structure provides a method of increasing the number of devices that may be combined. This number, however, must be binary, a disadvantage in certain cases. The isolation between outputs is high, and as will be seen in the next chapter,

an advantage over the n-way versions to be discussed. The efficiency, however, is reduced as the number of devices to be combined increases.

CHAPTER 5 PLANAR N-WAY COMBINERS/DIVIDERS

5.1 Introduction

The most efficient power combiner reported to date is is the cylindrical resonant cavity combiner that has been shown to have a combining efficiency of 98 percent. This device is radial and therefore non-planar when used in a complete amplifier system. As it is non-planar, there are difficulties associated with heat dissipation. One way of overcoming this heat dissipation problem is to design a planar combiner/divider. Such devices are available, for example, the fork combiner/divider first described by Z. Gallani and S. Temple[24] and later analysed by A.A.M. Saleh[33]. However, these combiners/dividers are constructed on microstrip which is lossy and as a result low combining efficiencies are obtained.

This chapter discusses the fork-combiner/divider and deals with the various losses associated in the design. Loss in microstrip will be discussed. Various techniques for reducing this loss such as as a new stripline structure will be presented. Finally, an 8-way planar combiner/divider with a combining efficiency of 94 percent will be presented.

5.2 Microstrip

5.2.1 Introduction

Microstrip transmission lines consisting of a conductive ribbon attached to a dielectric sheet with conductive backing are widely

used in both microwave and computer technology. Because such lines are easily fabricated by printed-circuit manufacturing techniques they have undoubted economic and technical merits. The general geometry of microstrip is shown in figure 5.1. Prior to 1965 nearly all microwave equipment utilised coaxial,

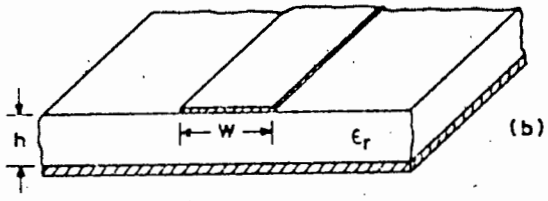

Fig. 5.1 General geometry of microstrip.

waveguide or stripline circuits. In recent years, with the advent of microwave integrated circuits, microstrip lines have been extensively used, for they provide one free and accessible surface on which solid state devices may be placed. The most important dimensional parameters are the microstrip width, w, and height, h, (equal to the thickness of the substrate). Also of importance is the relative dielectric constant of the substrate ε_r. The thickness, t, of the conducting strip is much less important and can often be neglected. Some properties and advantages of microstrip are as follows:

a) D.C. as well as A.C. signals may be transmitted.

b) The structure is rugged and can withstand moderately high power levels.

c) The line wavelength is much reduced because of the effect of the substrate dielectric. Hence distributed component dimensions are relatively small.

d) Active components such as FETs, can easily be incorporated.

There are two types of microstrip board available; these are hard and soft boards. Hard boards consist of a hard dielectric, gold plated on either side. The dielectics used are alumina, which has a dielectric constant of 10 and quartz which has a dielectric constant of 3,5.

The major disadvantage with these type of boards is that they are exceptionally hard and require special drilling and cutting tools, such as diamond tipped drills.

Approximately 20 years ago soft board was introduced. This was polyguide which had a dielectric constant of 2,33. The substrate was a PTFE (polyteraflouroethylene). At this stage of development, the copper was inclined to lift off the substrate on soldering and etching. This meant that the soft board did not catch on commecially and microstrip with alumina as the substrate continued to be used extensively. After 10 years 3M produced a better softboard, with dielectrics varying from 1,7 to 10. The board with the dielectric constant of 10 is often referred to as epsilam 10, and was primarily introduced as a substitute for the alumina hardboard.

Another firm, Rogers Engineering, also manufacture softboards - RTDUROID. Boards with a dielectric constant of 2,2 are referred to as RTDUROID 5880, those with a dielectric constant of 10, RTDUROID 6010. RTDUROID 5870 was developed to replace the polyguide board, and has a dielectric constant of 2,33.

5.2.2 Design Formulae for Microstrip

Various formulae are available to calculate the widths and lengths of line required on microstrip to give a specific impedance and transmission line length. The formulae used are quoted from T.C. Edwards[32]. The wavelength λ_m may be calculated using the formula

$$\lambda_m = \frac{\lambda_0}{\sqrt{\varepsilon_{eff}}} \qquad 5.1$$

where λ_0 is the wavelength in free space
and ε_{eff} is the effective relative dielectric constant of the substrate.

The effective relative dielectric constant is defined as the ratio of C/C_1 where C is the capacitance of the standard microstrip and C_1 is the capacitance of microstrip with the same dimensions but with a substrate consisting of air.

For known values of the characteristic impedance, Z_0, and relative dielectric constant, the following formulae may be used to determine the width of the line.

For narrow strips (ie. when $Z_0 > \{44 - 2\varepsilon_r\}$ ohms)

$$\frac{w}{h} = \left[\frac{\exp H}{8} - \frac{1}{4\exp H}\right]^{-1} \qquad 5.2$$

where

$$H = \frac{Z_0\sqrt{2(\varepsilon_r+1)}}{119,9} + \frac{1}{2}\left[\frac{\varepsilon_r-1}{\varepsilon_r+1}\right]\left[\ln\frac{\pi}{2} + \frac{1}{\varepsilon_r}\ln\frac{4}{\pi}\right] \qquad 5.3$$

and ε_{eff} is given by

$$\varepsilon_{eff} = \frac{\varepsilon_r+1}{2}\left[1 - \frac{1}{2H}\left[\frac{\varepsilon_r-1}{\varepsilon_r+1}\right]\left[\ln\frac{\pi}{2} + \frac{1}{\varepsilon_r}\ln\frac{4}{\pi}\right]\right]^{-2} \qquad 5.4$$

For wider strips (ie. when $Z_0 < (44 - 2\varepsilon_r)$ ohms

$$\frac{w}{h} = \frac{2}{\pi}\left[[d_e-1] - \ln[2d_e-1]\right] + \frac{\varepsilon_r-1}{\pi\varepsilon_r}\left[\ln[d_e-1] + 0,293 - \frac{0,517}{\varepsilon_r}\right] \qquad 5.5$$

where

$$d_e = \frac{59,95\pi^2}{Z_0\sqrt{\varepsilon_r}} \qquad 5.6$$

In all cases the shape ratio will be accurate to approximately 1 percent. For narrow lines ($w/h < 1,3$) ε_{eff} has the error range +0,5 - 0,0 percent. Equation 5.6 is accurate to 0,2 percent for $8 < Z_0 < 45$ ohms. Note that for microstrip having $t/h < 0,005$, $2 < \varepsilon_r < 10$ and $w/h > 0,1$ the effects of the strip thickness are negligible (within approximately 1 percent on Z_0 or ε_{eff}).

When the frequency of a signal exciting a microstrip line is doubled (say), the phase constant, $\beta = \frac{2\pi}{\lambda}$ is not exactly doubled. This effect is called dispersion. All microstrip lines are dispersive and it follows that the exact relationship between wavelength and frequency is very complicated. The fields are forced into the dielectric substrate to an increasing extent

as the frequency rises and as such a frequency dependent effective microstrip permittivity $\varepsilon_{eff}(f)$ may be defined. The limits of $\varepsilon_{eff}(f)$ are summarised below.

$$\varepsilon_{eff}(f) \longrightarrow \begin{cases} \varepsilon_{eff} & \text{as } f \longrightarrow 0 \\ \varepsilon_r & \text{as } f \longrightarrow \infty \end{cases}$$

Between the limits $\varepsilon_{eff}(f)$ changes continuously. This therefore means that in order to calculate the microstrip wavelength (λ_m) equation 5.7 must be used.

$$\lambda_m = \frac{c}{f\sqrt{\varepsilon_{eff}(f)}} \qquad 5.7$$

where $\varepsilon_{eff}(f)$ is given by

$$\varepsilon_{eff}(f) = \varepsilon_r - \frac{\varepsilon_r - \varepsilon_{eff}}{1 + \left[\frac{h}{Z_0}\right]^{1,33}\left[0,43f^2 - 0,009f^3\right]} \qquad 5.8$$

where h is in millimetres and f is in gigahertz. The estimated accuracy of equation 5.8 is approximately 0,8 percent. The above formulae were used for all microstrip designs and were implemented on a programmable calculator, the HP41C.

5.2.3 Losses in Microstrip

Power losses in microstrip can be split into three separate mechanisms: -

a) Conductor loss.

b) Dielectric loss, or dissipation of power in the dielectric of the substrate.

c) Radiation losses.

The first two items are dissipative whereas the last is parasitic. Both conductor and dielectric losses can be lumped together for the purposes of calculation and considered as an attenuation constant for a microstrip line.

a) Conductor loss

One expression for the conductor loss is

$$\alpha_c = \frac{0{,}072\sqrt{f}\lambda_m}{wZ_0} \quad \text{dB/microstrip wavelength} \qquad 5.9(a)$$

where the frequency f is in gigahertz and Z_0 in ohms.

In order to get equation 5.9 (a) in to a form that gives a loss in dB/m 5.9 (a) must be divided by λ_m. This then gives

$$\alpha_c = \frac{0{,}072\sqrt{f}}{wZ_0} \quad \text{dB/m} \qquad 5.9(b)$$

In practice equation 5.9 (b) gives somewhat low results and some account of surface roughness must be taken into account. In general the loss is increased by 60 percent when surface roughness is taken into account and equation 5.9 (b) modifies to

$$\alpha_c' = 1{,}6\,\alpha_c \qquad 5.10$$

b) Dielectric loss

The following expression gives the dielectric loss associated with microstrip.

$$\alpha_d = \frac{27{,}3\,\varepsilon_r(\varepsilon_{eff}-1)\tan\delta}{\sqrt{\varepsilon_r}(\varepsilon_r-1)\lambda_0} \quad \text{dB/m} \qquad 5.11$$

where λ_0 must be in metres and $\tan\delta$ is the loss tangent for the substrate material. The value used for $\tan\delta$ was 10^{-3} as this is the most general value. It varies with humidity and from substrate to substrate. However, the main objective is to see the effect various parameters have on the loss in microstrip, and for the frequencies of interest in the region of 4GHz. The dielectric loss is some ten times smaller than the conductor loss.

c) Radiation loss

Microstrip is an asymmetric transmission line structure and is often used in unshielded situations and as such is free to radiate. This means that there is further power loss.

In particular, discontinuities such as bends, steps and open ends, such as an open circuit will radiate to a certain extent. This radiation is however, small compared to the conductor and dielectric losses, at the frequencies of interest. The radiation loss also depends very much on the line widths, and for the most part they are quite narrow. In a later section, when the 8-way combiner/divider is discussed, radiation is considered in more detail, where it is shown that it is negligible for the board (RTDUROID 5880) used here.

The equations given for the various losses in microstrip were implemented on a programmable calculator and the results obtained are shown in figures 5.2, 5.3, 5.4 and 5.5. From these figures the main points to note are:

a) Loss increases with an increase in frequency; figure 5.2.

b) Loss increases with an increase in the relative dielectric constant ε_r; figure 5.3.

c) Loss decreases with an increase in h; figure 5.4.

d) Loss increases with an increase in impedance; figure 5.5.

Note that for a relative dielectric constant of 1, the dielectric loss, α_d, tends to zero. In general, however, a dielectric of 1 would be associated with air, in which case tanδ would be zero. The copper loss, α_c does not tend to zero unless w or Z_0 tend to infinity.

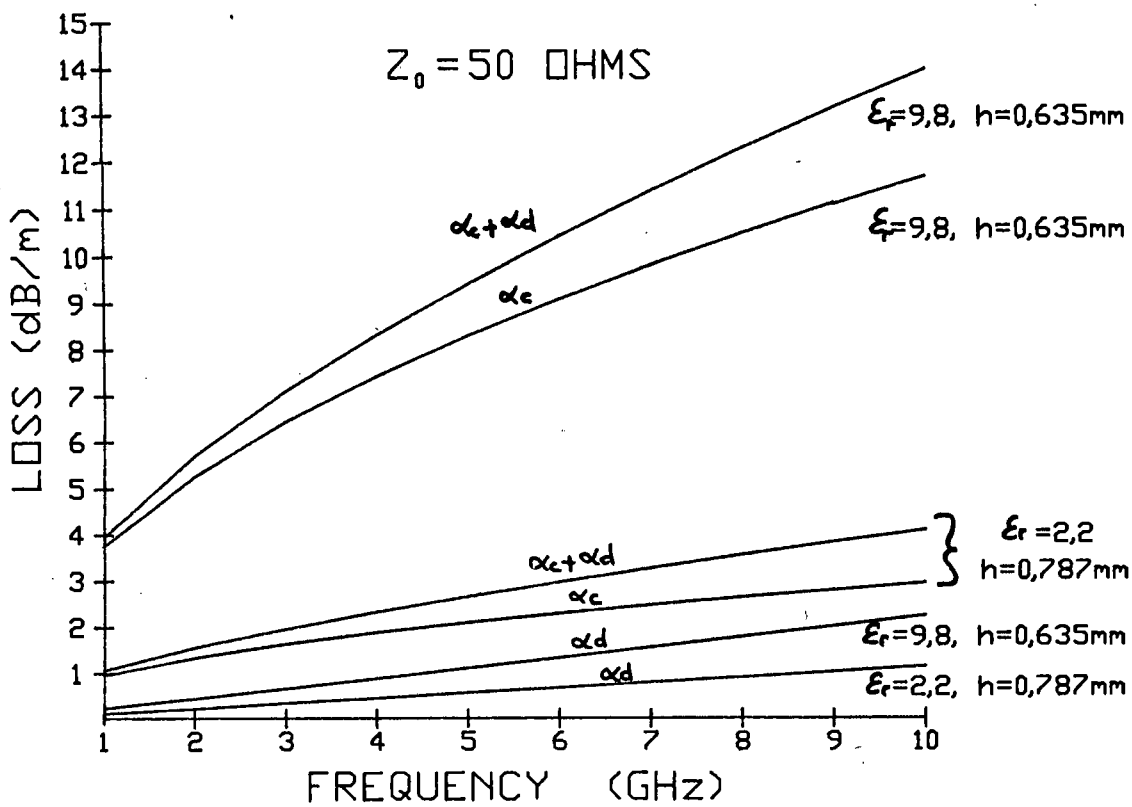

Fig. 5.2 Loss versus frequency.

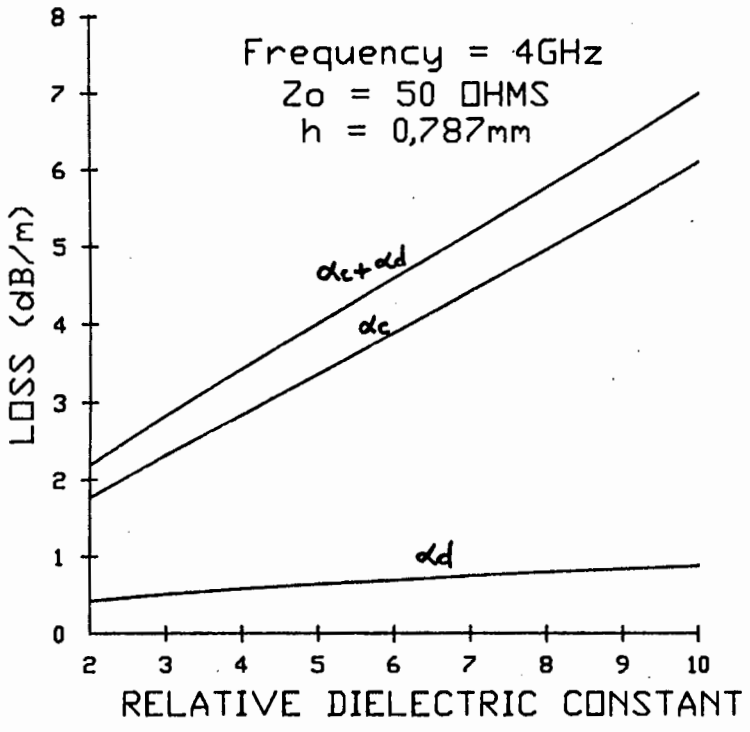

Fig. 5.3 Loss versus relative dielectric constant.

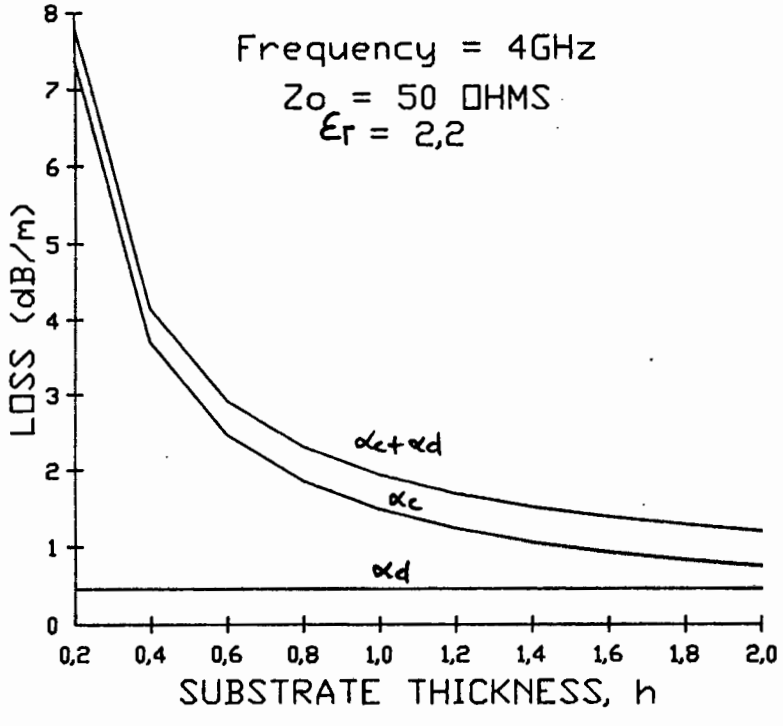

Fig. 5.4 Loss versus height, h.

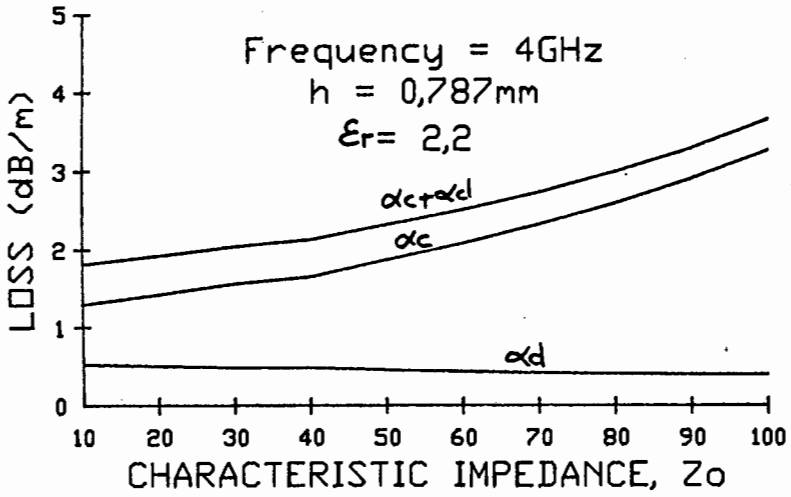

Fig. 5.5 Loss versus characteristic impedance.

The graphs do not take into account any radiation losses, because this loss depends very much on the type of line under consideration. If it is just a constant impedance line the radiation will be negligible in most cases. It is only at corners and step changes that radiation may become significant. A structure which prevents radiation is stripline and as a low loss planar combiner/divider is required this type of structure may be advantageous, especially if low dielectrics are to be used.

5.3 Stripline

Stripline shown in figure 5.6 used to be one of the most commonly used transmission lines at microwave frequencies. The mode of transmission is transverse electromagnetic (TEM), and the design data can be obtained completely by electrostatic analysis.

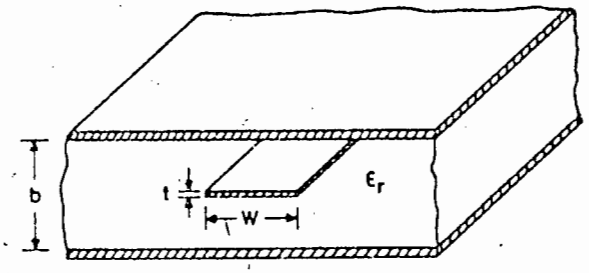

Fig. 5.6 Stripline structure.

5.3.1 Design Equations for Stripline

The design equations below are from K.C. Gupta et al[34].

For t, non zero

$$\frac{w}{b} = \frac{w_0}{b} - \frac{\Delta w}{b} \qquad 5.12$$

with

$$\frac{w_0}{b} = \frac{8(1-x)}{\pi}\sqrt{\frac{e^{\pi A}+0{,}568}{e^{\pi A}-1}} \qquad A = \frac{Z_0\sqrt{\epsilon_r}}{30\pi} \qquad 5.13$$

and

$$\frac{\Delta w}{b} = \frac{x}{\pi}\left[1 - \frac{1}{2}\ln\left[\left[\frac{x}{2-x}\right]^2 + \left[\frac{0{,}0796x}{\frac{w_0}{b} - 0{,}26x}\right]^m\right]\right] \qquad 5.14$$

where

$$x = \frac{t}{b} \qquad m = 2\left[1 + \frac{2}{3}\frac{x}{1-x}\right]^{-1} \qquad 5.15$$

5.3.2 Stripline Losses

These formulae are quoted for completeness and to show the relationship between the various parameters and the associated

loss. There are no radiation losses because of the shielding provided by the two ground planes. Therefore the total loss in stripline can be divided into two parts; the conductor loss and the dielectric loss.

$$\alpha_T = \alpha_c + \alpha_d$$

where α_T is the total loss, α_c the conductor loss and α_d the dielectric loss.

The dielectric loss for stripline (or any other TEM line) is given by

$$\alpha_d = 27{,}3\sqrt{\varepsilon_r}\,\frac{\tan\delta}{\lambda_0} \qquad \text{dB/m} \qquad 5.16$$

where $\tan\delta$ is the loss tangent of the dielectric. From this equation it is seen that the dielectric loss is directly proportional to the frequency and the loss tangent.

The conductor loss may be evaluated using the following relation,

$$\alpha_c = \frac{0{,}0231 R_s \sqrt{\varepsilon_r}}{Z_0}\left[\frac{\partial Z_0}{\partial b} - \frac{\partial Z_0}{\partial w} - \frac{\partial Z_0}{\partial t}\right] \qquad \text{dB/m} \qquad 5.17$$

where R_s is the sheet resistivity for the conductor and is given by $\sqrt{\pi\mu_0\rho f}$ with ρ being the resistivity of the conductor. In order to evaluate the above, an equation relating Z_0 with the parameters b, w and t is required. This is given by

$$Z_0\sqrt{\varepsilon_r} = 30\ln\left[1+\frac{4}{\pi}\frac{b-t}{w}\left[\frac{8}{\pi}\frac{b-t}{w}+\sqrt{\frac{8}{\pi}\left[\frac{b-t}{w}\right]^2+6{,}27}\right]\right] \qquad 5.18$$

where

$$\frac{w'}{b-t} = \frac{w'}{b-t} + \frac{\Delta w}{b-t} \qquad 5.19$$

and

$$\frac{\Delta w}{b-t} = \frac{x}{\pi(1-x)}\left[1 - \frac{1}{2}\ln\left[\left[\frac{x}{2-x}\right]^2 + \left[\frac{0,0796x}{\frac{w}{b}+1,1x}\right]^m\right]\right] \qquad 5.20$$

where m and x have been previously defined.

Equation 5.17 shows that the conductor loss is directly proportional to the square root of frequency for a particular stripline structure. In general, the dielectric loss is small compared to the conductor loss at microwave frequencies. But at millimeter waves it becomes comparable to the conductor loss because dielectric loss increases linearly with frequency, whereas conductor loss is proportional to the square root of frequency. The loss in stripline will vary much the same as microstrip with variations in the various parameters. Discrete differentiation would be required to solve for $\frac{\partial z_0}{\partial b}$, $\frac{\partial z_0}{\partial t}$ and $\frac{\partial z_0}{\partial w}$ if a large amount of arithmetical work is to be avoided. Gupta et al do have an equation which gives the conductor loss directly, however, there seems to be a printing error as the results obtained using it were nonsensical.

Figure 5.7 gives the variation of loss in stripline with frequency. Tan δ was chosen to be 10^{-3} as before and the differentiation was carried out in discrete steps on a programmable calculator.

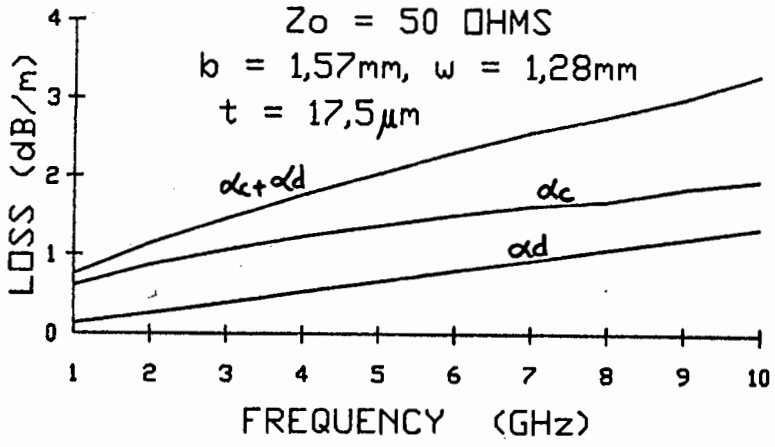

Fig. 5.7 Loss in stripline versus frequency.

From this graph it is seen that the variation of loss with frequency in stripline is similar to that found in microstrip structures. The values are slightly lower for the stripline structure, however, as the equations come from different sources, and in the case of microstrip are empirical, the two cannot be numerically compared. The trends are more important at this stage.

Practical results obtained for the loss in both stripline and microstrip will be given in a later section, where methods of reducing loss in these structures are discussed.

5.4 Planar N-way Combiner/Divider

The n-way planar combiner/divider that was considered to be the most promising was the fork combiner/divider proposed by Z. Gallani and S. J. Temple[24]. Figure 5.8 gives a schematic of the device. The input is split into n identical transmission lines of characteristic impedance Z_0, each a quarter of a wavelength long at the centre frequency. Adjacent output ports

are interconnected with equal resistors R_0. Analysis of this type of combiner was carried out by A. A. M. Saleh[33].

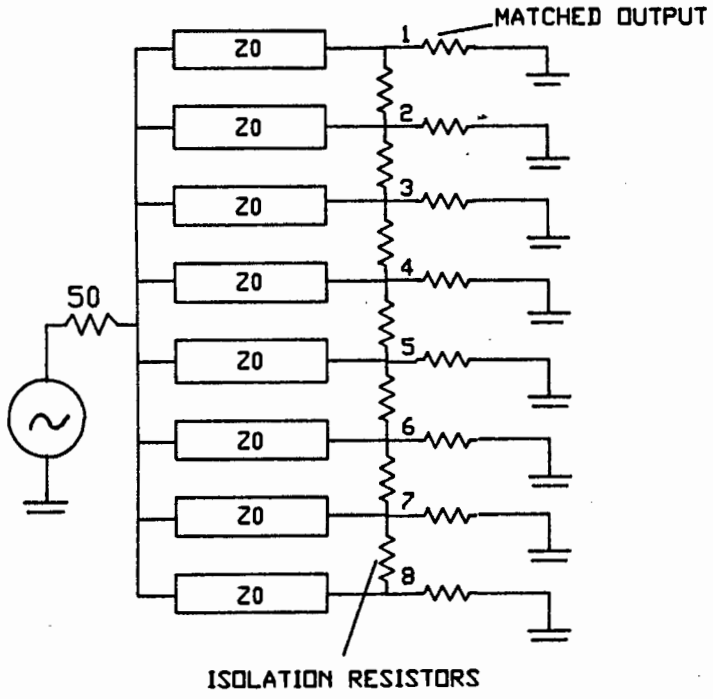

Fig. 5.8 Planar n-way combiner/divider.

5.4.1 Design of a Planar 4-way Combiner/Divider

In order to obtain a perfect match (consider the device as a divider unless otherwise stipulated) an input impedance of 50 ohms is required. Therefore the characteristic impedance Z_0 must be chosen so that

$$50 = \frac{Z_0^2}{nZ_{in}} \qquad 5.21$$

where Z_{in} is the output load, 50 ohms, and n is the number of ways the input is to be split. Therefore 5.21 reduces to

$$Z_0 = 50\sqrt{n} \qquad 5.22$$

The isolation resistors are chosen to give the best isolation between the output ports. According to the analysis carried out by Saleh[33] this would give a value of 70,7 ohms for a 4-way combiner/divider. The optimum isolation that would result is quoted as 14,5dB. For a four way version of figure 5.8, a characteristic impedance of 100 ohms would be needed for the quarterwave transformers. Although a transmission line of this impedance is relatively narrow it is still possible to etch. However, practically it is not ideal because of the step transition that would result at the 100/50 ohm transmission lines found at the output ports. This transition is from a width of 0,70mm for the 100 ohm line to 2,46mm for the 50 ohm line. Which would cause discontinuity problems. To overcome this, it is necessary to choose a lower impedance for the quarterwave transformers. A value of 70 ohms is a fairly good one to start with because the discontinuity effects with its previous use were acceptable. With 70 ohm transmission lines a further quarterwave transformer is required to transform the parallel combination to 50 ohms. The layout therefore used for this combiner/divider is shown in figure 5.9.

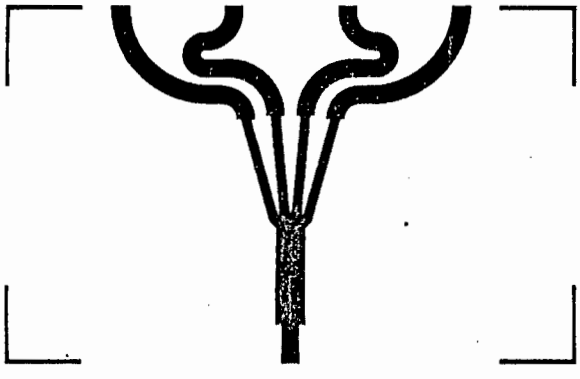

Dimensions

50 ohm as before

70 ohm w = 1,41mm

λ_m (at 4GHz) = 55,3mm

35 ohm w = 4,00mm

λ_m = 53mm

Fig. 5.9 Layout of the 4-way fork combiner/divider.

With the layout in figure 5.9, it was assumed that the isolation resistors may no longer be optimum. It was decided to model the combiner/divider on TOUCHSTONE, and optimise the circuit to give the best isolation possible by only varying the value of R_0. The value indicated by TOUCHSTONE was 80 ohms. Figures 5.10 (a) and (b) give the expected response for the combiner/divider shown in figure 5.9. Figure 5.11 shows the isolation between the output ports. From figure 5.10 (a) it is seen that the addition of a quarter wavelength at the input has the effect of increasing the bandwidth, with S_{11} being better than 15dB over the band 2,0 to 6,0GHz. The addition of this quarter wavelength section is in some ways similar to adding another section to broaden the bandwidth, a technique commonly used on Wilkinson combiners to obtain octave bandwidths. A. Saleh[33] gives an analysis on the two stage combiner. Note that these extra stages, although having the effect of increasing the bandwidth also increase the loss and hence decrease the efficiency of the combiner. Returning to figure 5.10 (a), it is also seen that the output match of S_{22} and S_{33} is 17dB at 4GHz (the centre frequency). Only two output matches are given due to the symmetry of the device. The isolation resistors control this parameter as well as the isolation, so a compromise must be taken. In general, the better the output matches, the better the isolation. Figure 5.10 (b) gives the expected through transmission, and as shown is flat over the band 2,0 to 6,0GHz. The poorest isolation is 15dB and occurs between ports 2 and 5. This is shown in figure 5.11

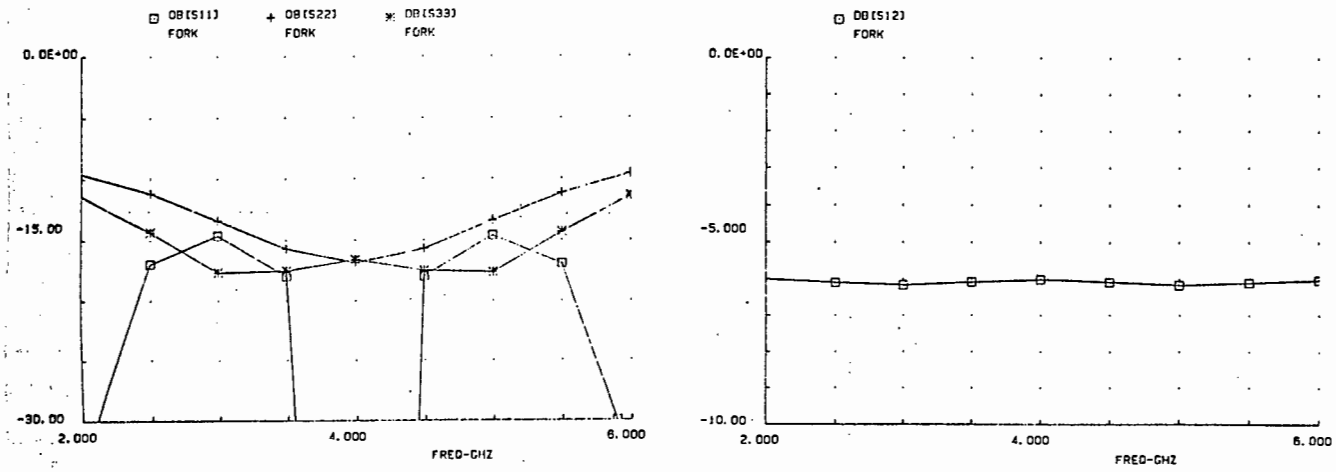

(a) (b)

Fig. 5.10 (a) Predicted S_{11}, S_{22} and S_{33} for the 4-way fork combiner/divider (b) Predicted S_{21} for the fork combiner/divider.

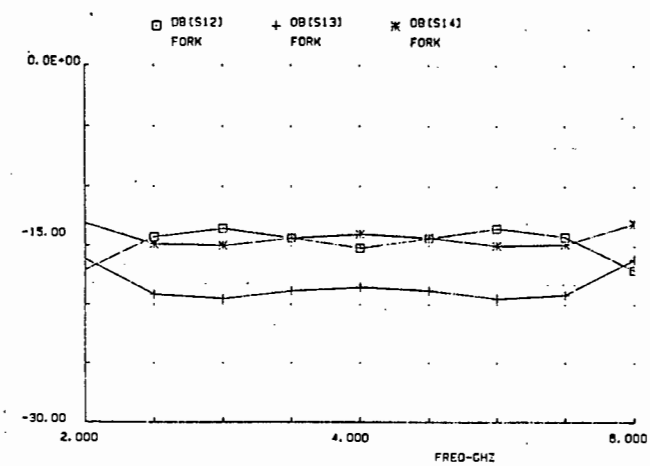

Fig. 5.11 Predicted S_{23}, S_{24} and S_{25} for the combiner/divider. (Because of TOUCHSTONE circuit layout S_{23}, S_{24} and S_{25} correspond to S_{12}, S_{13} and S_{14} shown on the diagram.)

With the predicted results looking promising the combiner/divider was constructed on microstrip (RTDUROID 5880) and analysed. The results are shown in figures 5.12 to 5.15. Figure 5.12 gives the

input match. The input return loss is 32,7dB at 4.1GHz. And the response is similar to that predicted by TOUCHSTONE, with best matches occuring at 2,8 and 5,8GHz. Over the frequency range 2,3 to 6,0GHz the return loss is better than 14,0dB (VSWR of 1,5).

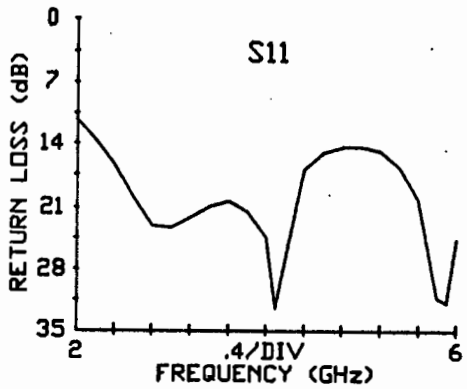

Fig. 5.12 Input match of the 4-way combiner/divider.

Figures 5.13 (a) and (b) show a return loss of 12dB at 4,0GHz for S_{22} and 20,6dB for S_{44}. The return loss for S_{44} is better than predicted and for S_{22} is worse. The reason for this departure from the predicted results is the use of chip resistors that were not 80 ohms. This particular value was not readily available, and as a result 100 ohm resistors were used. The variations in the match and isolation were shown by TOUCHSTONE not to be too dramatic and this is born out by the results obtained. It must be emphasised at this stage, that the prime objective is an eight way combiner/divider and these devices are a build up to this design, experience being one of the prime objectives.

Figures 5.14 (a), (b) and (c) show the isolations obtained between various ports. The worst isolation occurs between ports 2 and 5, and is 15,1dB at 4GHz. The other isolations are better as can be seen from the figures. These results could be improved by using the correct isolation resistor as already mentioned.

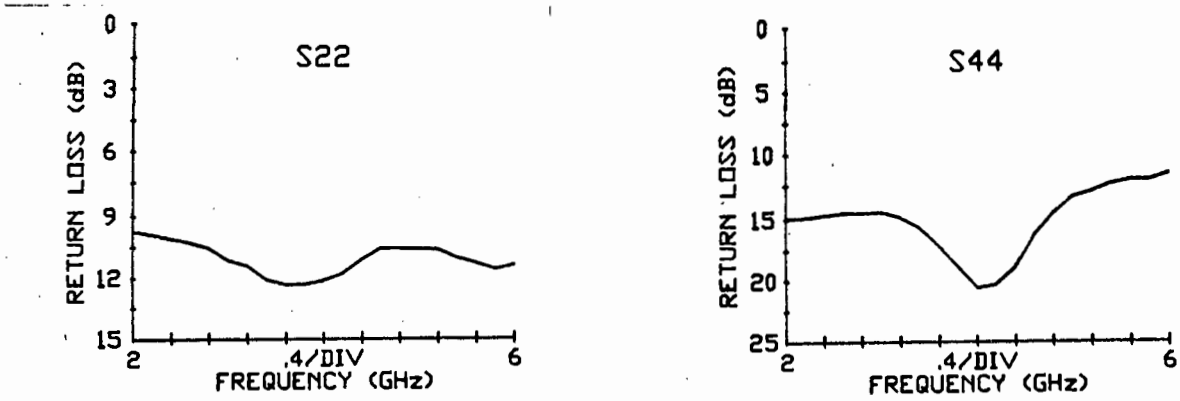

(a) (b)

Fig. 5.13 (a) S_{22}, (b) S_{44} for the 4-way combiner/divider.

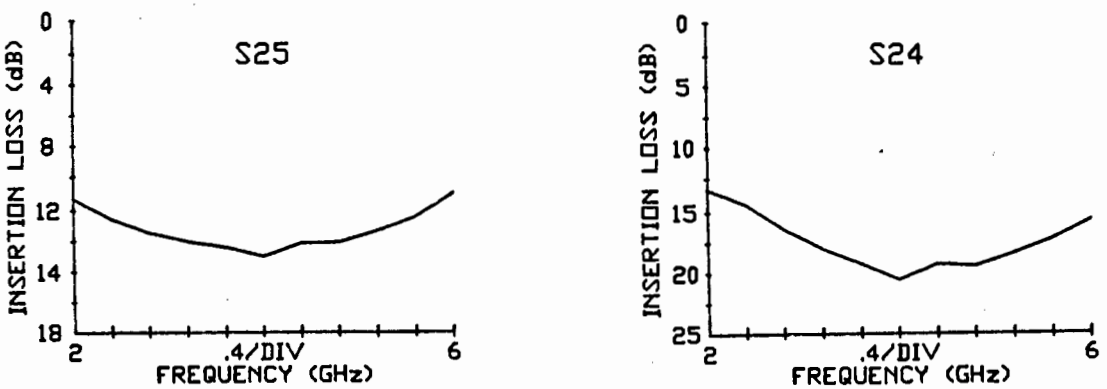

(a) (b)

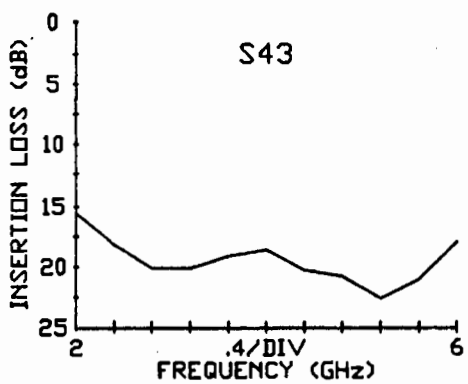

(c)

Fig. 5.14 (a) S_{25}, (b) S_{24} and (c) S_{43} for the 4-way combiner/divider.

Figures 5.15 (a), (b), (c) and (d) show the insertion losses obtained. From these figures it can be seen that the split is fairly even, with a maximum variation between ports of 0,4dB. The insertion loss with respect to 6dB measured at 4.1GHz is 0,3dB which results in a combining efficiency of 93,3 percent. This efficiency assumes of course that the phase variation between ports is not too large, ideally less than 5 degrees. Unfortunately, the phase response for this device was not very good at all. The phase error at 4GHz was 8 degrees. Note that this error occurs between ports 2 and 3 and between ports 4 and 5. The phase response between 2 and 5 being within 2 degrees over the whole band. This is also true between ports 3 and 4 which immediately indicates that the path lengths must be different.

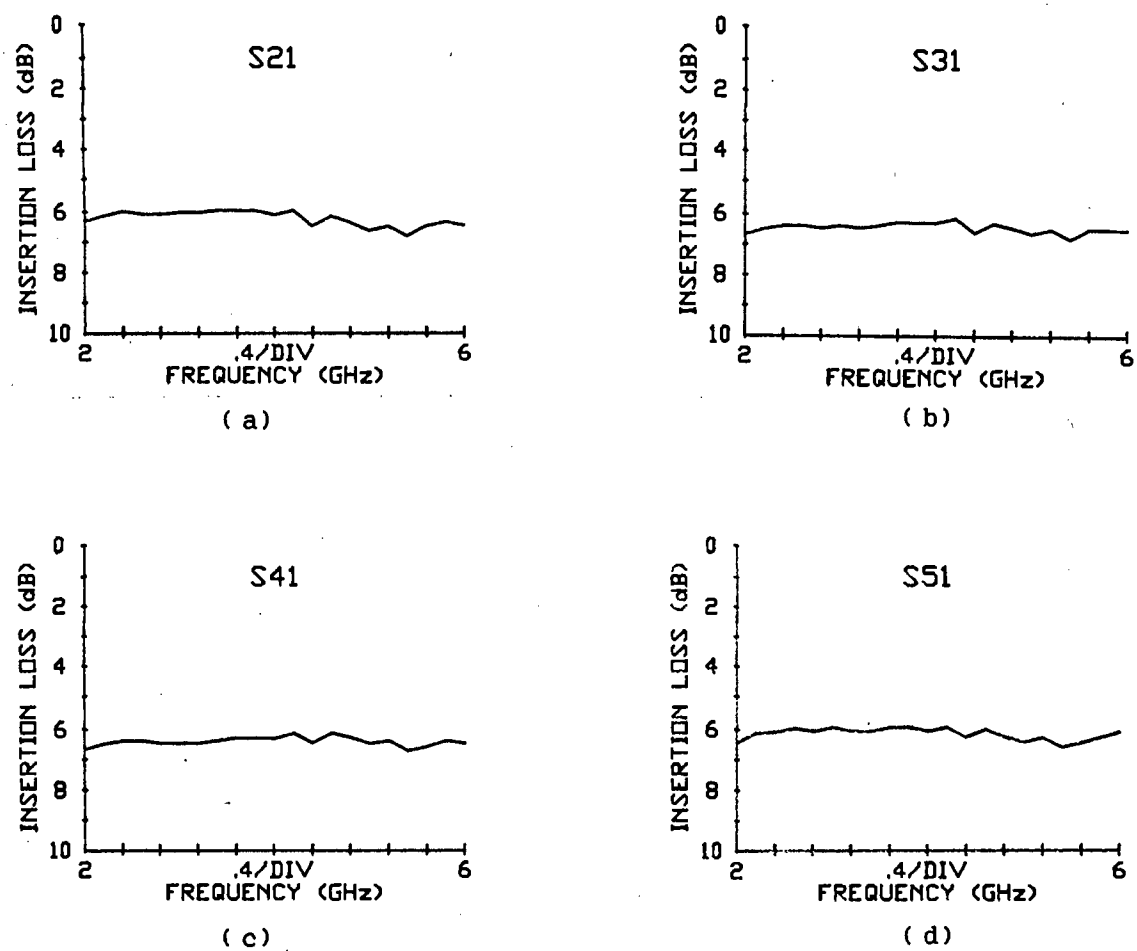

Fig. 5.15 (a) S_{21}, (b) S_{31}, (c) S_{41} and (d) S_{51}.

On examining the layout shown if figure 5.9 it is seen that the physical length is exactly the same. The only difference between the paths is the difference in meandering. As with the case mentioned for the corporate Wilkinson, the bends produce some phase variations. It is also possible that coupling occurs at the sharp bend where the line turns to run parallel with itself. At this stage it is important to try and find out where these phase discrepancies occur, especially if an eight way combiner/divider is to be constructed. It was decided to make another 4-way fork combiner on the same lines as this one, but change the layout of the meandering transmission lines at the output. The bends will be made shallower in an attempt to reduce any phase variations that could occur in a bend, and secondly make sure that the lines are separated by more than one line width to reduce any coupling that might be present. This was done, and the layout of the second 4-way combiner is shown in figure 5.16.

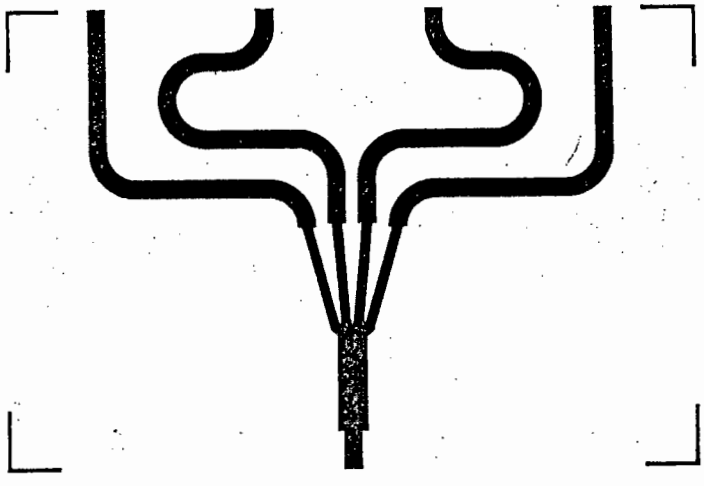

Dimensions as before.

Fig. 5.16 Layout of the second version of the 4-way fork combiner/divider.

From the layout it is seen that each of the bends have a much larger radius and that the lines are more separated. The results

obtained for this device are shown if figures 5.17, 5.18 and 5.19. Figure 5.17 shows the input return loss obtained with the best input match occurring at 5,2 GHz with a return loss of 24,2dB. This is probably the upper frequency match as predicted by TOUCHSTONE. The match is better than 15dB over the frequency range 2.5GHz to 6,4GHz. The output match for port 3 is given in figure 5.18 (a) and the isolation between ports 2 and 4 is shown in figure 5.18 (b). The through transmission measurements are shown in figure 5.19.

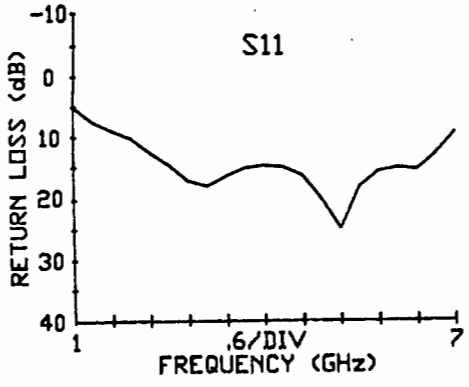

Fig. 5.17 Input match of the second version of the combiner/divider.

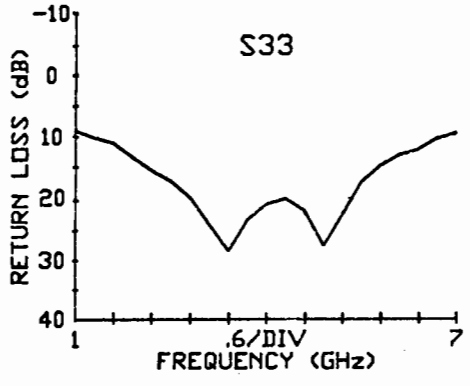

(a)

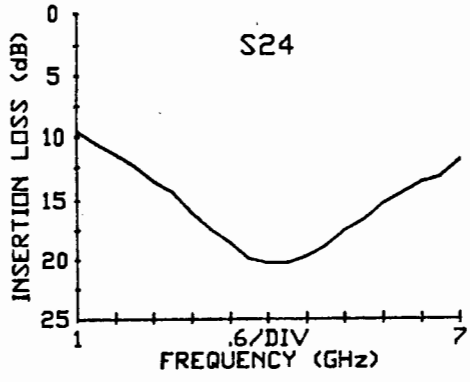

(b)

Fig. 5.18 (a) S_{33} and (b) S_{24} for the second version of the combiner/divider.

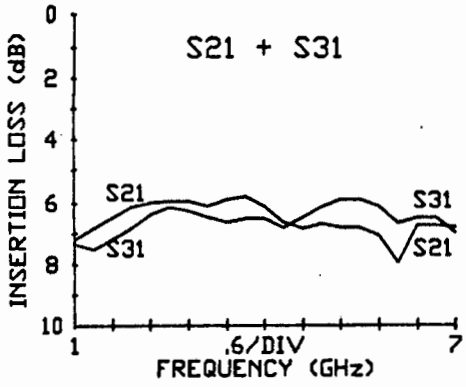

Fig. 5.19 S_{21} and S_{31} for the second combiner/divider.

These do not track as well as for the other combiner. The only reason for this can be the effect of the bends being transferred to the input and creating different loads, and as such changing the split. These effects probably also cause the other differences noted, as the only difference between the two combiners is the meandering lines. These lines were changed in an attempt to get the phase correct. The phase, however, does not track well. This can be seen from figure 5.20, where the maximum phase error is 41 degrees at 7GHz. It is 8 degrees at 1GHz.

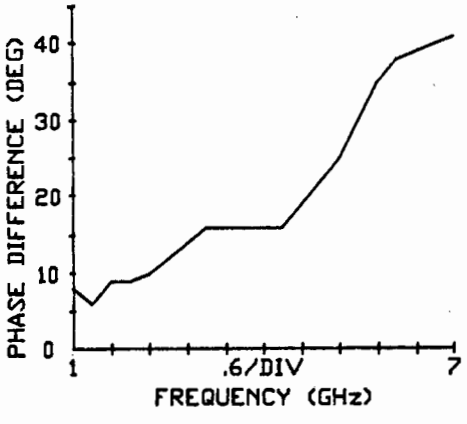

Fig. 5.20 Phase variation between ports 2 and 3.

As the physical lengths are the same, there must be phase errors introduced at some point. Coupling is obviously not a factor as the lines are too widely spaced. This leaves two possibilities. Either the phase errors are introduced by the curved bends, or they are introduced at the split, i.e. at the input port. By this, it is meant that the wave travelling to the outside branches might travel a further distance than the one travelling to the inside branches.

It has been suggested by Edwards[32] that for at least up to a frequency of about 10GHz, a mitred bend produces as good as, or better, performance than curved bends. It was decided therefore, to fabricate a combiner/divider that had mitred 90 degree bends for the meandering lines. One advantage with this is the ease of calculating the physical lengths and thus enabling all the lengths to be the same in a prescribed space. It was also hoped that the phase error may be reduced. The layout of this combiner/divider is shown in figure 5.21.

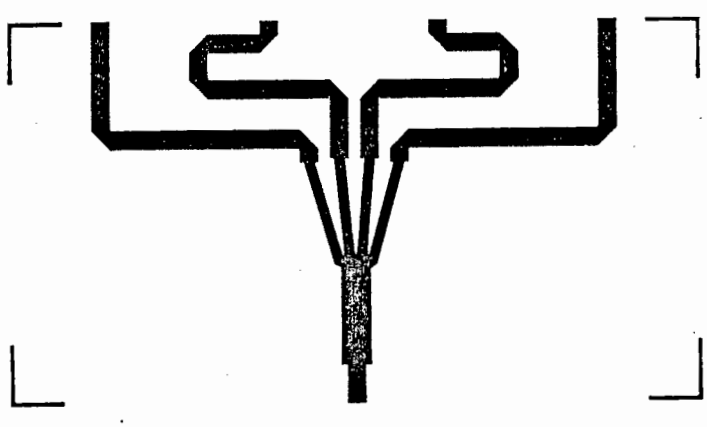

Fig. 5.21 The layout of the third version of the 4-way fork combiner/divider.

The results obtained for the through measurements are shown in figures 5.22 (a) and (b). Figure 5.22 (a) shows S_{21} and 5.22 (b) shows S_{21} and S_{31} superimposed on one another. From this figure it is seen that the outputs are fairly equal as regards amplitude. The maximum variation is 0,4dB which occurs at 6,7 GHz. Once again the phase response was poor. The difference in phase between ports 2 and 3 is shown in figure 5.23. This variation is the same as for ports 4 and 5. The other results obtained were similar to those obtained for the previous combiner/divider. The phase variation was, however, a factor of two better than for the previous combiner/divider, which tends to indicate that mitred corners are better than curves in this frequency range.

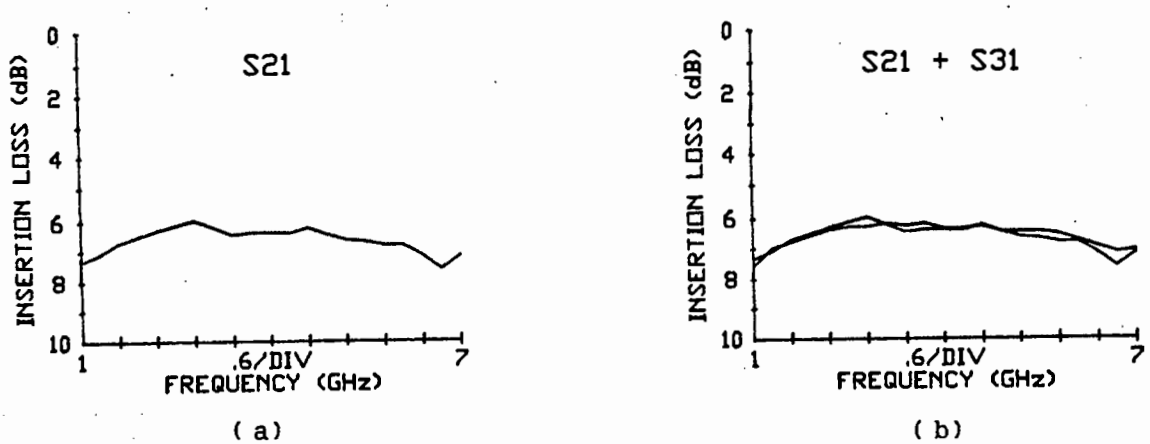

Fig. 5.22 (a) S_{21} (b) S_{21} and S_{31} for the third version of the 4-way combiner/divider.

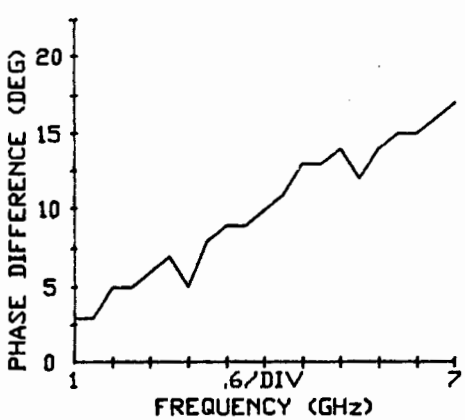

Fig. 5.23 Variation in phase between ports 2 and 3.

At this stage it was decided to make a four way divider without any 50 ohm lines at the output and no isolation resistors so that it could be determined whether a phase difference occurs before the output lines are added. The layout of the circuit is shown in figure 5.24. Note that the only major difference is the absence of meandering lines at the output and as a result the connectors are not in the same plane.

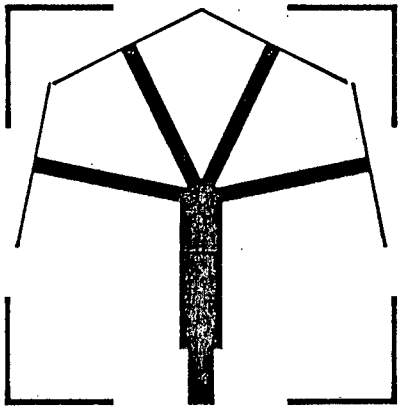

Fig. 5.24 Layout of the 4-way combiner to determine if any phase variation exists before meandering.

The results obtained for this layout are shown in figure 5.25.

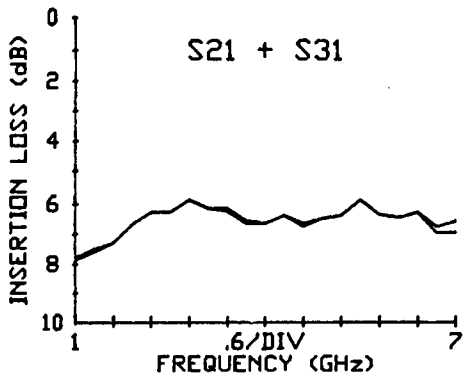

Fig. 5.25 S_{21} and S_{31} for the device.

The outputs track very well as can be seen from figure 5.25. The phase variation, as shown in figure 5.26, was however, poor. This immediately implies that this error must be introduced at the point where all the quarter wave transmission lines meet. In

other words, the width at this point is large, and as such must cause the variations in phase. It is also likely that the bends also introduce some phase variation.

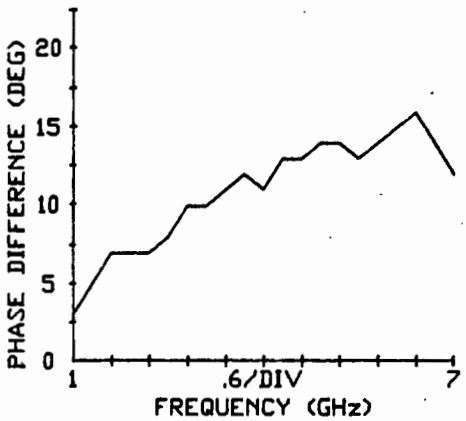

Fig. 5.26 Phase variation between ports 2 and 3 of this "combiner/divider".

From figure 5.26 it is seen that at 4GHz the phase variation is 10 degrees. This corresponds to a physical length of 1,5mm. As the outputs should ideally be in phase at 4GHz, it was decided to incorporate the difference of 1,5mm in the output lines. The outer lines were made 1,5mm shorter. The final layout of the fork combiner divider is shown in figure 5.27(a). Figure 5.27(b) is a photograph of the same device, as well as version two.

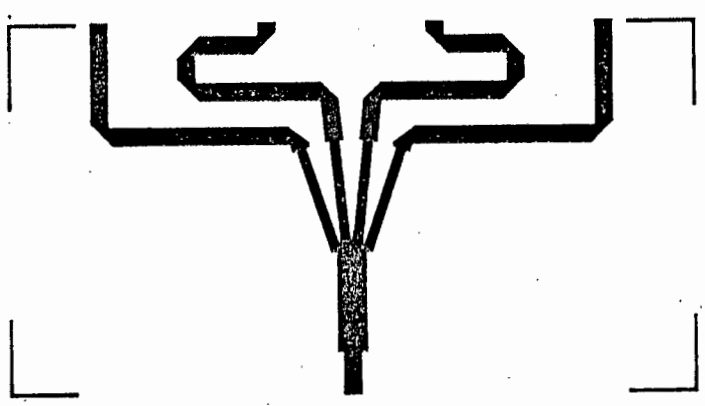

Fig. 5.27 (a) Layout of the 4-way fork combiner/divider.

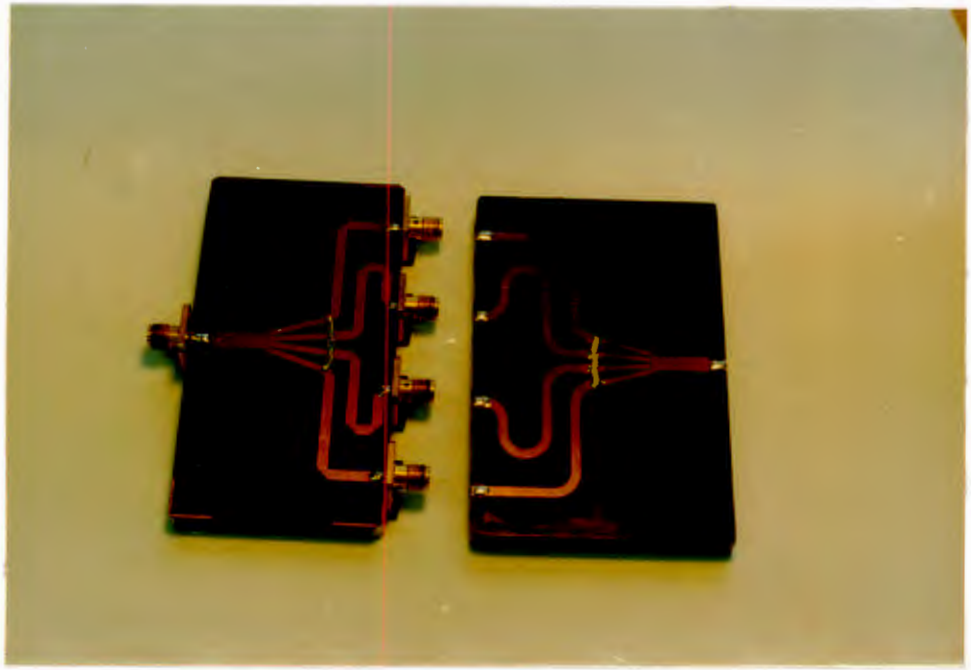

Fig. 5.27 (b) Photograph of two of the the 4-way combiners/dividers that were constructed.

The results obtained for this combiner/divider were once again very similar to those obtained previously. Figure 5.28 shows S_{31}. The average insertion loss with respect to 6dB is 0,4dB. Figure 5.29 gives the phase variation between ports 2 and 3.

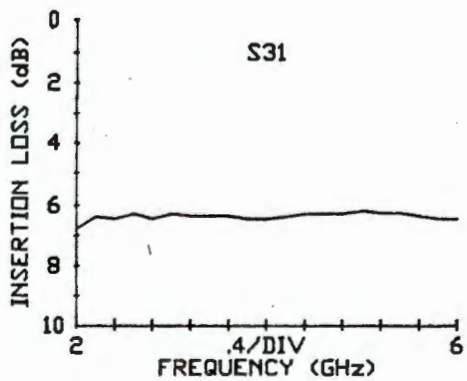

Fig. 5.28 S_{31} of the combiner/divider.

From this figure it is seen that the worst phase variation is 3 degrees. The isolation obtained is shown in figures 5.30 (a) and (b), S_{11} is shown in figure 5.31 (a) and S_{33} is shown in figure 5.31 (b). Note that S_{11} is not as good as that obtained

previously, however, the return loss is better than 14dB over the frequency range 2,5 to 6,0GHz. The poorer match is ascribed to

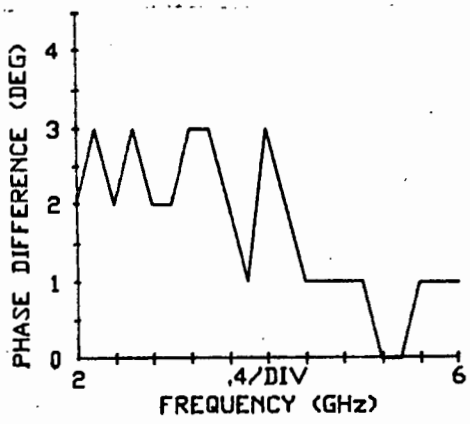

Fig. 5.29 Phase variation between ports 2 and 3

the slightly different impedances that might be presented at the outputs due to the bends. These impedances would then be transformed to the input and therefore cause a slight mismatch. The match however, is good enough. The good match at 6GHz is expected, refer to the ideal response of the combiner/divider. S_{22} is very much the same as for the other combiners/dividers.

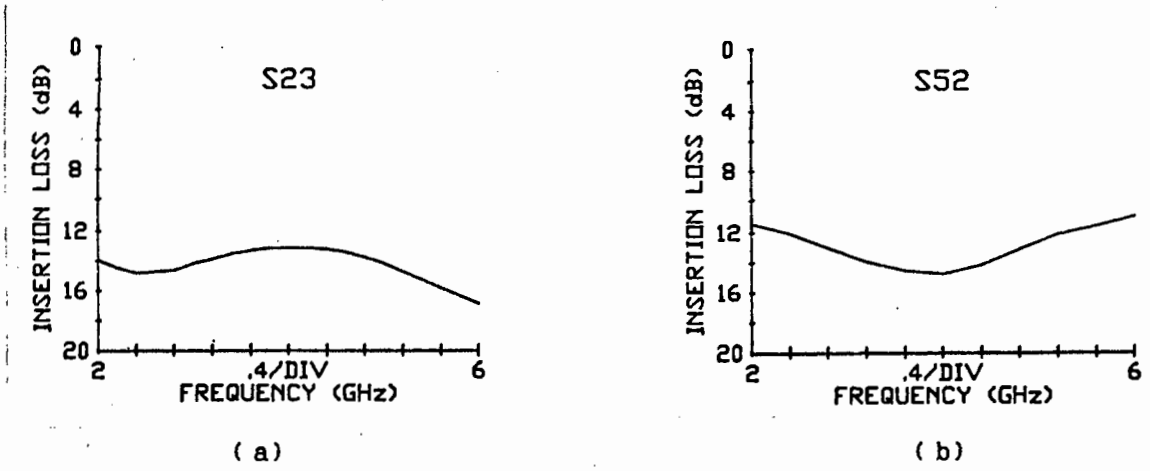

Fig. 5.30 (a) S_{23} (b) S_{32} for the 4-way combiner/divider.

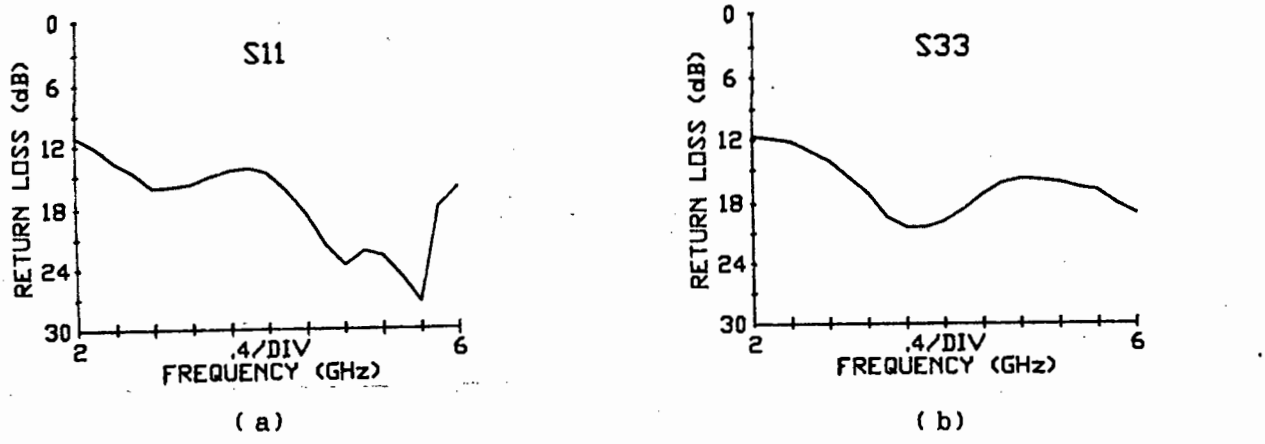

(a) (b)

Fig. 5.31 (a) S_{11} (b) S_{33} for the 4-way combiner/divider.

5.4.2 Conclusions

The final results obtained for the planar 4-way combiner/divider were satisfactory. Equiphased outputs on these combiners/dividers seem to be a problem, and it is difficult to estimate the change in lengths required to compensate. The experience gained however, should prove useful in the design of an 8-way combiner/divider along the same lines. Apart from this problem, the combiner/divider provides an easy method for power combination/division and is planar. The measured combining efficiency for the latter combiner is 90 percent. It is felt that this could be improved upon with improved construction. The combining efficiency is very similar to the 4-way corporate Wilkinson combiner which is expected because the path lengths are very much equal for the two combiners. However, a 5-way could be easily built with very much the same efficiency in the case of the fork combiner, but not in a corporate structure, as 5 is a non binary number.

the above type should be attempted. Once this has been fabricated in microstrip, attempts at increasing the combining efficiency will be looked into if the results obtained look promising.

5.5 An 8-Way Planar Combiner/Divider

5.5.1 Design of the Combiner/Divider

For an 8-way combiner/divider the characteristic impedance of the quarter wave transformers would have to be 141,4 ohms. Once again this impedance is too high, as the line widths would be 0,29mm, which is too narrow for the etching process and would introduce large discontinuities at the 50 ohm to 141,4 ohm junction found at the outputs. For this reason a quarter wave section is added at the input so that the impedance of Z_0 may be altered. A value of 100 ohms was chosen for the 8 quarter wavelength transmission lines. This value still gives a fairly large discontinuity at the output, but allows a reasonable value for the characteristic impedance for the input transformer of 35,35 ohms. The layout of the combiner/divider is shown in figure 5.32 (a). Figure 5.32 (b) shows a photograph of the combiner/divider.

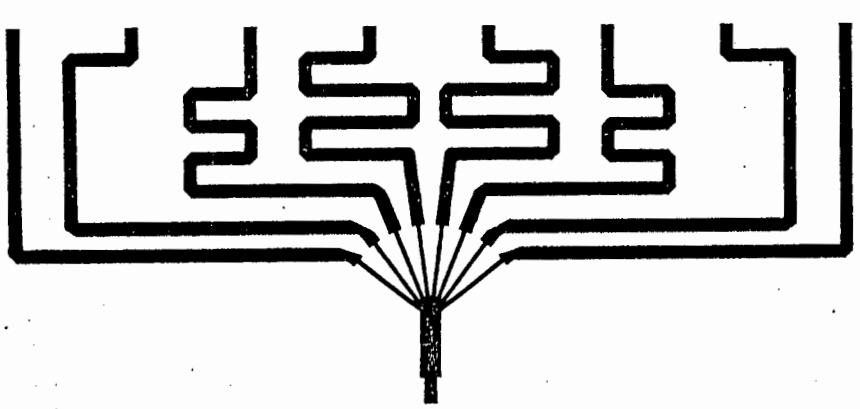

Dimensions

50 ohms as before

100 ohms w = 0,7mm

λ_m (at 4GHz) = 56,4mm

35,35 ohms w = 3,94mm

λ_m (at 4GHz) = 53,0mm

Fig. 5.32 (a) The layout of the 8-way combiner/divider.

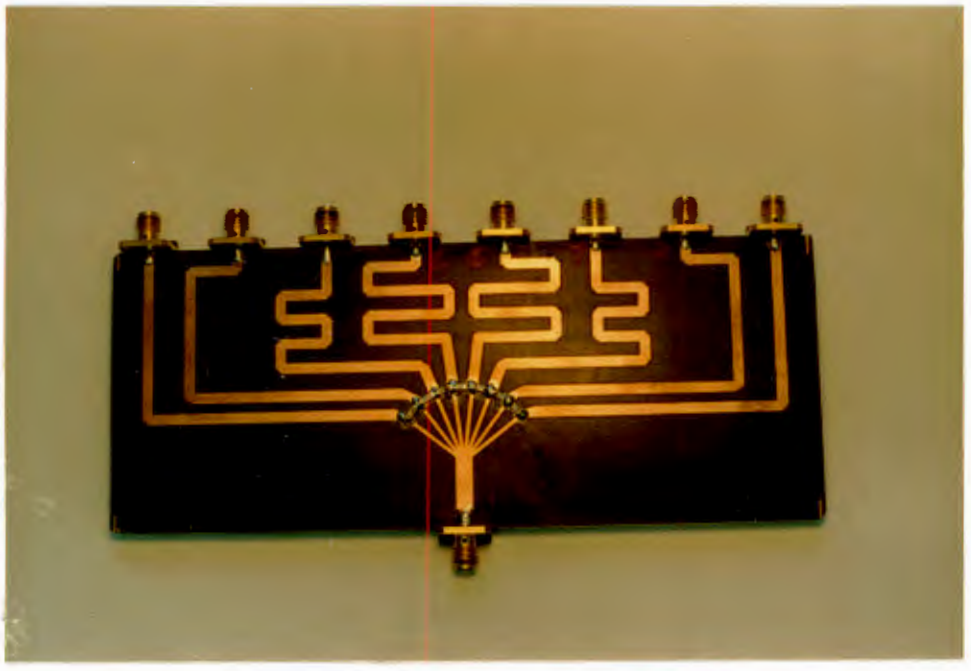

Fig. 5.32(b) A photograph of the 8-way combiner/divider.

The circuit as shown in figure 5.32 (a) was modeled on TOUCHSTONE using ideal transmission lines. Firstly, TOUCHSTONE was used to optimise the value of the resistors. A value of 65 ohms was found to be optimum. The value that A. Saleh[33] recommends is 85 ohms. The difference in value is due to the fact that his analysis is for a combiner/divider that does not have a quarter wave transformer at the input. The predicted results obtained from TOUCHSTONE are shown in figures 5.33 (a) and (b).

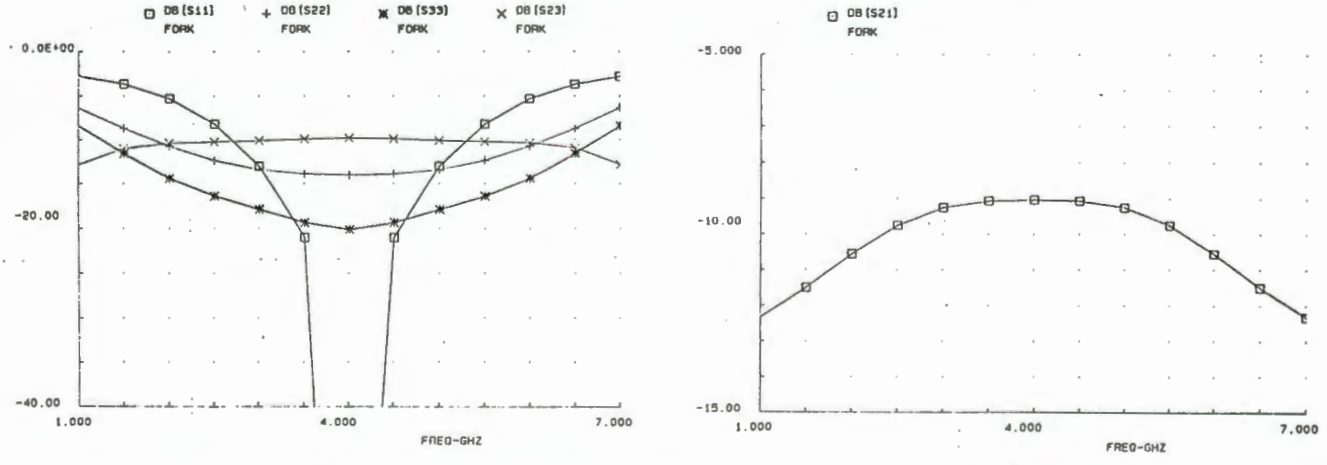

(a) (b)

Fig. 5.33 (a) The predicted values of S_{11}, S_{22}, S_{33} and S_{23} (b) predicted S_{21} for the 8-way combiner/divider.

The best return loss that could be obtained for S_{22} was just under 15dB. The optimum minimum isolation was 10dB for S_{23}. A. Saleh predicted an optimun minimum isolation/match of 10,8dB for the 8-way combiner/divider. Note that without isolation resistors the isolation would be 18dB, as discussed in chapter 3. The output matches would, however, be very poor. Figure 5.34 shows the isolation predicted by TOUCHSTONE.

With these results, the combiner/divider was fabricated in microstrip (RTDUROID 5880). Before going on to analyse the results obtained, a brief account on the meandering lines is given.

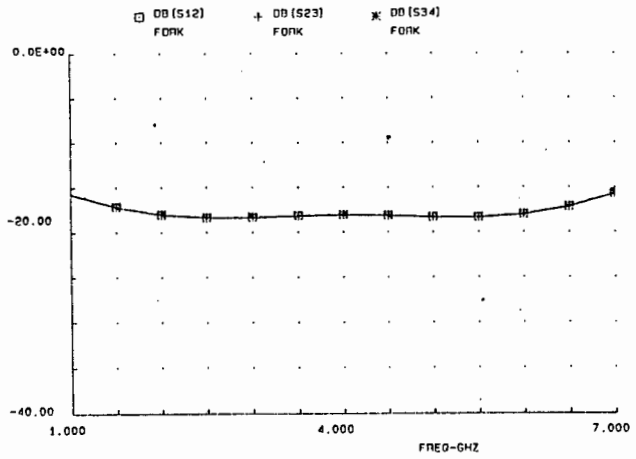

Fig. 5.34 Predicted isolation for the 8-way combiner without isolation resistors.

From figures 5.32 (a) and (b) the meandering lines provide a striking feature. As mentioned previously, this is necessary to obtain equiphased outputs. It must be emphasised that the positioning of the connectors is controlled by the size of the devices to be combined. They must also be in the same plane so that two combiners/dividers may be used back to back to allow the combination of several FETs in an amplifier.

In order to get all the lines the same length, a particular layout which has various limits associated with it is chosen. Such a limit might be the distance allowed between two lines. This information then allows a set of simultaneous equations to be written. These are solved, and if the solution is not practical a new layout must be tried. One variation in the layout may include a change in the number of meanders. This process is iterative and as such time consuming. However, this seemed to be the only way to lay the circuit out.

5.5.2 Results Obtained for the 8-Way Combiner/Divider

To start with figures 5.35 (a), (b), (c) and (d) show some results obtained without isolation resistors. Figure 5.35 (a) shows the isolation obtained between ports 9 and 2. From the graph it is seen that the isolation is greater than 16dB over the range 3,5 to 5,5GHz. The centre frequency was at 4,4GHz and at this frequency the isolation is in the vicinity of the expected 18dB. Figure 5.35 (b) shows the isolation between ports 9 and 4. The response should be the same as the device is now symmetrical. The results obtained show that this is almost the case. Figures 5.35 (c) and (d) show S_{22} and S_{44} respectively. From these figures it can immediately be seen that the output match is poor as was predicted, being in the vicinity of 3dB at 4,5GHz.

The results are now presented with isolation resistors inserted. Figure 5.36 gives the isolation obtained between port 2 and all other output ports. The graphs show that the worst isolation occurs between ports 2 and 3, which was predicted by TOUCHSTONE, and is approximately 10dB at the centre frequency.

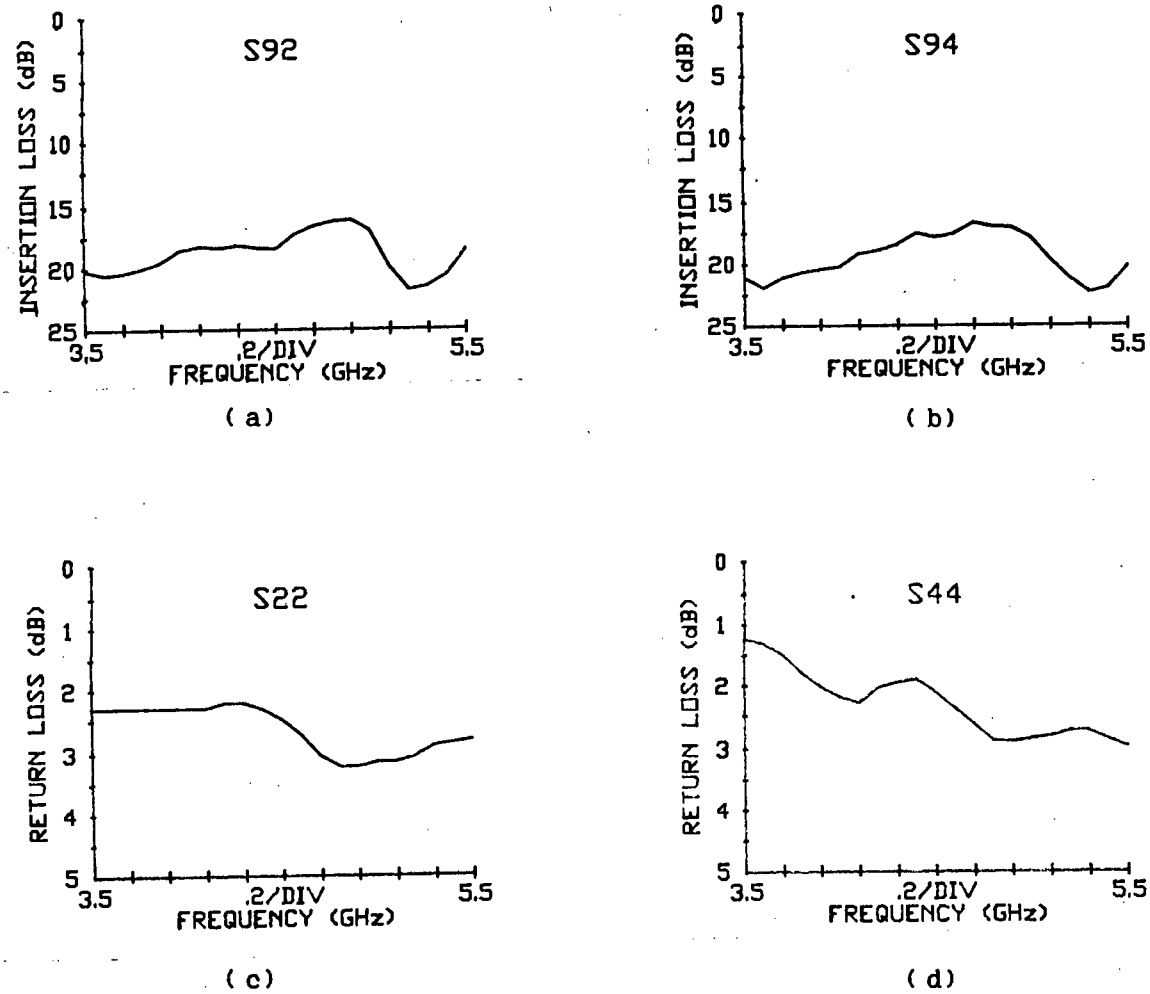

Fig. 5.35 (a) S_{92}, (b) S_{94}, (c) S_{22}, and (d) S_{44} for the combiner/divider without isolation resistors.

All the other isolation values should be fairly similar, and this is born out by the remaining graphs. The isolation is almost 20dB at the centre frequency. Figure 5.37 shows the match obtained for S_{22}, where it is seen that there has been a definite improvement compared to the case without isolation resistors. The shape of the graph is not easily explained because there are too many variables to be able to say exactly why good matches occur at any particular point.

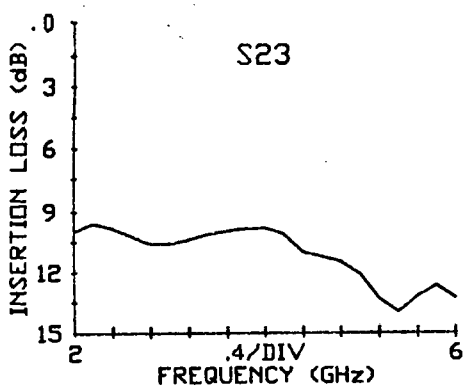

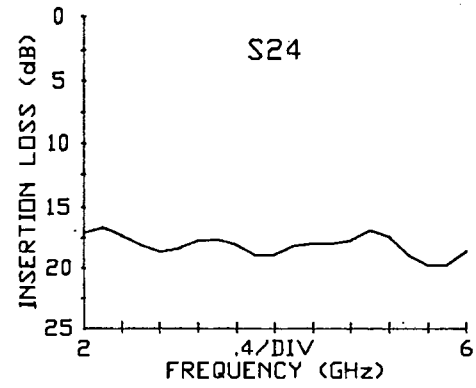

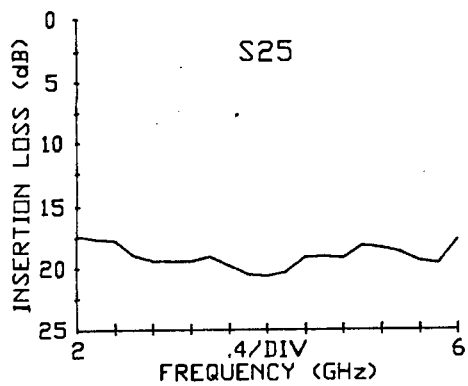

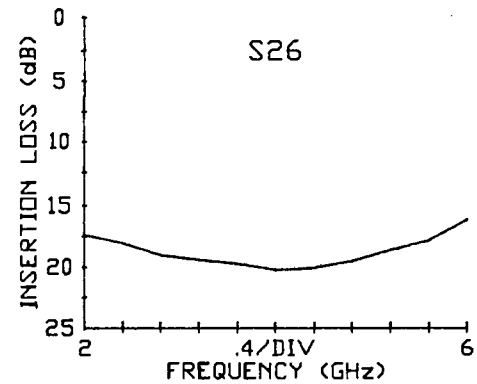

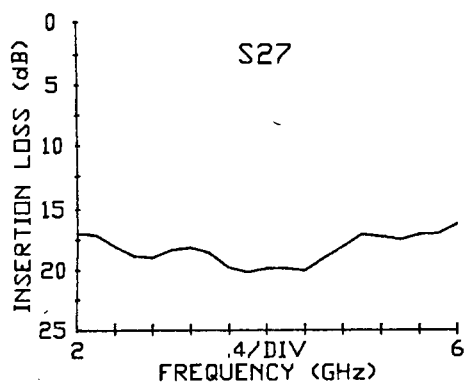

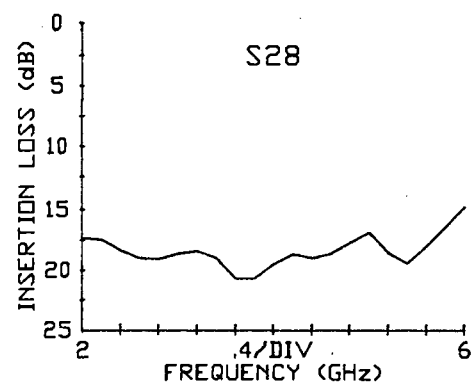

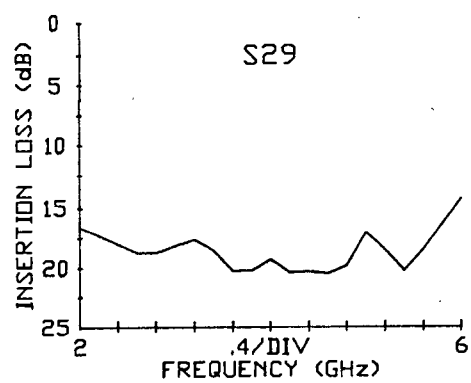

Fig. 5.36 Isolation obtained from port 2 to all other output for ports for the 8-way combiner/divider.

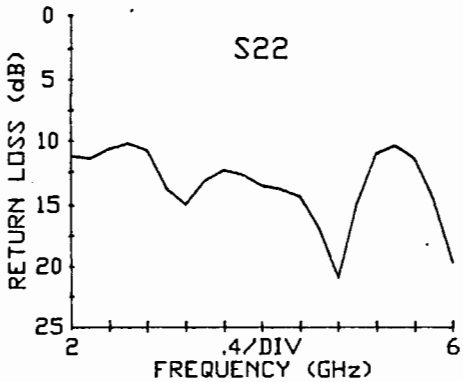

Fig. 5.37 S_{22} for the 8-way combiner/divider.

These variables include the parasitics caused by all the bends in the meandering lines, the distances between these bends, discontinuities at the impedance transistions, as well as discontinuity effects at the connection of all the quarter wave transformers.

S_{11} is shown in figure 5.38, where the best match occurs at 4,5GHz with a return of 32dB. The frequency is slightly on the high side because of the discontinuity at the transition between the 100 and 50 ohm lines. A step transistion has the effect of lengthening the wider line, which in effect causes the quarter wavelength to become shorter, and thus shift the frequency slightly. The other good match at about 5,5GHz is not easily explained and could be due to a number of factors.

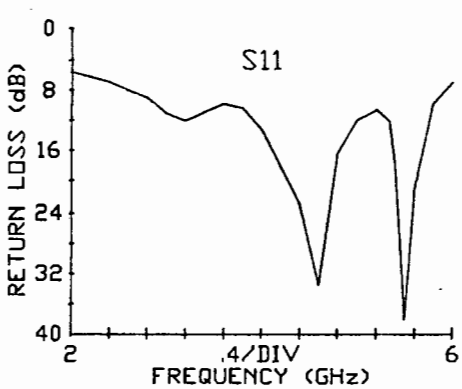

Fig. 5.38 The input match, S_{11}, of the 8-way combiner/divider.

Figure 5.39 shows all the transmission measurements obtained for the combiner/divider. These results show that the split is accepatable with a variation between ports of up to 1,2dB. This variation, is due to the effects caused by the bends in the meandering lines which change the impedances seen at each of the outputs. This means that the loads that are placed in parallel at the input will be different and hence the split will be different at this point. Another possible explanation for the difference in the split could be the loss of power due to radiation. Note that the meandering lines are in fact the same as a Rampart line antennae described by Wood et al[35], and as such must radiate to some extent. This was further investigated and will be discussed in section 5.6. If the above explanations are true it should be found that S_{21} and S_{91} are almost the same, as should be S_{31} and S_{81} etc, because of the symmetry. On examining the graphs shown in figure 5.39, it is seen that this is in fact true, with variations between pairs being in the order of 0,3dB.

The phase variations between ports 2, 3, 4 and 5 are once again very poor. The reasons for these phase variations are the same as for the 4-way combiner/divider but on a larger scale. The worst phase variation occurs between ports 2 and 5, and is shown in figure 5.40. The worst variation occurs between these ports because the path from ports 1 to 2 is the most outer and port 1 to 5 the most inner. From the investigation carried out for the 4-way fork, it was found that the phase discrepancy is mainly introduced at the point where the power is split. At this point, as can be seen from the layout given in figure 5.32a, the width of the line is large and as such can easily cause a path

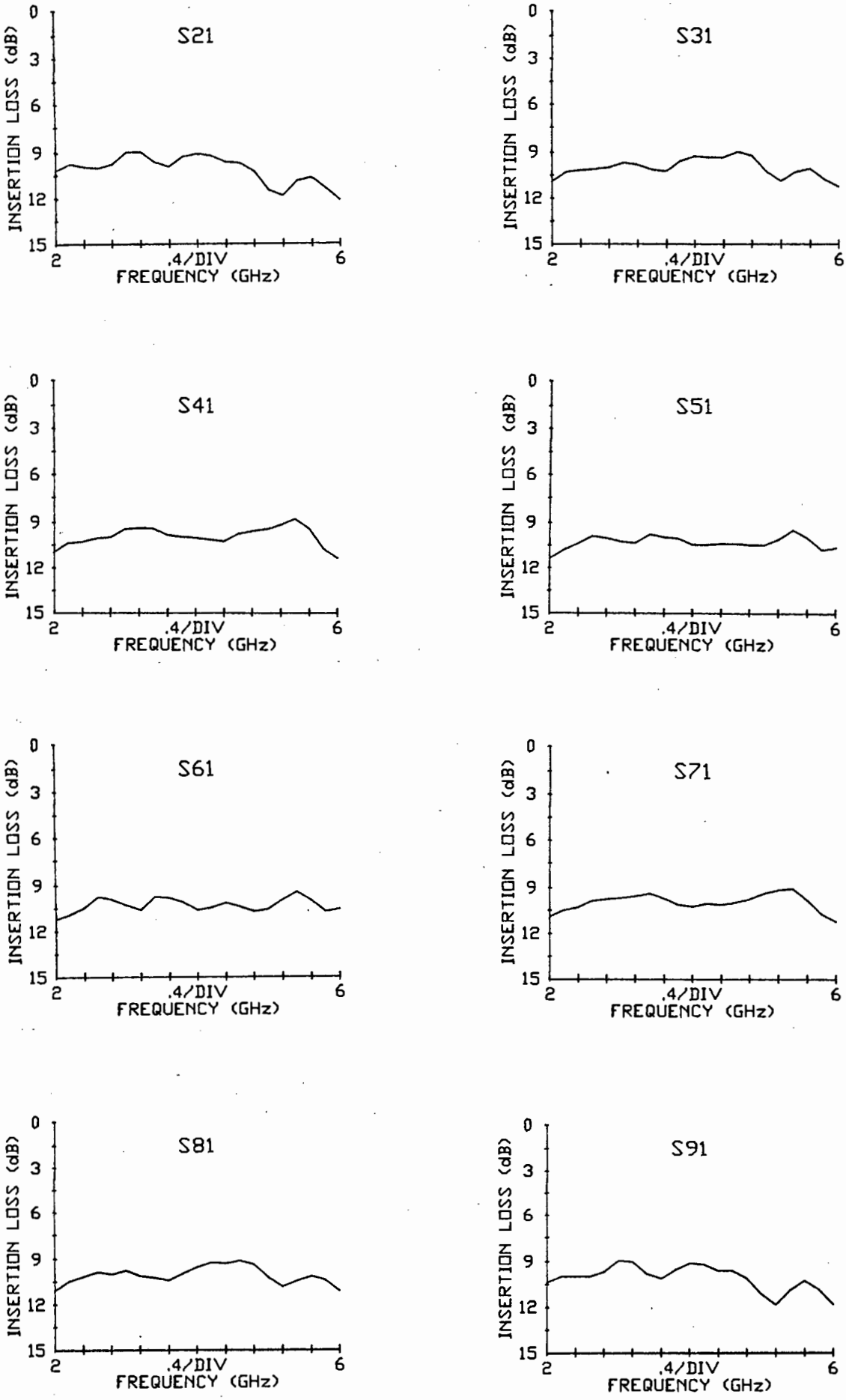

Fig. 5.39 S_{21}, S_{31}, S_{41}, S_{51}, S_{61}, S_{71}, S_{81} and S_{91} for the 8-way combiner/divider.

difference between the inner and outer paths. As it has already been shown that this is a straight forward proceedure to get the phase correct, it was decided not to build another just for this purpose as the size of board used is quite large and is expensive. It was decided to rather look more closely at the combining effeciency obtained with this device.

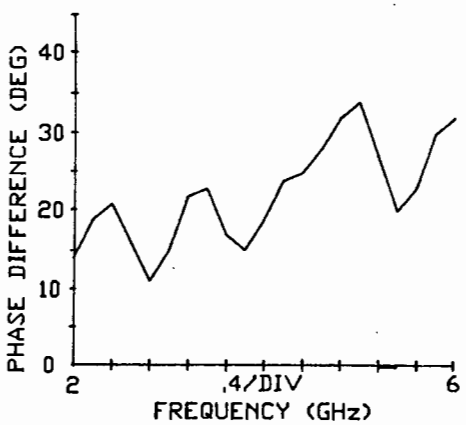

Fig. 5.40 Phase variation between ports 2 and 5.

5.5.3 Combining Efficiency of the 8-Way Combiner/Divider

In this discussion it is assumed that the outputs are in phase. The combining efficiency of the combiner/divider was determined by taking each of the through measurements (S_{j1}) and converting them to output powers with reference to 1 watt (dBW). For example, if S_{21} were -9,1dBW, the output power would be 0,123W. All the outputs in watts were then added to give the expected output and hence efficiency.

$$\text{Efficiency} = \text{output/input} \times 100\% \qquad 5.23$$

The results obtained for each frequency were plotted on a graph which is shown in figure 5.41. From this figure it is seen that

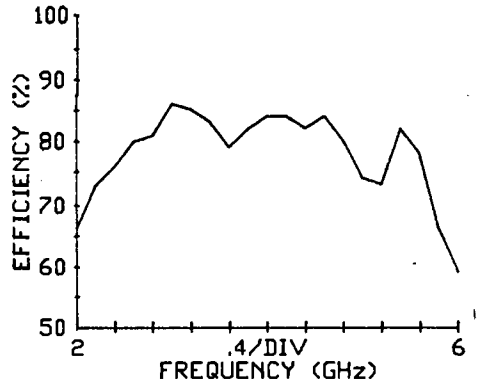

Fig. 5.41 Combining efficiency versus frequency for the 8-way combiner/divider.

the combiner is more than 80 percent efficient over the band 3,7 to 4,8GHz and better than 79 percent efficient over the band 2,6 to 4,8GHz. The peak efficiency is 86 percent and occurs at 3,0GHz. Note that over the narrow band of 3,8 to 4,7GHz the combiner is better than 82 percent efficient.

These results indicate a good efficiency for an 8-way planar combiner made on microstrip. The various losses consist of: the dielectric loss, conductor loss and possibly radiation losses from the discontinuities and bends. Before discussing methods of increasing the efficiency of this type of combiner, the loss associated with radiation from the antennae is investigated.

5.6 Loss from Rampart Antennae Structure on RTDUROID 5880

Rampart antennae usually consist of a microstrip transmission line that is made to meander. The lengths of line between each bend are chosen so that the radiation adds to give a particular type of polarization. The lengths may also be chosen so that the radiation at each of the corners cancel as shown in figure 5.4.2.

The dimensions are in wavelengths and are such as to give circular polarization. If no radiation is required the dimensions given in brackets must be used.

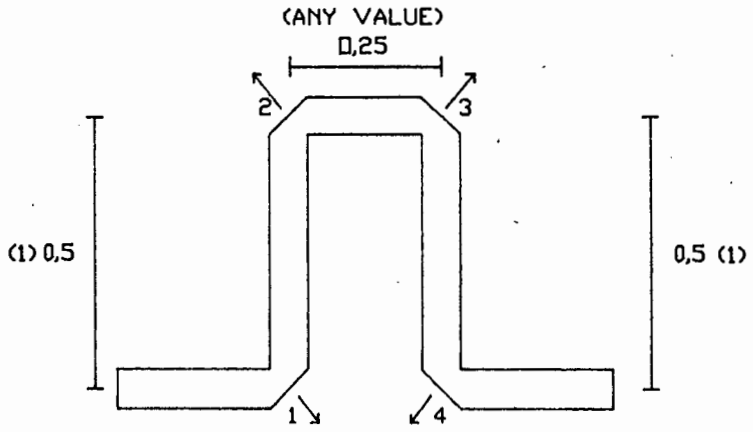

Fig. 5.42 Rampart antenna.

To find out if any radiation of significance occurs with RTDUROID 5880, it was decided to construct a radiating and non radiating meander line. The overall length was to be 3λ. A length of microstrip of the same dimensions was also fabricated and the insertion loss of each measured.

5.6.1 Results Obtained

One wavelength of 50 ohm line gives a physical length of 53,8mm at 4GHz on RTDUROID 5880. The layout of each antenna is shown in figures 5.43 (a) and (b).

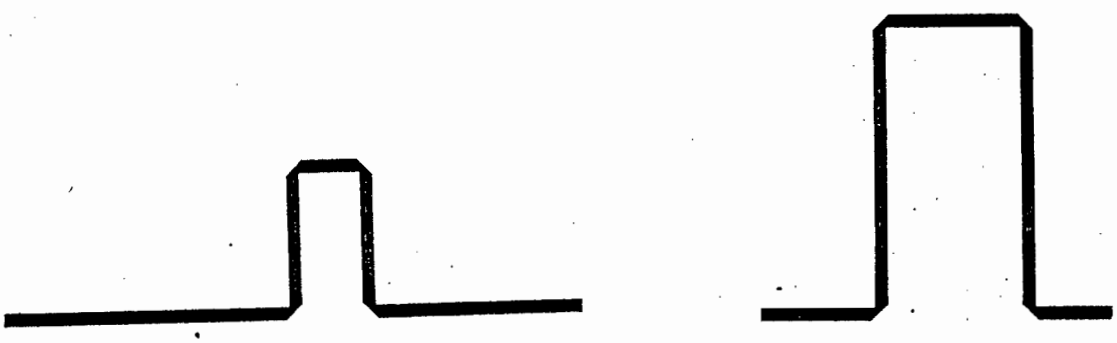

(a) (b)

Fig. 5.43 (a) Circularly polarised antenna (b) a "non radiating antenna".

The results obtained for these two antennae are shown in figures 5.44 (a), (b), (c), and (d). Figures 5.44 (a) and (b) give the return loss, which in both cases is better than 18dB over the range 2 to 6GHz. This indicates that the bends do not have too significant an effect on the match in this particular case. The through measurements are given in figures 5.44 (c) and (d). Here it is seen that the insertion loss for each is almost the same. At 4GHz, the design frequency, there is no difference between the two and both have an insertion loss of 0,4dB. This immediately indicates that the radiation losses are either very low or both antennae are radiating. To confirm which, all that had to be

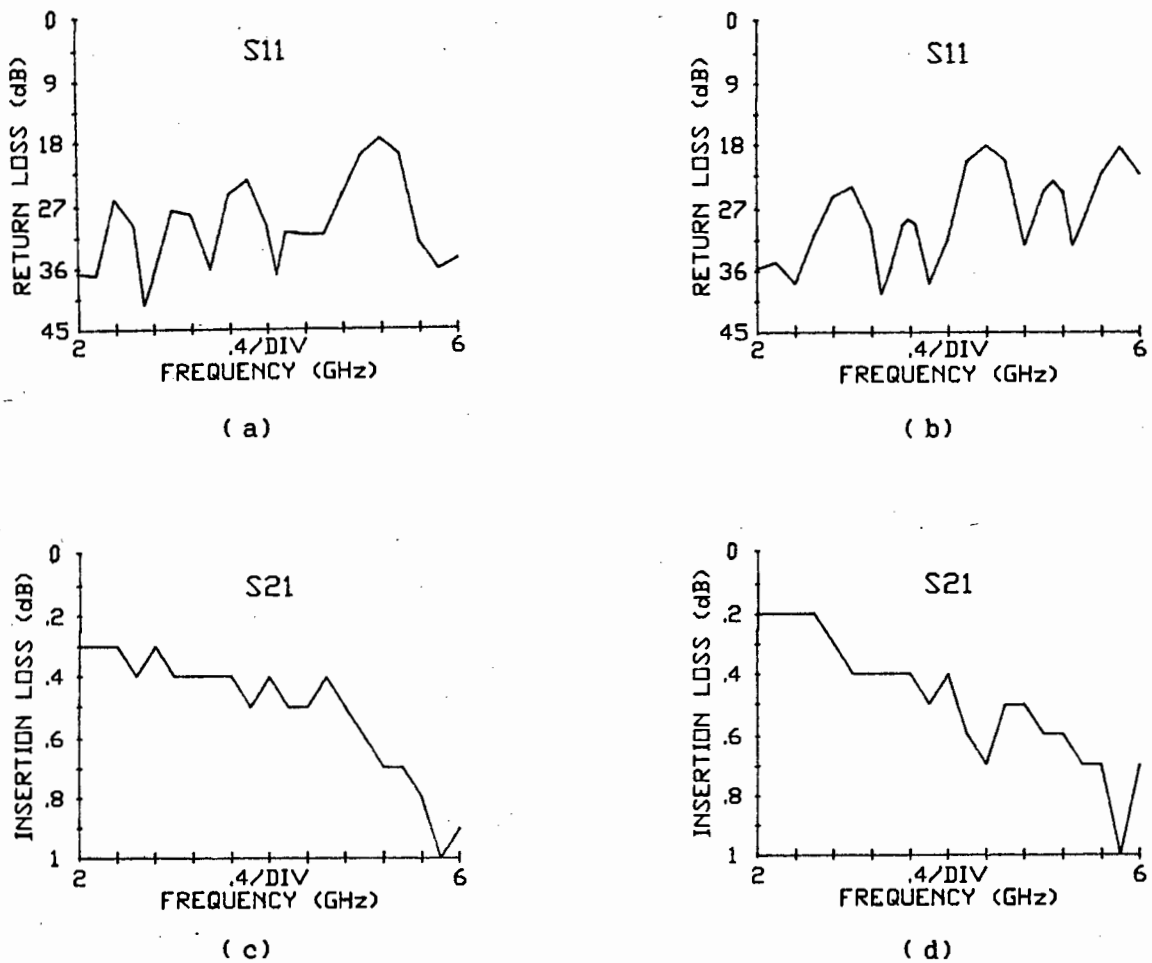

Fig. 5.44 (a) S_{11} for the antenna (b) S_{11} for the non radiating antenna (c) S_{21} for the antenna (d) S_{21} for the non radiating antenna.

done was to examine the insertion loss obtained with a 50 ohm transmission line of the same length on microstrip. The results obtained are shown in figures 5.45 (a) and (b). From these results it is seen that the return loss is once again greater than 18dB over the bandwidth 1 to 7 GHz. The insertion loss at 4GHz is also 0,4dB, the same as for the two antennae. The graphs for insertion loss are very much the same. The insertion losses are all within 0,2dB of one another and as the network analyser can only be calibrated to an accuracy of about 0,1dB, the radiation from the meandering lines of microstrip (RTDUROID 5880) can be concluded as been negligible per section.

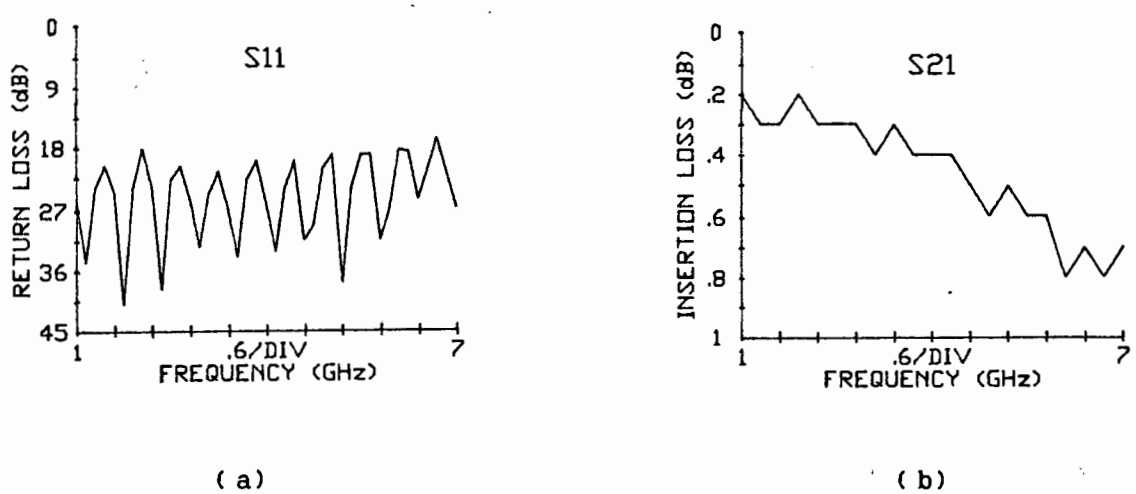

(a) (b)

Fig. 5.45 (a) S_{11}, (b) S_{21} for a 50 ohm line on microstrip RTDUROID 5880.

In general these antennae are made on board which have a thick

substrate with a low dielectric constant. This increases the width of the line and hence the radiating properties. At 4GHz, Rampart antennae were made on 1/16" (1,59mm) thick board with a dielectric constant of 2,2[35] which is twice the thickness of the board used. With this board a line width of almost 5mm for 50 ohms would result.

From these results it was evident that for the case on microstrip (RTDUROID 5880), h = 0,787mm, the effect of radiation is not as significant as first thought, so other methods to reduce the loss must be considered. This is the subject of the next section.

5.7 The Reduction of Loss in Microstrip and Stripline Structures

To reduce the loss in stripline and microstrip structures either the physical dimensions of the substrate or the substrate material have to be changed. In order to reduce the loss by changing some physical dimension, the height h of the substrate would have to be increased. This only changes the conductor loss because now the line widths become wider. The dielectric loss, however, remains the same. A difficulty associated with this change is that in the case of microstrip there is increased radiation losses, which increase rapidly if the line widths become too wide. In stripline, the line widths also become large, and the effects of discontinuities would probably be more detrimental than the gain obtained in the reduction of loss. If the material could be changed, such as to reduce the dielectric constant, both the conductor and dielectric losses would be reduced. This is not easily achieved, as most materials have a

dielectric constant in the vicinity of 2 to 5, and if the dielectric constant is less than 2, it does not necessarily have a low tanδ where the dielectric loss is directly proportional to tanδ. The ideal solution would be to have air as the substrate. This has a dielectric constant of 1 and a tanδ of zero. The only and major disadvantage is that it is difficult to incorporate into a physical structure that is reasonably robust and practical.

There are two possible structures that might be feasible. The first structure involves paper thin printed circuit board (PCB) that is placed over a ground plane that has been milled out to correspond to the circuit layout. Figure 5.46 shows a sketch of this configuration. Fabrication problems include accurate milling out of the circuit and keeping the PCB taught over the whole plane, especially if there are large areas.

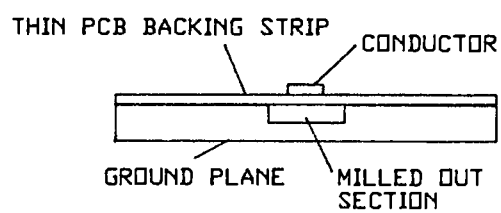

Fig. 5.46 Cross-section of milled out ground plane with thin PCB placed on top.

The second idea involves the same paper thin PCB that is glued onto an expanded closed cell polyethelene foam. This foam has a dielectric constant of 1,03 and the average tanδ would be very low as the structure consists mainly of air. The closed cell

structure prevents the absorption of moisture, which reduces the effect it has on loss. The higher the moisture content the higher the loss. The structure is shown in figure 5.47.

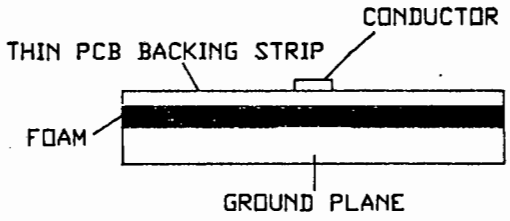

Fig. 5.47 Cross-section of second type of structure involving an air substrate.

These ideas are feasible, but the loss would be further reduced if a stripline structure were used as this would prevent any loss due to radiation.

These ideas were implemented. The first idea was implemented both in stripline and microstrip. The latter only in stripline, as the thinnest foam available was 3mm thick, which meant that the lines would be far too wide on microstrip. The stripline structure allowed the foam to be compressed to the desired thickness.

5.7.1 Results Obtained with the Air Substrates

The first structure fabricated was that shown in figure 5.46. The depth of the milled out section was 0,89mm (0,035"). The results obtained are shown in figures 5.48 (a) and (b). The length of line was 70mm. Figure 5.48 (a) shows the return loss obtained which was better than 16,5dB over the bandwidth. The insertion loss, shown in figure 5.48 (b) was 0,1dB at 1GHz and

0,3dB at 6GHz, this corresponds to a loss which is only slightly better than that obtained with microstrip (RTDUROID 5880) of the same length. Figure 5.49 shows the results obtained with RTDUROID 5880. From these results it appears that the structure used is not very good. The results indicate that the loss obtained for the lengths of line tested with the antennae should have been higher if the loss per unit length were to remain the

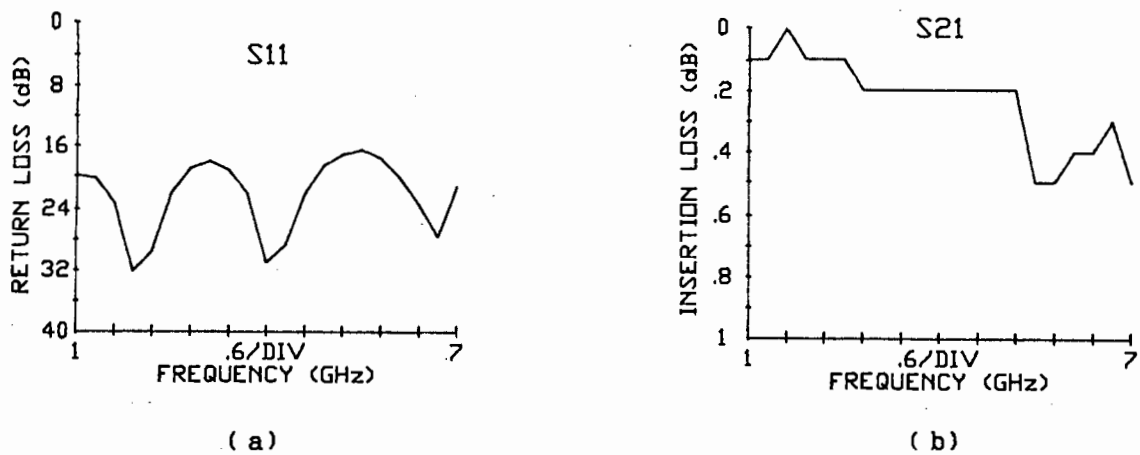

(a) (b)

Fig. 5.48 (a) S_{11} for microstrip with air as dielectric l = 70mm (b) S_{22} for same.

same. As this was not the case, it was decided that longer line lengths would give more reliable readings and comparisons as errors due to mismatch and calibrations would have less effect.

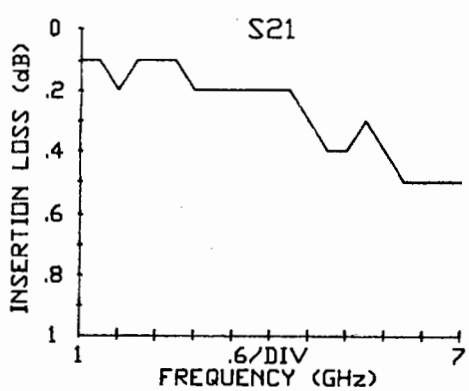

Fig. 5.49 S_{21} for microstrip, RTDUROID 5880, l = 70mm.

A stripline structure of the milled out version was fabricated. This gave promising results, and these are shown in figures 5.50 (a) and (b). The length of this structure was still 70mm and b, the width of substrate, was 1,78mm (0,07"). The results show a loss of 0,3dB at 6GHz and 0,2dB at 2GHz. The match is given in figure 5.50 (b). The return loss is better than 15dB over the bandwidth.

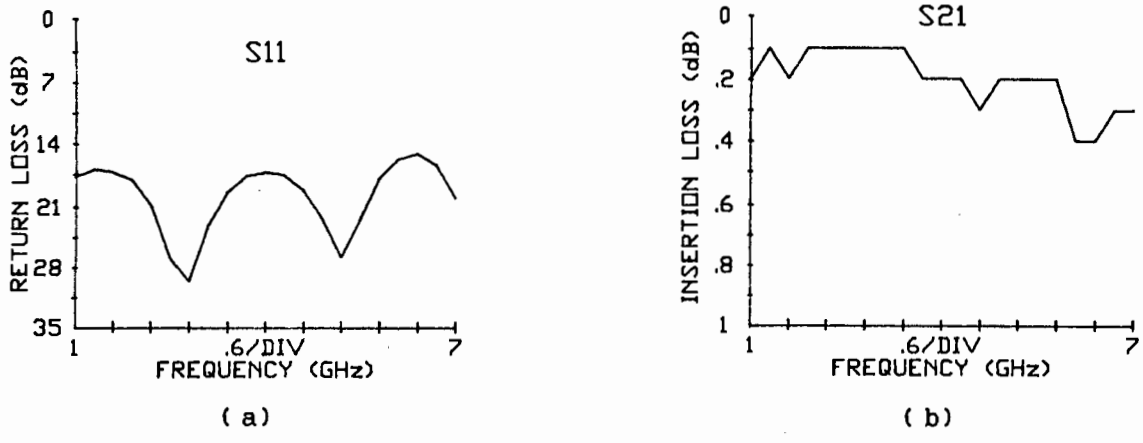

(a) (b)

Fig. 5.50 (a) S_{11}, (b) S_{21} for stripline with air as a dielectric.

For the following results, the length of the line was taken to be 160mm unless otherwise stipulated. Firstly, the loss obtained for a length of stripline made on RTDUROID 5880, b = 0,062" is shown in figure 5.51. From this diagram it is seen that the loss obtained is higher than that obtained for the antennae and microstrip given in the previous section. The results obtained for a stripline structure with a milled out section are shown in figures 5.52 (a) and (b). The results are poor. The main reason for this was that the construction was poor and the PCB was not taught enough. This meant that at some points along the line the copper conductor was close to the ground plane and was therefore not a 50 ohm line. This explains the poor match as shown in

figure 5.52 (a). Because the match is poor, a standing wave is

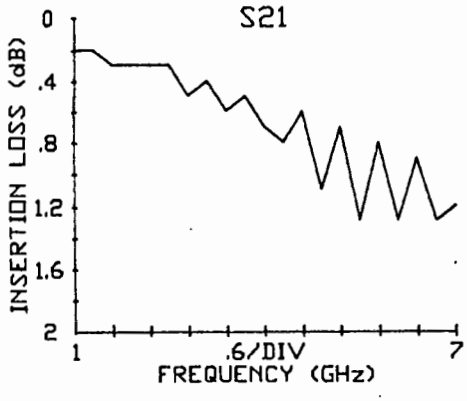

Fig. 5.51 Loss in stripline (RTDUROID 5880), b = 0,062".

set up and points of high electric field occur. This has the effect of distorting the actual loss obtained, so subtraction of the loss due to mismatch from S_{21} is not reliable.

A second attempt at this structure was made. The results were much better and are shown in figures 5.53 (a) and (b). The return loss was now better than 15dB over the bandwidth 1 to 7GHz and the insertion loss varied from 0,1dB at 1GHz to 0,6dB at

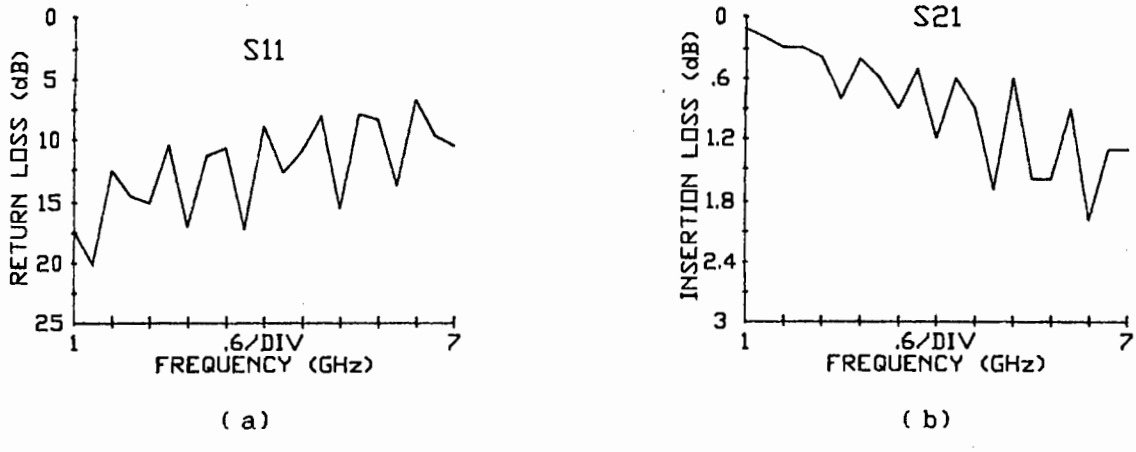

Fig. 5.52 (a) S_{11} of the first attempt at stripline structure with air as a dielectric (b) S_{21} of the same (substrate thickness, b = 0,07").

6GHz. This is an improvement of nearly a factor of 2 compared to the stripline structure with RTDUROID 5880.

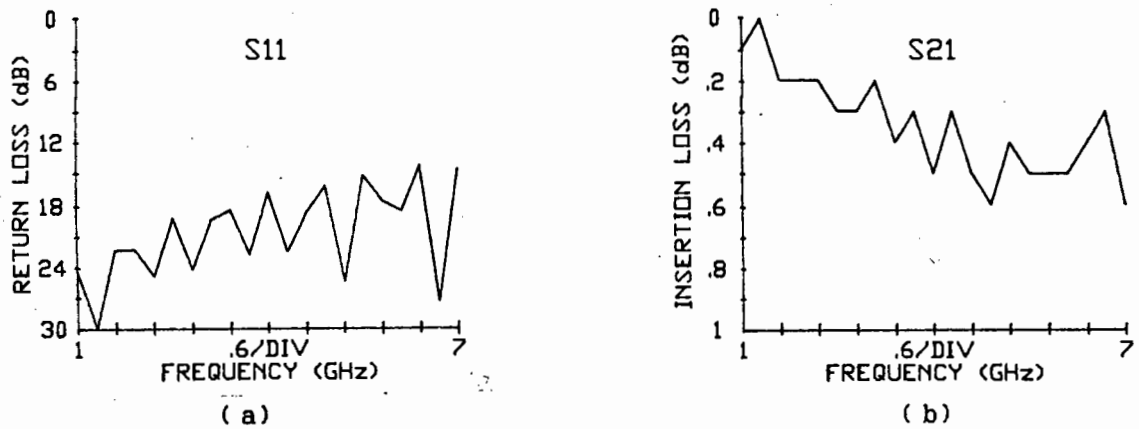

Fig. 5.53 S_{11} for second version of stripline with air as a substrate (b) S_{21}.

Microstrip structures were thought not to be robust enough, and were not built. Structures using foam were now fabricated. The results obtained are shown in figure 5.54 (a) and (b) which were very promising. Figure 5.54 (a) shows the match obtained with a return loss of better than 18,4dB over the bandwidth 1 to 7GHz. The advantage with this structure was that the height between ground planes and hence the match could be adjusted. The insertion loss was 0,4dB at 7GHz and 0,1dB at 1GHz. These results give an improvment approaching a factor of 3 to that obtained with standard stripline, and a factor of 2 with respect to microstrip. The main problem with these structures is the weak structure of the PCB which is very much like paper. It was thought that it could be stiffened up using various thin materials which were sturdy or brittle. However, most materials with this property had a high tanδ, for example thin cardboard gave the poor results shown in figure 5.55.

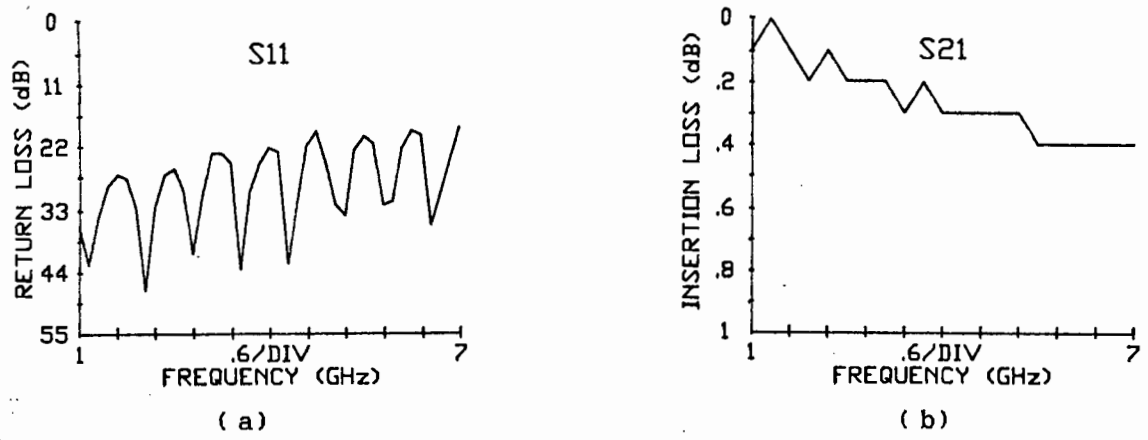

Fig. 5.54 (a) S_{11}, (b) S_{21} with foam as the substrate.

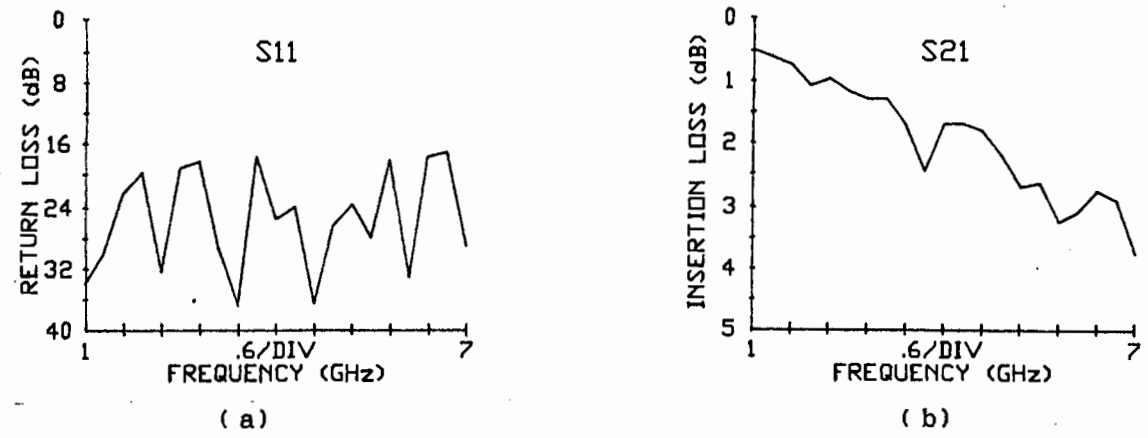

Fig. 5.55 (a) S_{11}, (b) S_{21} for structure using cardboard to enhance the strength of the PCB.

From the results obtained with the various stripline structures it was decided to build an 8-way combiner/divider using the stripline structure that incorporated the foam. Before going on to the disign, it must be mentioned that the backing strip of the PCB was found to have a very small effect on the impedance of lines. This was investigated using a finite element program that is in the process of being developed at UCT by a L. Watkins as an M.Sc. project. The loss associated with this backing strip is not easily measured. Note also that the conductor loss can never be zero and tends to a limit. Refer to the section on microstrip losses (section 5.2.3).

5.8 A Low Loss 8-Way Combiner/Divider

The layout of the circuit on the PCB is of the same form as that shown in figure 5.32 (a). The dimensions were obviously changed to take into account the new parameters of the substrate. The cross-section of the overall structure is shown in figure 5.56.

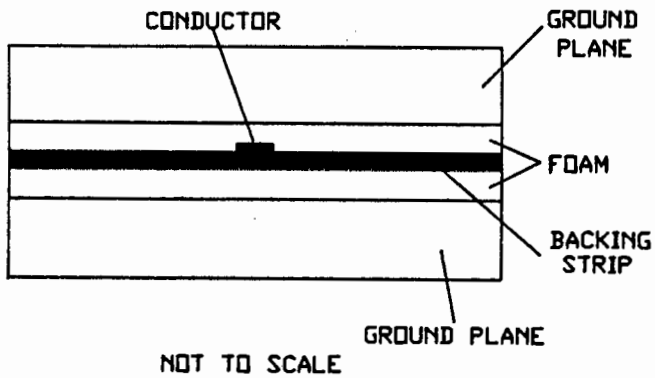

Fig. 5.56 Cross-section of the low loss 8-way combiner/divider.

Results obtained for this combiner/divider are as follows:
Figure 5.57 gives the input match of the combiner/divider. From this figure it is seen that the best return loss is only slightly better than 15dB. This match was improved by adjusting the

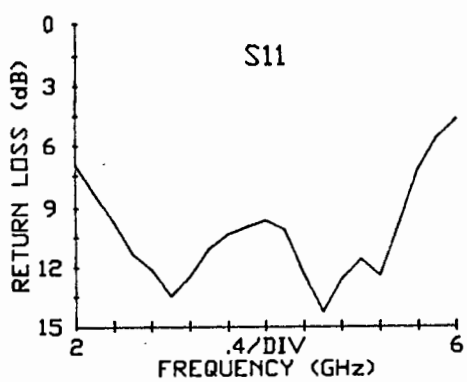

Fig. 5.57 Initial S_{11} for the 8-way combiner/divider.

distance between the ground planes. The best match obtained is shown in figure 5.58. The best return loss obtained is now 25dB

at 4,9GHz.

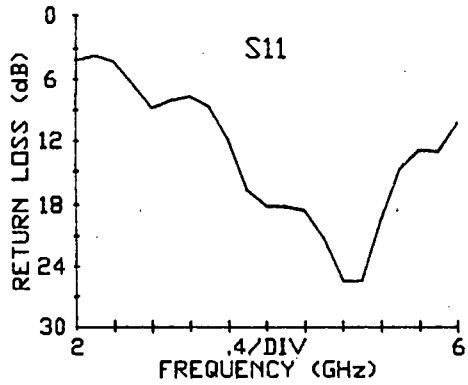

Fig. 5.58 Final S_{11} obtained for the 8-way combiner/divider.

The through transmission measurements are given in figure 5.59 and from this figure it is seen that the outputs track reasonably well. The phase response is once again poor, the explanations for this have already been given. Figure 5.60 gives the phase error between ports 2 and 5. Note that the shift in centre frequency to 4,9GHz is also due to the reason given before, namely discontinuities at the characteristic impedance changes. The difference in splits has also been accounted for previously. The isolation obtained is very similar to that measured for the combiner/divider fabricated on microstrip.

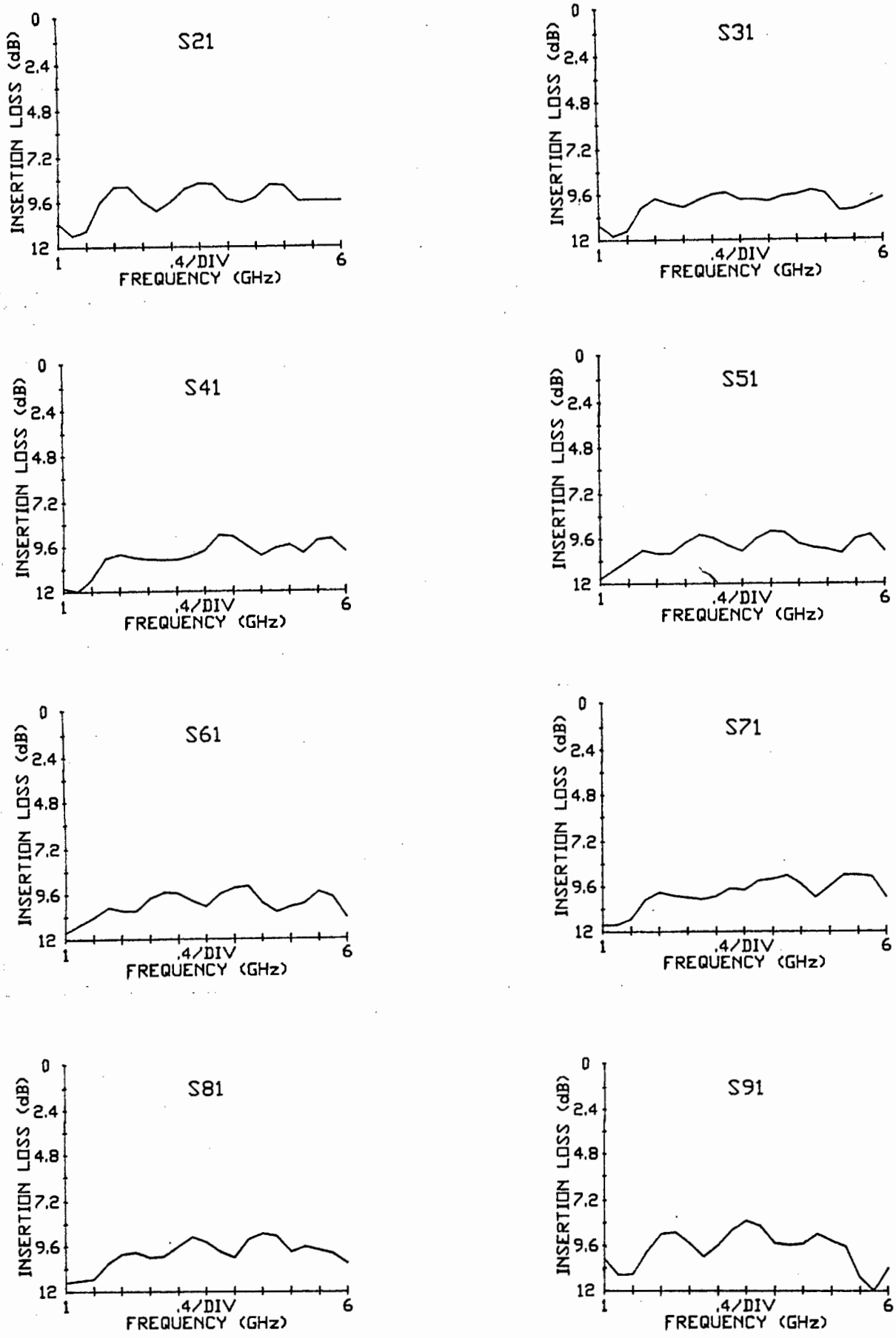

Fig. 5.59 S_{11} for the low loss 8-way combiner/divider.

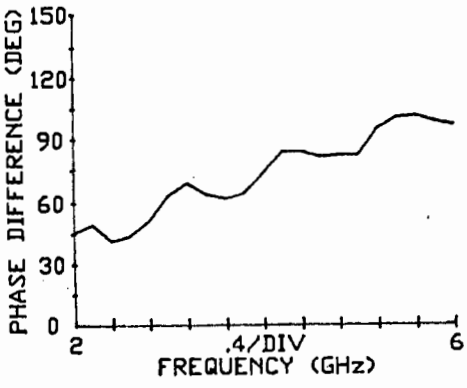

Fig. 5.60 Phase variation between ports 2 and 5 for this 8-way combiner/divider.

The combining efficiency for this combiner was calculated in the same way as for the 8-way combiner/divider constructed on microstrip RTDUROID 5880. The results obtained are shown in figure 5.61. From this figure it is seen that a peak combining efficiency of 94 percent at 4,2GHz is obtained. The efficiency

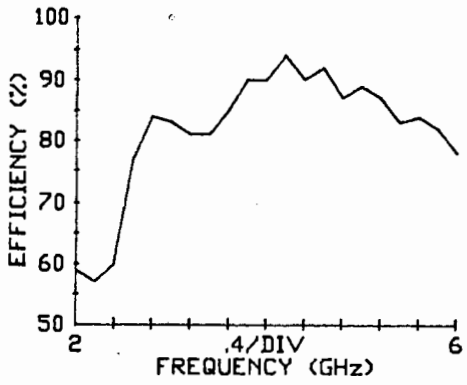

Fig. 5.61 Combining efficiency for this 8-way combiner/divider.

is better than 90 percent over the bandwidth 3,8GHz to 4,7GHz and better than 80 percent over 2,6 to 5,8GHz. This is a marked improvement over the microstrip version where the peak efficiency was only 86 percent. These results are very promising and the

major difficulty associated with this combiner/divider is in its construction. The difficulty in construction is associated with placing the thin PCB taughtly and smoothly onto the foam and simultaneously compressing the foam to the desired width evenly below and above the PCB. The phase errors may be removed as mentioned proviously, although the process may be rather time consuming.

5.9 Conclusion

This chapter dealt with planar n-way combiners/dividers. Firstly microstrip was introduced and design equations presented. Losses in stripline and microstrip were also discussed where factors such as dielectric constant and substrate thickness were found to affect the loss obtained. A 4-way fork combiner/divider was fabricated and analysed. The results obtained were good, although for this number of divisions there is not much to choose between a corporate Wilkilson or a fork combiner/divider. The 4-way combiner/divider was extended to an 8-way version which gave reasonable results and a peak combining efficiency of 86 percent. Methods at reducing the loss in stripline and microstrip were looked into with the aim of increasing the combining efficiency of such a combiner. This lead to a structure using foam which has a dielectric constant of 1,03 and a low tanδ . An 8-way combiner/divider was constructed and a peak combining efficiency of 94 percent was achieved. This gives a new n-way planar combiner/divider that is practically possible, provides a high combining efficiency and is planar, and as such allows heat dissipation. The isolation between ports is in the worst case 10dB, but can be 18dB if no isolation resistors are used.

Isolators can be used and are probably advisable as this would protect expensive power FETs if any were to fail.

CHAPTER 6 CONCLUSION

A low loss 8-way combiner/divider has been developed as the culmination in to the investigation of various types of combiners/dividers and their associated loss. The need for power combiners/dividers is evident from the fact that the maximim power available from a power FET is at the present stage of development only 10 watts at 4GHz. This compares very unfavourably with 100 watts output power available from commercial travelling wave tube amplifiers. For higher powers levels to be achieved using power FETs, power combiner/dividers are required.

The first type of combiners investigated were resonant cavity types. The most successful of these is the radial combiner. This type of combiner/divider was found to be very efficient (98 percent at 4,2GHz). Its major disadvantage is however, that it is non planar and therefore causes heat dissipation problems for the combined amplifier. There are various types of planar combiner/divider available, but in general they are generalisations of the Wilkinson combiner/divider and are used in a corporate structure. They are therefore less efficient and can only combine 2^N devices, where N is a positive integer. These combiners/dividers were investigated. They provide good results, are planar but are not very efficient.

Planar n-way combiners were investigated. These were more efficient and an 8-way version manufactured on microstrip (RTDUROID 5880) gave a peak efficiency of 86 percent. This however, was still not as good as the radial resonant cavity

combiner/divider. Methods of increasing the combining efficiency were investigated. This meant that various methods of reducing the loss in stripline and microstrip structures had to be investigated. The most efficient structure that was investigated was stripline that used a closed cell expanded polyethelene foam as the substrate. The circuit was etched on paper thin PCB that was placed between two layers of foam. This structure was used to make an 8-way combiner/divider. The results obtained were very promising, and a peak combining efficiency of 94 percent was obtained at 4,2GHz.

A low loss planar 8-way combiner/divider was therefore developed which has an efficiency approaching that of a circular resonant cavity combiner. The bandwidth of the former was much broader and its planar structure allows better heat dessipation for the combined amplifier. The isolation resistors allow graceful degredation, not found in the resonant cavity structure.

The planar combiner/divider developed has much to offer and is worthy of further investigation. Techniques for improving its construction should be considered as well as possible low loss materials which could replace the foam. The initial steps have however, been taken and with further work the planar combiner/divider with comparable combining efficiency to a radial resonant cavity combiner could become a viable commercial device allowing solid state power amplifiers to compete with TWTAs.

Table A.1 Bessel functions of the first kind $J_0(x)$.

x	0	1	2	3	4	5	6	7	8	9
0.	1.0000	.9975	.9900	.9776	.9604	.9385	.9120	.8812	.8463	.8075
1.	.7652	.7196	.6711	.6201	.5669	.5118	.4554	.3980	.3400	.2818
2.	.2239	.1666	.1104	.0555	.0025	−.0484	−.0968	−.1424	−.1850	−.2243
3.	−.2601	−.2921	−.3202	−.3443	−.3643	−.3801	−.3918	−.3992	−.4026	−.4018
4.	−.3971	−.3887	−.3766	−.3610	−.3423	−.3205	−.2961	−.2693	−.2404	−.2097
5.	−.1776	−.1443	−.1103	−.0758	−.0412	−.0068	.0270	.0599	.0917	.1220
6.	.1506	.1773	.2017	.2238	.2433	.2601	.2740	.2851	.2931	.2981
7.	.3001	.2991	.2951	.2882	.2786	.2663	.2516	.2346	.2154	.1944
8.	.1717	.1475	.1222	.0960	.0692	.0419	.0146	−.0125	−.0392	−.0653
9.	−.0903	−.1142	−.1367	−.1577	−.1768	−.1939	−.2090	−.2218	−.2323	−.2403

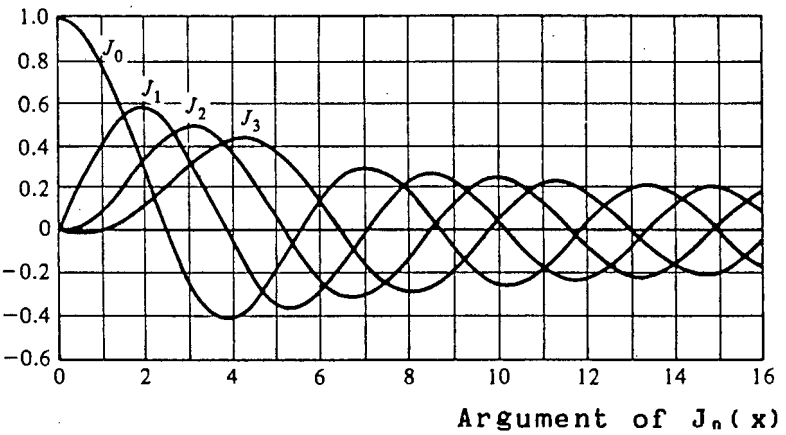

Fig. A.1 Graph of Bessel functions of the first kind.

Table A.2 p^{th} Zeros of $J_n(x)$.

p \ n	0	1	2	3	4	5
1	2.405	3.832	5.136	6.380	7.588	8.771
2	5.520	7.106	8.417	9.761	11.065	12.339
3	8.645	10.173	11.620	13.015	14.372	
4	11.792	13.324	14.796			

APPENDIX B TOUCHSTONE/RF-VERSION 1.3 1985

TOUCHSTONE is a product of EEsof and is a software programme written by Bill Childs and Chuck Holmes for RF computer aided engineering. The program runs on IBM and IBM compatible personal computers. It uses a nodal description for circuits; random optimisation and has a complete element and measurement catalogue.

TOUCHSTONE is commanded via function and cursor pad keys on the keyboard. Various features that are offered by TOUCHSTONE are:

i) The program can be operated with both a monochrome and colour graphics display. This enables viewing of both files and graphics simultaneously.

ii) There is a full-screen editor which allows the creation of new text and edition of the old, this is displayed as an entire page on the screen.

iii) A tuner is incorporated that allows data to be changed in a particular circuit. By pressing enter, a new sweep is initiated which is plotted on to the same graph as the previous sweep. This allows the effect a particular change has on a circuit to be seen.

iv) An optimiser is available that allows optimisation of a particular response for the circuit under consideration by changing parameters specified by the user. The optimiser is interactive and uses random exploration. That is, it searches for a global minimum of the error function. The program displays updated responses for as many trials as are specified. The optimisation may be stopped as soon as the response seems satisfactory to the user.

v) TOUCHSTONE is programmed to utilise the Intel 8088-8086, and has been optimised for the Intel 8087 numerical coprocessor. This makes the program up to 10 times faster than Basic based programs.

vi) TOUCHSTONE has an element catalogue, these elements are listed below.

a) Lumped elements These include resistors, inductors and capacitors in standard condigurations as well as ideal transformers and mutually coupled coils.

b) Electronic models These include voltage controlled current and voltage sources, FET, PIN diode and op-amp.

c) Transmission lines These include ideal transmission lines, ideal short and open circuited transmission lines. and short and open circuited transmission line physical models.

d) Ideal coupled line

e) S-parameters The element library allows up to 4-port networks. The S-paramerers are interpolated for simulation frequencies between those in the S-parameter file and extrapolated for those simulation frequencies outside the range of frequencies in the file.

f) Defining networks TOUCHSTONE allows the naming of any network in the circuit up to a maximum of 4-ports. This network can be used as if it were an element as many times as required.

Other features include the possibility of storing S-parameters that have been computed from a particular circuit model. Variables in a circuit file may also be defined at the beginning. This means that a particular impedance, for example, does not have to be continually typed in, but just the variable name.

The structure of a circuit file is divided into 9 different blocks. The variable block, here variables that may be used throughout a circuit are defined. The circuit block describes the circuit layout. The output block is where the outputs are specified as well as format of the output. Either magnitude, magnitude and phase, real and imaginery etc. The outputs are also directed to one of the output grids, or in tabular form or in polar form on a Smith chart. The frequency block sets up the simulation frequencies. The grid block defines the rectangular plotting grids. The optimisation block, sets up the optimiser. There is a dimension block that allows the overiding of default dimension. There is also a terminations block that allows different terminations to be used other than 50 ohms. The processor block is used to perform calculations on the S-parameters for a new network. Uses networks defined in the circuit block. These blocks are usually specified in a particular order in the circuit file and is shown below.

VAR	Variables
CKT	Circuit
PROC	Processor
OUT	Output
FREQ	Frequency
TERM	Termination
GRID	Grid
OPT	Optimisation
DIM	Dimension

The above gives a brief description of TOUCHSTONE. The program provides an easy method of analysing various circuits and helps in the design of amplifiers where matching circuits need to be

optimised to give an optimum gain. An example of a circuit file is given in chapter 3 where the rectangular waveguide combiner/divider was analysed.

APPENDIX C METHOD EMPLOYED TO SHOW OUTPUT MATCHES WHEN A DIVIDER IS USED AS A COMBINER

This appendix presents the model used on TOUCHSTONE to show that the output ports of a 2-way Wilkinson combiner without isolation resistors are matched when driven simultaneously.

In order to show that the outputs are in fact matched at the centre frequency when the output ports are being driven simultaneously consider the below circuit.

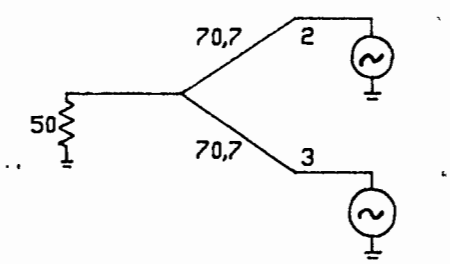

Fig. C.1 Circuit of Wilkinson combiner/divider being used as a combiner.

When s-parameters are determined, only one input is fed at a time. This means that when using TOUCHSTONE, a method must be implemented such that when port 2 is driven so is port 3. One way of achieving this is to use an ideal voltage controlled voltage source that has a gain of 1. In other words, for an input of 1 volt, the output from the voltage source is also 1 volt.

The model of the controlled voltage source on TOUCHSTONE is given in figure C.2.

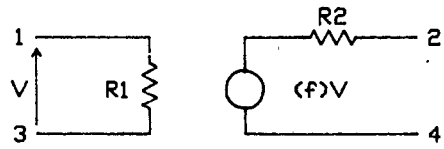

Fig. C.2 Schematic of the voltage controlled voltage source used by TOUCHSTONE.

The format of entering this into the circuit file on TOUCHSTONE is VCVS n1 n2 n3 n4 M=x1 A=x2 R1=x3 F=x4 T=x5

where n1, n2, n3 and n4 are the connecting nodes.

M = magnitude of voltage gain at dc.

A = angle of voltage gain at dc.

R1 = input resistance.

R2 = output resistance.

F = frequency at which voltage gain is down by 3dB.

T = time delay associated with voltage gain.

For an ideal voltage source

F = 0 => F -> infinity

T = 0 => T =0

R1 = 0 => R1 -> infinity

R2 = 0 => 0

For this particular use R1 was chosen as 0, implies that there is

no input impedance for the driving source. R2 was also chosen to be 0. A 50 ohm load is placed in parallel to the voltage source so that port 3 will see a 50 ohm load. M was chosen to be 1, A = 0, F = 0 and T = 0.

The final circuit entered into TOUCHSTONE is shown in figure C.3.

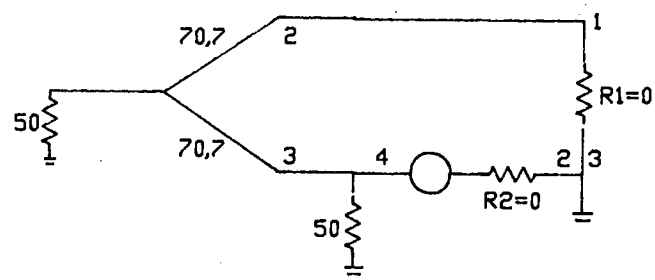

Fig. C.3 Layout of model used on TOUCHSTONE.

The circuit file is given in figure C.4, the results with their explanations are given in chapter 4.

```
CKT

   TLIN 1 2 Z=70.7 E=90 F=4
   TLIN 1 3 Z=70.7 E=90 F=4
!  RES 1 0 R=50
   RES 3 0 R=50
!  RES 2 3 R=100
   VCVS 2 0 0 3 M=1 A=0 R1=0 R2=0 F=0 T=0
   DEF2P 1 2 WILK

OUT
   WILK DB[S11] GR1
   WILK DB[S22] GR1
   WILK DB[S21] GR2
   WILK DB[S12] GR2

FREQ
   SWEEP 2 6 .25

GRID
   GR1 0 -40 5
   GR2 6 -6 1
```

Fig. C.4 Circuit file.

REFERENCES

1. J. Thomas and D. Condron, "M/W Small Signal Bipolar Transistor", Microwave Journal, February 1973, p43.
2. C.A. Liecht, "Microwave Field Effect Transistors -1976", IEEE Trans. Microwave Theory Tech., Vol.24, No.6, June 1976, pp279-285.
3. R. Allison, "Silicon Bipolar Microwave Power Transistors", IEEE Trans. Microwave Theory Tech., Vol.27, No.5, May1979, pp415-421.
4. H.V. Shurmer, "Microwave Semiconductor Devices", Pitman Publishing, 1971).
5. J.V. Dilorenzo and W.R. Wisseman, "GaAs Power MESFET's: Design, Fabrication and Performance", IEEE Trans. Microwave Theory Tech., Vol.27, No.5, May 1979, pp367-377.
6. F. Sterzer, "GaAs Field Effect Transistors", Microwave Journal, Nov. 1978, pp73-78.
7. B. Turner et al, "GaAs Microwave Power FET with Polymide Overlay Interconnection", Electronic Letters, Vol.17, No.5, 5th March 1981, pp185-187.
8. Y. Mitsui et al, "10-GHz 10-W Internally Matched Flip Chip GaAs Power FETs", IEEE Tran. Microwave Theory Tech., Vol.26, No.2, February 1978, pp70-74.
9. F.M. Megalhaes et al, "A Microwave GaAs FET Power Module with GaAs Matching Circuits", Microwave Journal, May 1985, pp205-224.
10. S.Y. Narayan et al, "Medium Power GaAs MESFETs", Microwave Journal, February 1976, p47,48.
11. R. Basset and M.D. McCombs, "Production Bipolars Edge Out FETs at 4GHz", Microwaves, February 1981, pp43-49.

12. Y. Mitsui et al, "Flip Chip Mounted GaAs Power FET with Improved Performance in the X to Ku-Band", Electronic Letters, Vol.15, No.15, 19th July 1979, pp461-462.

13. S. Rehnmark, "Wide-Band Balanced Line Microwave Hybrids", IEEE Trans. Microwave Theory Tech., Vol.25, No.10, October 1977, pp825-830.

14. G.P. Riblet, "A Directional Coupler with very Flat Coupling", IEEE Trans. Microwave Theory Tech., Vol.26, No.2, February 1978, pp70-74.

15. J. Reed and G.J. Wheeler, "A Method of Analysis of Symmetrical Four Port Networks", IRE Trans. Microwave Theory Tech., October 1956, pp246-252.

16. C.Y. Ho, "Transform Impedance with a Branch-Line Coupler", Microwaves, May 1976, pp47-52.

17. R.M. Osmani, "Synthesis of Lange Couplers", IEEE Trans. Microwave Theory Tech., Vol.29, No.2, February 1981, pp168-170.

18. A. Presser, "Interdigitated Microstrip Coupler Resign", IEEE Trans. Microwave Theory Tech., Vol.26, No.10, October 1978, pp801-805.

19. Y. Tajima and S. Kamashi, "Multiconductor couplers", IEEE Trans. Microwave Theory Tech., Vol.26, No.10, October 1978, pp795-801.

20. K.J. Russell, "Microwave Power Combining Techniques", IEEE Trans. Microwave Theory Tech., Vol.27, No.5, May 1979, pp472-478.

21. Y. Tokumitsu et al, "A 6GHz 80-W GaAs FET Amplifier with a TM-Mode Cavity Power Combiner", IEEE Trans. Microwave Theory Tech., Vol.32, No.3, March 1984, pp301-308.

22. R. Aston, "Techniques for Increasing the Bandwidth of a TM_{010}-Mode Power Combiner", IEEE Trans. Microwave Theory Tech., Vol.27, No.5, May 1979, pp479-482.

23. G.W. Swift et al, "A Radial Wave Power Combiner Designed by Broadband Techniques", European Microwave Symposium, 1985, pp973-978.

24. Z. Gallani and S.J. Temple, "A Broadband Planar N-Way Combiner/Divider", IEEE MTT-S Int. Microwave Symposium Dig., June 1977, pp499-501.

25. A.G. Bert and D. Kaminsky, "The Travelling-Wave Divider/Combiner", IEEE Trans. Microwave Theory Tech., Vol.28, No.12, December 1980, pp1468-1473.

26. N. Nagai et al, "New n-Way Hybrid Power Dividers", IEEE Trans. Microwave Theory Tech., Vol.25, No.12, December 1977, pp1008-1012.

27. M. Dydyk, "Efficient Power Combining", IEEE Trans. Microwave Theory Tech., Vol.28, No.7, July 1980.

28. S.Y. Liao, "Microwave Devices and Circuits", Prentice-Hill, Inc., Englewood Cliffs, N.J., 1980, pp95-137.

29. A.F. Harvey, "Microwave Engineering", Academic Press London and New York, 1963, p14.

30. E.J. Wilkinson, "An N-Way Hybrid power Divider", IRE Trans. Microwave Theory Tech., Vol.8, No.1, Jan 1960, pp116-118.

31. L.I. Parad and R.Z. Moyanihan, "Split-Tee Power Divider", IEEE Trans. Microwave Theory Tech., Vol.13, No.1, Jan. 1965.

32. T.C. Edwards, "Foundations for Microstrip Circuit Design", John Wiley & Sons, 1981.

33. A.A.M. Saleh, "Planar Electrically Symmetric N-Way Hybrid Power Dividers/Combiners", Trans. Microwave Theory Tech., Vol.28, NO.6, June 1980, pp555-563.

34. K.C. Gupta et al, "Computer Aided Design of Microwave Circuits", Artech House, Inc., 1981, pp57-60.

35. C.P. Wood, P.S. Hall and J.R. Jones, "Design of Wideband Circularly Polarized Microstrip Antennas and Arrays", Royal Military College of Science, U.K., pp312-316.